Leachability of polycyclic aromatic hydrocarbons from coal tar and synthesis of the nanohybrid photocatalyst for their degradation

S Maswanganyi

orcid.org/ 0000-0001-8719-1775

Dissertation submitted in fulfilment of the requirements for the degree *Master of Engineering in Chemical Engineering* at the North West University

Supervisor: Prof E Fosso-Kankeu

Co-supervisor: Dr Neeraj Kumar, Prof J Bunt

Graduation: 2021

Student number: 33628033

ABSTRACT

There exists a great number of industrial processes that produce coal tar as a by-product. The rate of coal tar production is higher than the rate at which it is converted to other products, and its application is very limited. As a result, coal tars produced as by-products end up being discharged into the environment and occupy the unused land.In addition, the disposal of coal tar in the environment poses threats because of the toxic, carcinogenic, mutagenic, teratogenic and skin irritants compounds it contains.These compounds are known as polycyclic aromatic hydrocarbons (PAHs). PAHs can leach into surface waters since they are mobile. It is therefore important that the water contaminated by these harmful compounds is properly treated to avert the health and environmental problems they cause.

Different techniques for the removal of PAHs from water have been investigated and explored. Photocatalysis has emerged to be a promising method in terms of efficiency, sustainability, economic impact and reliability in the removal of persistent organic pollutants such as PAHs. Even though photocatalysis has been found to be effective in purifying wastewater, there is a search for an appropriate photocatalyst to degrade these organic pollutants in water.

This research focused on assessing the coal tar PAH profile and investigated the factors influencing the leachability of PAHs from coal tar into the environment. It was discovered that coal tar contains the majority of the most popular PAHs, which generally include 16 priority PAHs. It was also found that the mobility of PAHs from coal is highly influenced by contact time between coal tar and chemical properties of the aqueous solution the tar may be exposed to. The findings suggest that PAHs can leach from coal tar and enter water bodies, while the leachability of low molecular weight PAHs is much higher than the leachability rate of high molecular weight PAHs. Even though the amount of HMW PAHs that is leached into the water is very small, if the leaching process takes place for prolonged periods, the amount of HMW PAHs in waters can be significant. Therefore, it is important that a photocatalyst that is able to degrade both LMW and HMW PAHs is found.

In this study, RGO-Bi_2MoO_6 was investigated as potential photocatalyst to degrade PAHs in water. Thus, this photocatalyst was synthesised using hydrothermal methods because it allows the use of elevated temperatures, at which the RGO-Bi_2MoO_6 nanocomposite forms, and it is easy to operate.

This research focused on using the synthesised photocatalyst in the photo degradation of coal tar PAHs. To test the photocatalytic performance of RGO-Bi_2MoO_6 in degrading PAHs, a degradation test was carried out using naphthalene as representative of PAHs. It was found that RGO-Bi_2MoO_6 is a highly effective material in degrading naphthalene. The material showed a photo degradation efficiency of about 95%, and the results also indicated that RGO-Bi_2MoO_6 can be reused for about five times and still achieve a photo degradation efficiency of over 80%. The small amount of RGO that was added in the photocatalyst played a significant role in improving the performance of the material.

Key words: photocatalyst, leaching, PAHs, photo degradation, graphene oxide, lixiviant, coal tar, naphthalene, Bi_2MoO_6, demin water, synthetic water, river water

ACKNOWLEDGEMENTS

I am grateful for all the support I received during the study. In truth, I would not have managed to submit this dissertation without a strong support sysytem. Therefore, I would like to thank and acknowledge the following:

- My supervisor, Prof Elvis Fosso-Kankeu, for his enormous support and for pushing me to work hard. Thank you for your patience and guidance.
- The Water Research Commission (WRC, Project 2974) for funding this study.
- North West University for financial support.
- Eskom, South Africa for providing facilities for the characterisation of materials.
- Council for Scientific and Industrial Research (CSIR) for allowing me to use their facility to conduct my experiments.
- Dr Neeraj Kumar and Dr Rashi Gusain for assisting me with the experiments at CSIR and for their warm welcome and hospitality.
- My co-supervisors, John Bunt and Neeraj Kumar for their valuable inputs.
- Mr Nicco Lemmer for laboratory assistance.
- Mr Gideon van Rensburg for assistance with HIRA.
- My family for supporting me throughout the study.
- Mr Champion Mtileni for encouraging me to apply for this Masters and for moral support.
- God for granting me wisdom, understanding and strength to start and complete this study.

LIST OF ACRONYMS

ACE	Associated chemical enterprise
BET	Branauer-Emmett-Teller
DHHS	Department of Health and Human Services
DNA	Deoxyribonucleic acid
EPA	Environmental Protection Agency
FTIR	Fourier-transform infrared spectroscopy
GC	Gas chromatography
GCXGC-TOF	Two-dimensional gas chromatography and time-of-flight mass spectrometry
HMW	Heavy molecular weight
HRTEM	High resolution transmission electron microscopy
IARC	International Agency for Research on Cancer
LMW	Light molecular weight
MGP	Manufactured gas plant
MS	Mass spectroscopy
MW	Microwave
ORP	Oxido-redox potential
PAC	Polycyclic aromatic compounds
PAHs	Polycyclic aromtaci hydrocarbons
PL	Photoluminescence
ROS	Reactive oxidisng species
SANS	Small-angle neutron scattering
SAXS	Small-angle X-ray Scattering
SCL	Sasol chemical industires
SEM	Scanning electron microscope
SSA	Specific surface area
SSF	Sasol synthetic fuels
TEF	Toxic equivalency factors
TEM	Transmission electron microscopy
TEQ	Toxic equivalency
UCG	Underground coal gasification
UV	Ultraviolet
XPS	X-ray photoelecton spectroscopy
XRD	X-ray diffraction

RESEARCH OUTPUTS

CONFERENCE PROCEEDINGS

1. S Maswanganyi, E Fosso-Kankeu, N Kumar, R Gusain, F Waanders, J Bunt, Ss Ray, T. Tamane and A. Lombard. PAHs profile of coal tars generated from coke production process and their toxicity. Conference: 17th Johannesburg International Conference on Science, Engineering, Technology and Waste Management (SETWM-19) At: Johannesburg, South Africa. DOI: 10.17758/EARES8.EAP1119275.
2. S Maswanganyi, E Fosso-Kankeu, N Kumar, R Gusain, F Waanders, J Bunt and S. S. Ray. A Comparison Study of Different Photocatalyst Preparation Methods: A Review on RGO-BI_2MoO_6 Photocatalyts Synthesis Methods. 18th Johannesburg International Conference on Science, Engineering, Technology and Waste Management (SETWM-20) At: Johannesburg, South Africa. https://doi.org/10.17758/EARES10.EAP1120220
3. S Maswanganyi, E Fosso-Kankeu, N Kumar, R Gusain, F Waanders, J Bunt, SS Ray.Removal of Naphthalene from Wastewater using RGO-Bi_2MoO_6 Nanocomposite: Adsorption Assisted Photocatalysis Degradation and Kinetics. IMWA Conference in 2022 in New Zealand (Ready to submit)

PUBLICATIONS (READY YO SUBMIT)

1. Shelter Maswanganyi, Elvis Fosso-Kankeu, Neeraj Kumar, Frans Waanders, John Bunt, Suprahkas Sinha Ray. Mobilisation of PAHs from coal tar by various environmental aqueous solutions.
2. Shelter Maswanganyi, Rashi Gusain, Neeraj Kumar, Elvis Fosso-Kankeu, Frans Waanders, Suprakas Sinha Ray. Bi_2MoO_6 nanoplates supported on reduced graphene oxide: An effective nanocomposite for removal of naphthalene via adsorption-photodegradation.

TABLE OF CONTENTS

LIST OF TABLES

LIST OF EQUATIONS

LIST OF FIGURES

CHAPTER 1: INTRODUCTION

1.1 BACKGROUND AND MOTIVATION

South Africa obtains about 70% of its energy from coal processing (Khethane *et al.*, 2017). As a result, most of the country's industrial processes involve conversion of tonnes of coal for energy production. Coal processes are mostly aimed at energy production, steel making, oil and coke making (Jin *et al.*, 2019). Industrial coal processing, such as gasification of biomass, combustion and pyrolysis, can result in tar formation, which is generated as either a by-product or main product, depending on the end-use of coal product. Coal tar is defined as a complex and valuable mixture of phenols, polycyclic aromatic hydrocarbons (PAHs) and heterocyclic compounds. Tars are classified according to their hydrocarbon chains and boiling points. The ones with short rings are referred to as phenols, and the larger ones are called PAHs (Abdel-Shafy & Mansour, 2016). The transition of tars from lower to higher hydrocarbons is a function of temperature, as shown in Figure 1-1. Tars are considered a threat to the environment when disposed, as it is known to be the largest source of polycyclic aromatic hydrocarbons, which are known to be toxic, mutagenic and carcinogenic (Mulder *et al.*, 2001).

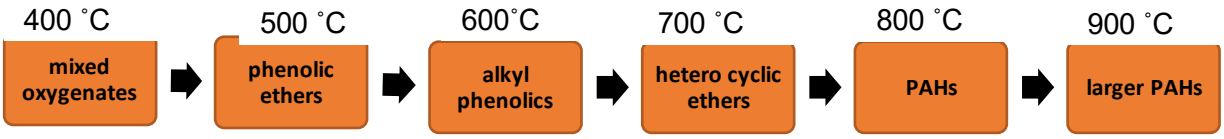

Figure 1-1: Tar Maturation with increasing temperature

This research project focuses on the leachability of PAHs from coal tar and the synthesis of a photo catalyst for their degradation. The leachability of PAHs from coal tar pitches produced from different coal samples is assessed. Although the characterisation of tar and the compositions thereof have been reported intensively in the literature, there is limited information on the impact of tar on water. Furthermore, there are many literature studies that focus on the leachability of PAHs from soil. Larsson *et al.* (2017) only focused on the existance and mobility of polycyclic aromatic compounds (PACs) in contaminated soils, and Zand *et al.* (2010) looked at the determination of leaching behaviour of PACs. Few research studies have been done on the leachability of PAHs from coal tar as well as the degradation of PAHs by a modified photocatalyst; hence this topic was chosen as the research focus of this project.

PAHs are an important group of organic compounds of serious environmental concern (Gupta & Gupta, 2015). They are compounds that consist of at least two aromatic hydrocarbons (benzene) rings. PAHs have been reported to be extremely carcinogenic and mutagenic in humans; hence,

they are considered an environmental hazard when in contact with water. There are several sources of these aromatic hydrocarbons; some sources can be natural, and some are due to anthropogenic activities. Anthropogenic sources are, however, considered the most significant contributors of PAHs to the environment (Bergendahl, 2007). Among the anthropogenic sources, pyrolytic and petrogenic sources are considered to be the most important. PAHs are also called secondary tars, as they start forming at a temperature of at least 800℃ and decompose at a temperature of 1000℃ and above. Naphthalene, phenanthrene, pyrene and benzopyrene are examples of PAHs (Roetsa *et al.*, 2014). Due to the fact that PAHs have the potential to be easily transported by rainwater to nearby water sources, it is therefore important to test their leachability from coal tar pitch. PAHs that end up in water sources lead to increased risk for human beings and aquatic life. Leachability tests will assist in determining how much hazardous PAHs from coal tars can be leached to the environment. Previous researchers have focused on the leachability of PAHs from soil, and they have found that the leaching process is slow. The minimisation of PAH mobility or leachability could have been caused by the fact that PAHs tend to bind strongly to soil (Zand *et al.*, 2010). However, it is not yet clear how easily the PAHs could leach from the coal tar; this study is therefore partly designed to address this issue, such as to provide relevant information for environmental risk assessments.

The inadequate removal of PAHs from waste treatment plants has led researchers to identify the most effective method for the degradation of these aromatics (Tayade, 2012). Different techniques have been utilised in the remediation of PAHs, including thermal desorption, containment, and biodegradation. However, these techniques have limitations; containment, for example, is a temporary solution (Tayade, 2012). The costs of utilising thermal desorption are too high, and microbial degradation of high molecular weight PAHs requires effective maintenance of optimised conditions and is very slow due to their high stability. Photodegradation is a favourable solution for the removal of PAHs and other persistent organic pollutants. Photocatalytic processes are more effective in decontaminating water and soils containing dangerous organic chemicals. There is ongoing research on finding the best photocatalyst for the degradation of pollutants in water. Semiconductors have been identified as materials that can be used to synthesise a catalyst, owing to their band gap, efficient light absorption, high chemical stability, high oxidation power, non-toxicity, low cost and relative abundance in nature. These semiconductors have their limitations (Tayade, 2012). Their limitations can be surmounted by modifying the surface of a semiconductor (Milne & Evans, 1998). There are several studies on the modification of semiconductors. Modifications of semiconductor photocatalysts (metal based materials) can reduce their high cost and heavy metal toxicity. The modifications can allow the use of metal semiconductors that have good catalytic properties but are expensive. In recent years, non-metal based photocatalysts have been explored. These non-metal materials include phosphorus, sulphur, nitrogen and carbon (Zhao *et al.*, 2018). In this study, the synthesis of an improved photocatalyst through modification with a carbon based non-metal known as graphene oxide is considered.

1.2 RESEARCH PROBLEM

Coal tar, which is a by-product of the coke-making process, contains PAHs. PAHs are carcinogenic and toxic. The disposal of coal tar in the environment may result in the contamination with these carcinogens of water sources meant for human use. The leachability of PAHs from coal tar may result in their dispersion in receiving water sources, which are also used by humans. The dispersion potential of PAHs from coal tar into various water sources has not been established yet. Furthermore, the removal of PAHs from water remains challenging, as conventional methods have shown some limitations.

1.3 RESEARCH AIM

The purpose of this study is to assess the leachability of PAHs from coal tar and synthesise effective photocatalysts for PAH removal from water.

1.4 OBJECTIVES

- To assess the leachability of PAHs from coal tar.
- To synthesise and characterise an effective photocatalyst for PAH degradation.
- To determine conditions suitable for the effective removal of naphthalene from water through photodegradation.
- To develop a sustainable technique for the treatment of PAH contaminated water.

1.5 RESEARCH QUESTIONS

- What is the susceptibility for PAHs in coal tar to disperse in water?
- What factors influence the leachability of PAHs in coal tar?

How effective is Bi_2MoO_6 nanoplates supported on reduced graphene oxide in the degradation of naphthalene?

1.6 ORGANISATION OF DISSERTATION

1.6.1 Chapter 1 Introduction

This section discusses the background and motivation of the study. It also includes the objectives, purpose and problem statement of the project.

1.6.2 Chapter 2: Literature review

Chapter 2 contains the literature relevant to the research topic and the objectives of the study. Definition of PAHs is discussed in detail and this includes its sources, how it can be generated, its health and environmental impact, and remediation techniques. It also discusses in detail PAHs removal technique applied in this study.

1.6.3 Chapter 3: Paper 1

This chapter contains the paper written on PAH profile of coal tars generated from coke production process and their toxicity

1.6.4 Chapter 4: Paper 2

This includes the study done on the Mobilisation of PAHs from coal tar by various environmental aqueous solutions

1.6.5 Chapter 5: Paper 3

Bi2MoO6 nanoplates supported on reduced graphene oxide: An effective nanocomposite for removal of naphthalene via adsorption-photodegradation

1.6.6 Chapter 6: Overall Conclusion and Recommendations

Includes key findings from the study as well as the recommendations.

REFERENCES

Abdel-Shafy, H.I. & Mansour, M.S.M. 2016. A review on polycyclic aromatic hydrocarbons: Source, environmental impact, effect on human health and remediation. *Egyptian Journal of Petroleum*, 25(1):107-123.

Gupta, H. & Gupta, B. 2015. Photocatalytic degradation of polycyclic aromatic hydrocarbon benzo[a]pyrene by iron oxides and identification of degradation products. *Elsevier Chemosphere,* 138:924-31

Khethane, T.C., Fosso-Kankeu, E., Waanders, F. & J.J. 2017. PAHs Content of Tar Produced from Fischer Assay of Medium Rank C Bituminous South African Coal. *Science, Engineering, Technology & Waste Management, 9th Int'l Conference on Advances in Science, Engineering, Technology & Waste Management (ASETWM-17).* November 2017, Parys, South Africa. Editors: F. Waanders, E. FossoKankeu, B. Topcuoglu, M. Plaisent, Y. Thaweesak. ISBN: 978-81-934174-6-1.27-28.

Larsson, M. et al., 2017. *Occurrence and leachability of polycyclic aromatic compounds in contaminated soils: Chemical and bioanalytical characterization.* s.l.: Science of the Total Environment, 622-623:1476-1484 .

Milne, T.A. & Evans, R.J. 1998. *Biomass Gasifier "Tars": Their Nature, Formation,and Conversion.* s.l.:National Renewable Energy Laboratory. Report No.NREL/TP-570-25357, National Renewable Energy Laboratory: Golden Mulder, E., Brouwer, J.P., Blaakmeer, J. & Frénay, J.W. 2001. Immobilisation of PAH in waste materials. Waste Management, 21: 247–253.E.

Roetsa, L., Bunta, J.R., Neomagusa, H.W. & Van Niekerk B.D. 2014. An evaluation of a new automated duplicate-sample Fischer Assay setup according to ISO/ASTM standards and analysis of the tar fraction. *Journal of Analytical and Applied Pyrolysis,* 106:190-196.

Tayade, R.J. 2012. *Photocatalytic Materials and Surfaces for Environmental Cleanup.* s.l.:Trans Tech Publications, Limited.712: 217

Bergendahl, J. 2007. Batch Leaching Tests: Colloid Release and PAH Leachability. *Soil & Sediment Contamination, An International Journal,* 14(6):527-543.

Jin, L. et al., 2019. Effect of temperature and simulated coal gas composition on tar production during pyrolysis of a subbituminous coal. *Fuel,* 241:1129–1137.

Zand, A.D., Grathwohl, P., Nabibidhendi, G. & Mehrdadi, N. 2010. Determination of leaching behaviour of polycyclic aromatic hydrocarbons from contaminated soil by column leaching test. *Waste Management & Research, 28(10):913-920*.

Zhao, G., Yang, H., Liu, M. & Xu, X. 2018. Metal-Free Graphitic Carbon Nitride Photocatalyst Goes Into Two-Dimensional Time. *Review*. *Front Chem*, 6:551.

CHAPTER 2: LITERATURE REVIEW

2.1 An Overview of Polycyclic aromatic aydrocarbons

2.1.1 Introduction

This chapter provides an overview of polycyclic aromatic hydrocarbons (PAHs), mainly the most popular 16 PAHs (Table 2-1). In this section, there are 11 subsections that describe sources, formation, mobility, exposure risk, health effects of PAHs, and remediation techniques for PAH contaminated environments.

Table 2-1:16 EPA priority PAHs

PAH Name	Molar Mass(g/mol)
Naphthalene	128
Phenanthrene	178
Anthracene	178
Fluoranthene	202
Acenapthylene	152
Acenaphthene	154
Fluorene	166
Pyrene	202
Chrysene	228
Benzo(a)Pyrene	252
Indeno(1,2,3-cd)Pyrene	276
Benzo(k)Fluoranthene	252
Benzo(b)Fluoranthene	252
Benz(a)Anthracene	228
Benzo(g, h, i)Perylene	276
Dibenz(a, h)Anthracene	278

2.1.2 What Are polycyclic aromatic hydrocarbons?

Polycyclic aromatic hydrocarbons are a group of organic compounds that are made up only of hydrogen and carbon, with many rings attached to each other in angular, cluster or linear

arrangements (Chen *et al.*, 2019). Under normal conditions, most PAHs are found as light yellow, colourless, or white solids at room temperature (Abdel-Shafy & Mansour, 2016). They are also known as lipophilic, having low water solubility, low vapour, high boiling and melting points compounds (Abdel-Shafy & Mansour, 2016). PAHs may contain hydrogen and carbon arranged in a very simplified benzene structure to complex structure systems. Chemically, PAHs contain two or more benzene rings without hetero atoms and substituents (Abdel-Shafy & Mansour, 2016). Although PAHs are made up of only hydrogen and carbon, in some conditions, these two atoms may be replacedby other elements and cause PAHs to transition to heterocyclic aromatic compounds, which are normally classified together with PAHs (Gitipour *et al.*,2018). PAHs are typical environmentally persistent organic pollutants with varied toxicity and carcinogenicity. They are known to have acute health effects on humans and animals. Research has proved that PAHs have an ability to give rise to mutagenic and carcinogenic effects and are strong immune suppressants (Alegbeleye *et al.*, 2017). PAHsare organic contamintsthat can be found in any segment of the environment, exhibiting mild to low water solubility, which promotes adsorption and absorption processes to particulates and build-up of PAHs in sediments. PAHs can be found in water, soil, sediments and air; as a result, they can be declared ubiquitous pollutants

There are more than 100 PAHs found in the environment, of which 16 can be said to be the most common (Dobaradaran *et al.*, 2020). PAHs that are deemed as the priority PAHs by the Environmental Protection Agency (EPA) of the United States of America include anthracene, naphthalene, pyrene, acenapthylene, fluoranthene, acenaphthene, indeno(1,2,3-cd)pyrene, fluorene, chrysene, phenanthrene, benzo(b)fluoranthene, benzo(k)fluoranthene, benzo(a)anthracene, dibenzo(a, h)anthracene, benzo(a)pyrene, and benzo(g, h, i)perylene (Gitipour *et al.*, 2018). In this report, the abbreviation PAH refers only to those listed above, due to the vast amount of information available. All these PAHs differ according to their benzene ring number and arrangement. Some PAH ring arrangement systems may be structured in such a way that carbon atoms are the centre of two or three interconnected benzene rings. PAHs with this kind of arrangement are referred to as compounds with linear ring arrangements (Abdel-Shafy & Mansour, 2016). However, many PAHs are found as hybrids surrounded by diverse structural components, and these are called PAHs with clustered or angular arrangements.

PAHs that contain at most four benzene rings are classified as light-weight compounds, and those that possess at least four rings are referred to as heavy-weight PAHs (Rubio-Clemente *et al.*, 2014). The number of benzene ring play a big role in defining the characteristics of PAHs. Heavy molecular weight PAHs exhibit a more stable structure and are more toxic compared to light-weight PAHs (Alegbeleye *et al.*, 2017). In general, heavy and more angular PAHs have higher hydrophobicity, lipophilicity and electrochemical stability, low water solubility and vapour pressure (Abdel-Shafy & Mansour, 2016a). Angular and clustered structured PAHs tend to dissolve more easily in water than linear structured molecules. For each addition of rings, PAHs become more resistant to oxidation

and reduction (Qu *et al.*, 2020). PAHs are detrimental, persistent environmental pollutants, but the heavy molecular weight (HMW) PAHs are much more harmful to human health and the environment. HMW PAHs are more persistent in the environment because of their hydrophobicity and molecular stability.

PAHs dissolve easily in organic solvents due to their highly lipophilic property. Most PAHs emit light when they are excited. They also show a variety of characteristics, which include heat resistance, conductivity and sensitivity, and corrosion resistance. PAHs have characteristic UV absorbance spectra. Each PAH ring displays a distinctive UV spectrum; consequently, each individual isomer exhibits a distinct UV absorbance spectrum. All the above-mentioned characteristics are useful in identifying PAHs.

Many PAHs have very little commercial purpose. PAHs are mainly utilised in agricultural products as intermediaries, lubricating materials, thermosetting plastics, pharmaceutical and other chemical operations (Alegbeleye *et al.*, 2017). Table 2-2 summarises the general uses of some PAHs. Others may be found in asphalt, which is used in road making or roofing. Some processed PAH products are applied in the field of electronics, liquid crystals and functional plastics (Gitipour *et al.*, 2018).

Table 2-2: PAHs application

PAH Name	Application
Acenaphthene	Dyes, Manufacture of Pigments Plastics, Pesticides And Pharmaceuticals
Anthracene	Diluent For Wood Preservatives, Manufacture Of Dyes and Pigments.
Fluoranthene	Manufacture of Pharmaceuticals, Agrochemical, And Dyes
Fluorene	Manufacture of Pigments, Pharmaceuticals, Dyes, Thermoset Plastic and Pesticides
Phenanthrene	Manufacture of Pesticides and Resins
Pyrene	Manufacture of Pigments

2.1.3 Common PAH sources

PAHs can be produced naturally or through anthropogenic activities; many PAHs are uncontrollable and exhibit toxic properties. Forest and bush fires, waste burying, petroleum seeps, volcanoes, and erosion of sedimentary rocks that contain petroleum hydrocarbons are natural sources of PAH release (Qiu *et al.*, 2019; Qu *et al.*, 2020). Anthropogenic sources of PAHs are formed mostly as a

result of human activities, including fossil fuel burning. Anthropogenic sources of PAHs are categorised into big point sources and small point sources (Rubio-Clemente *et al.*, 2014). Big point sources are partial combustion of fossil fuels such as waste incineration and other industrial processes (Rubio-Clemente *et al.*, 2014). Distributed sources that include automobile exhausts, smoke from wood stoves, and jet aircraft exhausts are considered small point sources of PAHs (Rubio-Clemente *et al.*, 2014). Other human-made sources of PAHs are creosote waste materials, sewage sludge, and petroleum spills. PAHs from human made sources are extensively dispersed environmental pollutants that have harmful biological effects, toxicity, carcinogenicity and mutagenicity (Abdel-Shafy & Mansour, 2016).

Pyrogenic, biological, and petrogenic processes are major emitters of PAHs in the environment (Qu *et al.*, 2020). PAHs produced through pyrolysis processes are referred to as pyrogenic PAHs and are formed via exposing organic substances to elevated temperatures at low oxygen or in the absence of oxygen conditions. Processes such as destructive distillation of coal into coal tar and coke, or the breaking down of petroleum product remains into smaller hydrocarbons using heat, are known as pyrolytic processes that take place intentionally and also result in PAH formation (Peng *et al.*, 2018). In contrast, the partial burning of motor fuels in trucks and cars, and partial combustion of fuels in heating systems are pyrogenic process that occur unintentionally. The temperature at which pyrolysis occur ranges from 300 ^{o}C to a maximum of 1200 ^{o}C (Abdel-Shafy & Mansour, 2016). Pyrogenic PAHs normally appear in higher concentrations in urban locations and in places within the vicinity of industrial operations that produce coke or coal tar. Alternatively, PAHs can be produced at temperatures lower than 300 ^{o}C (Abdel-Shafy & Mansour, 2016). Crude oil contains PAHs that developed over thousands and thousands of years at temperatures as low as 100 to 150 ^{o}C (Lawal, 2017). In this respect, petrogenic PAHs can be defined as PAHs that form during the process of crude oil maturation or any other similar processes. The widespread use of crude oil for fuelling purposes in transportation, and the utilisation of crude oil products and oil increase the presence of petrogenic PAHs in the environment. Major contributors of petrogenic PAHs in the environment include fresh water and oceanic oil spills, leaks from under and above ground storage tanks, and build ups of small releases of motor oil, gasoline and other transportation related products (Mahmoudi *et al.*, 2013). PAHs produced from biological processes are either created by particular bacteria and plants or formed during the process of degrading vegetative matter. It is important to note that partial combustion of organic materials either anthropogenically or naturally is the largest source of PAHs in the environment (Kim *et al.*, 2013). Incomplete combustion of these organic materials mostly occurs during steel making, coke production, coal tar production and other related processes (Abdel-Shafy & Mansour, 2016).

Mixtures of PAHs emerging from petrogenic sources and pyrogenic sources exhibit different characteristic profiles; petrogenic PAHs contain a higher percentage of alkylated compounds. (Gitipour *et al.*, 2018). As previously mentioned, these two processes occur at significantly different

temperature ranges; therefore, the temperature at which PAHs are formed can give one key to pin pointing PAH sources because it is known that higher temperatures tend to produce lower alkylated PAH chains compared to PAHs produced at a low temperature conditions. For instance, PAHs found in a power plant slack discharge, which are mostly heavier PAHs, will exhibit a different structure of PAHs compared to a PAH profile of mixtures found at a crude oil spill because they are formed at rapidly rising temperatures. PAHs from pyrogenic and petrogenic sources can be distinguished by examining the size of the five-membered rings in the structure of the PAH compound (Abdel-Shafy & Mansour, 2016). The five-member rings are found in greater abundance in crude oil (petroleum) products than in pyrogenic substances, because the longer period of petroleum products formation favours the marshalling of the rings. In pyrogenic processes, the reactant materials are transformed into a more stable product with six rings. Even though there are many PAH sources that have been identified, advances in research have been made and are still continuing to identify these other unknown sources and differentiating between petrogenic and pyrogenic sources. Temperature is not the only factor that can be used to identify PAH sources; concentration ratios of specific pair PAHs can also be used (Gitipour *et al.*, 2018). PAH specific pair ratios are known as PAH molecular diagnostic ratios and are utilised for PAHs found in soils, sediments and air (Abdel-Shafy & Mansour, 2016). PAH diagnostic ratios are used to distinguish PAHs from petroleum combustion, petroleum products and biomass /coal burning. The compound included in each single ratio exhibits the same molar mass; therefore, it is assumed that the compounds participating in each ratio will have the same physiochemical properties.

2.1.4 Coal tar generation

There exists a variety of coal tar production processes, which include gasification, underground coal gasification, and coking of coal (Fosso-Kankeu, 2019). In South Africa, large amounts of coal tar come from coking processes. Coking is a process that involves the production of metallurgical coke for purposes in iron-making blast furnaces and for use in other smelting processes (Fosso-Kankeu, 2019). This process entails the heating of coal at temperatures as high as 1200 ^{o}C in the absence of oxygen in order to distil oils and tars. Coal tar is a thick, dark, black, viscous liquid formed as a by-product of the coking process. The coking process takes place in an oven battery (Seo *et al.*, 2020). A coke oven battery is simply a series of 10 to 100 ovens stacked together. When by-products such as oven gas, water and sulphur from the oven battery are thermally removed, there remains a material called coke (Guo *et al.*, 2020). The water removed from the oven is usually rich in organic matter (e.g. PAHs) and inorganic matter. Recently, there has been a shift in how coal tar is applied or utilised. For instance, there has been a reduction in the amount of tar used in road construction due to the high content of carcinogenic and toxic PAHs in coal tar (Chen *et al.*, 2019). As a result, thousands of tonnes of coal tar being produced as by-products from coking processes end up being discarded into the environment. Apart from the possibility of the disposal space running out, PAHs

in the tar may leach into ground water or surface water and thus start affecting the environment negatively. Figure 2-1 is showing the general process of producing coke.

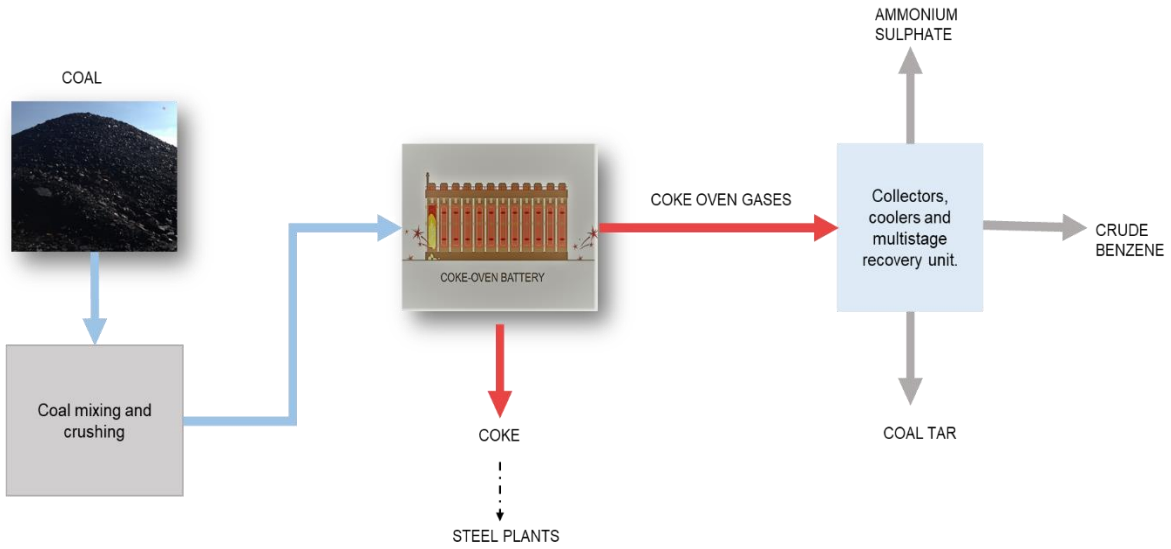

Figure 2-1: General flow diagram of coke production process

2.1.5 Fate and transfer of PAHs in the environment

In general, PAHs reach the environment via different routes and are commonly found in the environment as a complex mixture that contains at least two different PAH compounds, e.g. soot, a component of coal tar or crude oil (Abdel-Shafy & Mansour, 2016). Although PAHs occur as mixtures, they can be individually manufactured for use in research studies and for utilisation in certain industrial processes such as the production of medicine, dyes and plastics (Abdel-Shafy & Mansour, 2016). Research is done on single PAH compounds to reduce the number of variables, even though they exist and enter the environment as a mixture. PAHs enter the environmental matrices via natural or anthropogenic routes (Gitipour *et al.*, 2018). The amount of PAHs in the environment varies significantly, contingent upon the vicinity of the polluted site to the PAH source site, the mode of PAH transport and the level of industrial development (Abdel-Shafy & Mansour, 2016). PAHs occur in high concentrations in the products of fossil fuels, biomass burning, charcoals and wood smoke. In some places, petroleum refineries and transport activities are major contributors of PAHs in the environment, while in other places, coal burning processes are the biggest contributor.

PAHs have been found in surface water, soil, air, ground water, as well as in sediments (Chen *et al.*, 2020). PAHs that end up in the aquatic environment originate from wastewater effluent discharge, transportation or industrial use of petroleum, combined sewer overflows and urban runoff, as well as natural seeps (Huang *et al.*, 2020). As previously mentioned, PAHs enter the environment through different routes. For instance, PAHs in the air are introduced as by-products primarily from the partial combustion processes of organic matter. The atmospheric emissions of airborne PAHs are the result

of power and heat generation processes, vehicle emissions, and industrial processes such as coke production. Vehicular traffic is the largest contributor of airborne PAHs, and their concentration is found in higher levels in urban areas than in rural areas. Once emitted in the atmosphere, PAHs can be found in two different phases, a solid phase and a vapour phase, in which PAHs adsorb into atmospheric particulate matter, depending on the atmospheric conditions and the properties of individual PAHs (Zhang *et al.*, 2019). On the earth's surface, atmospheric PAHs are continuously transported via dry or wet deposition. PAHs can also enter surface soils through leaching process if material disposed of or sitting on the earth's surface contain PAHs, e.g. leachate tar road. When organic compounds such as PAHs are released into the environment, particularly on the the earth's surface, they become active and mobile. As a result, they penetrate into the soil (Chen *et al.*, 2020). Nonetheless, most of the PAHs found in soil are bound to soil particles. PAHs mobility in the soil surface is affected by the sorbent throat size and particle size of the soils. If particles which PAHs get adsorbed to cannot penetrate the soils, then the movement of PAHs becomes limited, since they have a tendency to be adsorbed to surface particles. PAHs found in sediments are deposited by a similar process as the one governing the deposition to surface soils. PAHs adsorbed to the atmospheric particulate matter can accumulate on the surface of oceans, streams and lakes by wet or dry deposition. They then are dispersed by currents and eventually become mixed with the sediments. PAHs also enter the sediments from sewage effluents as well as tar-roadway runoffs. In addition, PAHs produced from oil and coal combustion can add to sediment pollution, particularly in the vicinity within former manufactured gas plant (MGP) sites (Chen *et al.*, 2020). After a certain period, some PAHs from MGP will be adsorbed to particles, settle and form part of the sedimentary record. Once PAHs settle beome part of the sedimentary record, they become somewhat stagnant because their non-polar structures hinder them from dissolving in water (Abdel-Shafy & Mansour, 2016). Nevertheless, not all PAHs are insoluble in water; the lower molecular weight PAHs may dissolve in water. Therefore, a very small quantity of PAHs may dissolve in water and become part of the water system. In addition, not all PAHs are incorporated in the sediments; some may remain in the water for longer periods.

2.1.6 PAH occurrence in water

PAHs were first discovered and measured in coastal waters (Abdel-Shafy & Mansour, 2016). A concentration of PAHs in aquatic ecosystems is commonly found at the lowest level in water, intermediate in biota and highest in sediments. However, this is dependent on the source of PAHs, phase or form at which the PAH mixtures are entering the aquatic environment, as well as the properties or characteristics of that particular water. For instance, the majority of PAHs coming from coal tar mixtures might end up in the water rather than in the sediments, and PAHs from solids such as coal may end up mostly in sediments rather than in water. In addition, PAHs aggregate in sediments since they will in general adsorb to atmospheric aerosol particles that accumulate at the bottom of the aquatic ecosystems, but if the water body is near a point of contamination source, such

as an industrial site, a significantly higher amount of PAH concentration may be found in water compared to the PAHs in sediments. PAHs reach the water on the earth's surface mostly via atmospheric particulate matter deposition, contaminated ground and urban runoff, municipal waste discharges and industrial effluents (Kim *et al.*, 2013). Some PAHs in ground water and surface water originate from polluted water bodies, leaching from solid waste disposal sites and irrigation with contaminated water. Mostly, higher concentrations of PAHs were found in surface water than in ground water (Alegbeleye *et al.*, 2017). A study done by Zhao *et al.* (2017b) indicated that the lower molecular weight PAHs found in coastal water came from fuel oil combustion products and petroleum, as well as other pyrogenic sources. Zhao *et al.* (2017a) identified that PAHs in water come from mainly coal and biomass combustion. Kim *et al.* (2013) stated that toxic compounds from disposed coal tar could leach and pollute surface water. PAHs may be detected in drinking water as well (Dobaradaran *et al.*, 2020). The existence of PAHs in potable water may be associated with raw water sources from contaminated surface or ground water or the usage of pipe coated with coal tar in public water supply systems. It has been proven that chlorination does not degrade PAHs; however, it prompts the development of chlorinated and oxygenated PAHs, which are even more harmful than the parent PAH compounds.

2.1.7 Route and risk of PAHs exposure

The major routes of PAH exposure in the general population include breathing indoor air and ambient, smoking cigarettes, eating food containing PAHs, dermal contact and drinking PAH contaminated water in both workplace and non-workplace environments (Abdel-Shafy & Mansour, 2016). Smoking Tobacco may result in inhalation of PAHs, because some PAHs including benzo(a)pyrene and other possible carcinogens are contained in tobacco smoke (Abdel-Shafy & Mansour, 2016). Most crops including rye, wheat and lentils may produce PAHs or absorb them via air, water or soil; therefore ingestion of food from these crops may result in PAH exposure in humans (Kim *et al.*, 2013). Water also contains certain PAHs from industrial effluent, disposed waste leachates and seawater accidental spills during oil shipment. Exposure to PAHs from water sources can occur through drinking or dermal contact. In addition, people who are exposed to PAHs from occupational environments include street vendors, mechanics, workers in mining, metal, coke production and oil refining plants. PAHs are widespread contaminants in the environment; therefore avoiding their exposure is very difficult.

2.1.8 Human health and eco-toxic effects of PAHs

Exposure to various occupational environments with a high level of pollution mixtures containing PAHs is known to have caused short- and long-term health impacts (Lawal, 2017). The effect of PAHs on the health of human beings is dependent on the route and period of exposure and the amount of toxic PAHs an individual may be exposed to. A variety of other factors, such as age and underlying health conditions, can also contribute to the health impact. Exposure to high levels of

contaminant solutions containing PAHs has caused symptoms such as vomiting, diarrhoea, eye irritation, nausea, confusion, skin irritation and inflammation (Abdel-Shafy & Mansour, 2016). Nevertheless, exposure to PAH pollutants never occurs on an individual or single level of PAH, but rather a mixture. For example, mixtures of benzo(a)pyrene, naphthalene, and anthracene have been discovered as skin irritants, while mixtures of anthracene and benzo(a)pyrene are known to be skin sensitisers, i.e. they cause an allergic skin response in animals and humans beings. Therefore, it is usually not easy to identify exactly which components of these mixtures are responsible for the health effects. PAH exposure may result in long-term or chronic health effects, which include cataracts, breathing problems, lung function abnormalities, kidney and liver damage, decreased immune function, and asthma-like symptoms (Kim *et al.*, 2013). Frequent contact with PAHs may induce skin inflammation and redness. Ingestion or inhalation of huge amounts of naphthalene may cause the breakdown of red blood cells.

The toxicity of PAHs to the aquatic environment is mainly influenced by photo-oxidation and metabolism (Abdel-Shafy & Mansour, 2016). PAHs in the aquatic environment are generally more toxic when exposed to ultraviolet light. In soil, terrestrial invertebrates can be badly affected when the soil is heavily contaminated with PAHs. Harmful effects that may occur in organisms include immunity deficiency and tumours. Mammals absorb PAHs via different routes, e.g. ingestion, inhalation and dermal contact. On the other hand, plants are also able to absorb PAHs through their roots, from which they are transported to other parts of the plant. However, PAH-induced phyto-toxic effects are very rare, because some plants are able to protect themselves against PAH effects using certain inherent substances (Alegbeleye *et al.*, 2017). The 16 PAHs have been declared as compounds of the greatest risk with regard to potential exposure and harmful health effects on humans, and are therefores considered as a group when analysing them. The international agency Research for Cancer classified PAHs as carcinogens, possible carcinogens, and probably carcinogenic to humans and animals; these three categories are named group 1, group 2A and group 2B, respectively. Some PAHs are well known to beteratogenic, carcinogenic, and mutagenic and are considered to pose critical threat to the health and wellbeing of humans (Alegbeleye *et al.*, 2017).

2.1.9 Teratogenicity, carcinogenicity, mutagenicity and toxicity

The increasing rate of industrialisation is slowly leading to a higher concentration of contaminants in the environment, and PAH pollution is most likely to reach overwhelming levels in the future. PAHs are recognised for their mutagenicity, carcinogenicity, teratogenicity and toxicity. Benzo(a)pyrene is the greatest carcinogen among the different PAHs (Abdel-Shafy & Mansour, 2016). When PAHs enter agricultural soil and surface water through sewage sludge and leachates from the contaminated sites, they pose a danger to the environment, crops grown in the soil, and consequently, humans who eat food from PAH polluted environments. Excessive contact with PAHs causes lung cancer, a very well-known deadly disease. Once PAHs enter the body, they will require

metallic activation to start exerting their carcinogenic effects (Gbeddy *et al.*, 2020). The activation pathway occurs via a three-stage sequence, leading to the development of diol epoxides, which then react with DNA to give rise to adducts that can subsequently cause mutations and start the carcinogenic activity. Exposure to PAHs is also associated with human liver toxicity. It is vital to note that PAHs are the main cause of different types of cancers, primarily lung cancer, more than any other carcinogens. Exposure to PAHs in the air may result in asthma in children, bronchitis, impaired pulmonary function and respiratory problems (Kim *et al.*, 2013).

2.1.9.1 Carcinogenicity

Evidence shows that mixtures of PAHs cause cancer in humans (Dobaradaran et al., 2020). This evidence emerges from the research done on occupational workers in contact with mixtures containing PAHs. The research has indicated an increase of predominantly lung and skin cancer, as well as gastrointestinal and bladder cancer. Laboratory experiments were conducted on animals, and results showed that animals vulnerable to certain concentrations of some of the most common PAHs have developed skin cancer from dermal contact, stomach cancer from consuming PAHs in food, and lung cancer from inhalation over long periods (Dobaradaran *et al.*, 2020).

2.1.9.2 Immune suppression

Research reports show that immune suppression is one of the most frequent effects caused by exposure to PAHs. Furthermore, the literature indicates that immune-potentiation occurs after atmospheric exposure(Kim Gehle, 2009). It has been reported that some PAHs, when ingested through food, may give rise to DNA adducts in the lungs (Kim Gehle, 2009).

2.1.9.3 Genotoxicity

Genotoxic impacts for some PAHs have been shown both in in-vitro and rodent test systems using mammalian cells. It is to mention that most PAHs are not naturally geno-toxic; for them to induce geno-toxic effects, they requirre to undergo the metabolism process in order to form diol epoxides that then react with DNA (Kim *et al.*, 2013). Geno-toxicity plays an important role in the process of PAHs becoming carcinogenic and in their developmental toxicity process (Kuppusamy *et al.*, 2017).

2.1.9.4 Teratogenicity

During experimental analysis, PAHs displayed embryo toxic effects in animals exposed to PAHs such as benzo(a)pyrene, benzo(a)anthracene and naphthalene (Alegbeleye et al., 2017). Laboratory studies showed that consumption of large amounts of benzo(a)pyrene by mice during pregnancy caused birth defects and also resulted in reduced body mass in the offspring. It has not been confirmed that these same effects can take place in humans. However, it was investigated and reported that human exposure to PAH contamination during pregnancy can cause unusual birth outcomes such as low birth weight, heart malformations and premature delivery. In addition, high

exposure to PAHs during pregnancy or before giving birth is related to lower intelligence quotient at age 3, increased behaviour problems at age 6 and 8, as well as childhood asthma (Kim et al., 2013; Abdel-Shafy & Mansour, 2016).

2.1.10 Monitoring of PAHs in the environment

The physical and chemical properties of PAHs vary widely; therefore monitoring and measurement are often difficult and very costly. Cheaper methods and approaches have been developed to monitor and identify the existence of PAHs in the environment. Approaches such as the build-up of PAHs in biological representatives such as animals and plants (biomonitoring) are commonly used methods for monitoring PAHs. Biomonitoring has been widely used to capture the results of PAH exposure regardless of route, and it has been found to be an excellent method (Abdel-Shafy & Mansour, 2016). For instance, fish can collect PAHs, while other aquatic organisms such as oysters, mollusks and mussels can build up heavier PAHs because they are found in high concetrations in water, and they do not have the ability to efficiently metabolise all PAHs. The average levels of PAHs is higher in the tissues of mollusks than in fish musculature, since fish is capable of oxidising and metabolising PAHs into water-dissolvable compounds that are released by the living organisms (Kim *et al.*, 2013). Although biological samples can give an indication of PAH presence in the environment (in soil and water), they do not indicate the overall concentration of PAHs in polluted waters.

2.1.11 Remediation techniques of pollutants in the environment

Owing to teratogenic, carcinogenic and mutagenic effects of the PAHs in humans, their removal from the environment using various methods such as chemica, physical, and biological processes, have been studied by several researchers to protect the environment from contaminants. These approaches and techniques have been utilised, developed, and optimised to reduce the effects of the pollutants and remediate polluted sites. Biological remediation methods are effective methods for cleaning up organic pollutants, including volatile organic compounds and PAHs using plants (rhizomediation) or microorganisms (bioremediation) such as bacteria or fungi (Gitipour *et al.*, 2018). Bioremediation methods include fungal, bacterial, and biosurfactant bioremediation. Phytoremediation is the biological method of removing PAHs using plants. Roots in the plants are capable of absorbing contaminants and transporting them to other parts of the plant, where they are broken down (Mahmoudi *et al.*, 2013). Bioremediation is another biological process that uses microorganisms to reduce the concentration of contaminants in soils, and it occurs either anaerobically or aerobically (Peng *et al.*, 2018). It has been used in several countries to change contaminants into non-reactive and non-harmful substances like carbon dioxide and water. Biological techniques have been widely used due to their greater efficiency in degrading compounds with complex structures, low cost, greater safety, no secondary pollutants generation, simple operation, and the availability of microorganisms in many soils (Lawal, 2017). Despite the advantages listed above, biological methods have limitations relating to the treatment of PAH

contaminants. Bioremediation limitations include: they are effective in soils only, little information is available on the degradation pathway, and it involves longer cycles.

Previously, it was mentioned that biological techniques do not always yield the best results, especially for wastewater treatment and treatment of surface water contaminated with PAHs. The ineffectiveness of treating wastewater using biological processes is related to the fact that PAHs produced from industries are more toxic and resistant to treatment using microorganisms or plants (Abdel-Shafy & Mansour, 2016). Due to the negative impact of PAHs on aqueous solutions, physical and chemical methods have been widely used as PAH removal techniques in the aqueous environment. The problem associated with physical methods is their inability to degrade pollutants at ambient temperatures (Alegbeleye *et al.*, 2017). This method reduces the amount of PAHs in water through adsorption, filtration or volatilisation. Some of the examples of physical methods include sorption, soil washing/solvent extraction and membrane techniques. Sorption is a process where a porous solid surface is used to trap or catch contaminants together with adsorbents (Abdel-Shafy & Mansour, 2016). Adsorbents such as biochar, activated carbon, and modified clay minerals have been widely used to reduce the levels of PAHs in aqueous solutions (Chen et al., 2020). Meanwhile, solvent extraction removes PAHs from water or soil through the use of agents like methanol, dimethyl ether, acetone, and n-hexane (Chen *et al.*, 2020). Even though these solvents can extract PAHs successfully, they can contaminate the environment as well. As a result, more research needs to be conducted to find environmentally friendly solvents. Some oils, such as vegetative and peanut oil, have been identified as non-toxic and cleaner extraction solvents. As mentioned, treatment methods depend on various factors, such as solubility and the concentration of contaminant in the polluted sites. Different treatment methods are used in different polluted environments. Thus, membrane techniques are used in the treatment of aqueous environments, in which the driving force is the difference in concentration across the membrane. Membrane technologies, such as nanofiltration, microfiltration, ultrafiltration, and reverse osmosis, have been used for the removal of PAHs (Abdel-Shafy & Mansour, 2016). A disadvantage of physical methods is that they are inefficient, time consuming, and most of them are expensive. In addition, physical methods are efficient in removing some PAHs, but they do not change the chemical structure of these compounds (Kuppusamy *et al.*, 2017). Therefore, chemical methods have been used as alternative to completely remove PAHs from water or soil by breaking them down into simpler molecules. The most prominent chemical approaches used for PAH degradation are oxidation and photocatalysis. PAH photodegradation is the most widely investigated technique, and it has been proven to successfully remove most organic pollutants from water.

2.2 Photocatalysis processes

2.2.1 Introduction

This section provides detail on the mechanism of photocatalytic degradation of pollutants, the best semiconductors used as photocatalysts, factors affecting the degradation process, physicochemical characterisation techniques for semiconducting materials, methods of preparing photocatalysts, and ways of improving photocatalytic materials, as well as a brief description of PAH degradation potential photocatalyst (RGO-Bi_2MoO_6).

2.2.2 Photocatalytic degradation of organic pollutants

Photocatalytic degradation is defined as a process of breaking down contaminants using chemical reactions started by light absorption (Peng *et al.*, 2018). These reactions take place when the light absorbed by compounds excites the electrons that are within the molecules. The excitation of these electrons creates an unstable structural arrangement (Theerakarunwong & Phanichphant, 2018). As a result, the unstable structural arrangements allow chemical and physical processes to take place on the surface of the PAH compound. Photocatalysis is also a useful technique in the remedaition of organic matter such as PAHs and other organic pollutants in wastewater. Photodegradation works efficiently when pollutants are in water because, when PAHs occur in soil or the atmosphere, they bind to particles, thus allowing little photodegradation to take place (Peng et al., 2018). The process involves the chemical transformation of PAHs. In photocatalysis, a semiconductor material interacts with light of enough energy and a certain wavelength to form reactive oxidising species (ROS) (Shen *et al.*, 2020). It is important to emphasise that photocatalytic reactions occur under the action of light or photons. Different sources of light, such as ultraviolet (UV), visible, and UV- visible, have been used to study the photodegradation of PAHs. UV and visible light both come from the solar radiation spectrum. UV light emits radiation of wavelengths that range between 100-400 nm, while on the other hand, visible light has a wavelength that ranges from 400-700 nm. Some of the examples of light sources in photocatalytic reactions include low pressure, medium pressure UV lamps, and Xe arc simulating sunlight. The efficiency of light to degrade pollutants relies on the properties of the PAH to be degraded and its ability to absorb radiation at certain wavelengths. UV light has been considerably used for the degradation of organic pollutants.

Recent studies have focused on utilising visible light to degrade pollutants because it is cheaper and easier to harvest compared to UV light. Solar radiation may cause either direct or indirect photochemical reactions (Hernández-Ramírez & Medina-Ramírez, 2015). Direct photocatalytic reactions involve the photodegradation of PAHs by the direct excitation of separate molecules by light. During photocatalytic reactions, at least two events must take place at the same time in order to successfully form ROS. Generally, the first path involves the oxidation of dissociative adsorbed water by photo induced holes, and the second involves reducing dissolved oxygen (electron acceptor) by photoexcited electrons. The first and second reactions lead to the formation of hydroxyl

and superoxide radical anion, respectively. From the explanation above, it is easy to understand that photocatalytic process implies a photo-assisted generation of catalysts' active species rather than the activity of light as a catalyst. The two photoreaction paths can occur on different surfaces, if the first photoexcitation reaction takes place in the adsorbate molecule, which subsequently reacts with the lowest energy state of the catalyst substrate; the reaction is therefore called catalysed photoreaction. In contrast, if the starting photoexcitation occurs in the substrate and the excited catalyst reacts with the lowest energy state absorbance molecule, then the process is called sensitised photoreaction. In many cases, heterogeneous photocatalysis is associated with a semiconductor photocatalysis or semi-conductor-sensitised photoreactions. Heterogeneous photocatalysis is when the photocatalyst and reaction medium are not in the same phase (Laursen & Poudyal, 2015).

In photocatalysis, electrons are excited from the valance band to the conduction band by the light that has energy greater than the band gap of the semiconductor. The absorption of a photon excites an electron to the conduction (e_{CB}-) and generates a positive hole in the valence band (h_{VB}-) (Candal & Cruz, 2015) (Equation 2-1). Titanium dioxide is the most studied and used photocatalyst in the degradation of pollutants; therefore it will be used to describe the mechanism of the photodegradation of pollutants. In the case of TiO_2 (visual representation of the mechanism is shown in Figure 2-2, charge carriers can be trapped as Ti^{3+} and O^- defect site in the TiO_2 or they can recombine, releasing energy (Candal & Cruz, 2015). As an alternative, the charge carriers can move to the catalyst surface and start redox reactions with adsorbents. Positive holes can oxidise OH^- or water at the surface to generate •OH radicals (represented in Equation 2-2 and 2-3), which are tremendously powerful oxidants (Candal & Cruz, 2015). The hydroxyl radicals can then oxidise organic species with mineralisation, producing carbon dioxide, mineral salts, and water.

$$TiO_2 + h_v = h_{VB^+} + e_{CB^-}$$ Equation 2-1

$$e_{CB^-} + h_{VB^+} \rightarrow energy$$ Equation 2-2

$$H_2O + h_{VB^+} \rightarrow \bullet OH + H^+$$ Equation 2-3

$$O_2 + e_{CB^-} \rightarrow O_2\bullet^-$$ Equation 2-4

$$\bullet OH + pollutant \rightarrow\rightarrow\rightarrow H_2O + CO_2$$ Equation 2-5

$$O_2\bullet^- + H^+ \rightarrow \bullet OOH$$ Equation 2-6

$$OOH + \bullet OOH \rightarrow H_2O_2 + O_2$$ Equation 2-7

$$O_2\bullet^- + pollutant \rightarrow\rightarrow\rightarrow CO_2 + H_2O$$ Equation 2-8

$$\bullet OOH + pollutant \rightarrow CO_2 + H_2O$$ Equation 2-9

The electron in the conduction band can instantaneously get trapped by the molecular oxygen adsorbed on the titanic particle, which is lessened to generate the super oxide radical anion, $O_2^{\bullet-}$ (Equation 2-4) that may further react with H^+ to produce hydroperoxyl radical (•OOH) (Equation 2.6) and stimulate an electrochemical reduction that yields H_2O_2 (Equation 2-7). These reactive oxygen species may also play an important role in the oxidative pathways such as the degradation of the pollutant (Equation 2-8 and 2-9) (Candal & Cruz, 2015). The recombination of photogenerated charge carriers is the biggest limitation in photocatalysis, as it requires overall quantum efficiency (Theerakarunwong & Phanichphant, 2018). When recombination takes place, the excited electrons revert to the valence band without interacting with adsorbed species, emitting energy as heat or light. Recombination may take place either in the bulk or on the surface and is generally facilitated by defects, impurities or factors that introduce surface or bulk imperfection into the crystal. Different methods, such as doping photocatalysts with ions, have been reported to improve catalyst efficiency by promoting the separation of the electron-hole pair and reducing recombination.

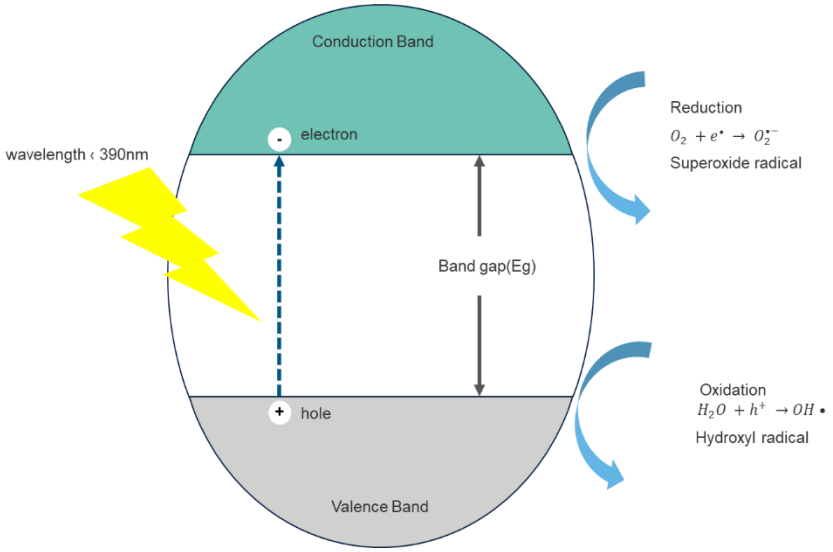

Figure 2-2: Degradation mechanism of pollutant with TiO_2

2.2.3 Factors affecting photodegradation

The photocatalytic degradation of organic contaminants is influenced by several factors, such as reaction temperature, pH, photocatalyst loading and its particle size, the initial concentration of pollutants, surface area, and oxidising agents (Gbeddy *et al.*, 2020). The effect of these parameters depend on the type of degradation process taking place; some parameters have no effect on some photocatalytic reactions, i.e. they are kept constant throughout the reaction.

2.2.3.1 pH of the solution

pH plays an important role in the effectiveness of the photocatalytic activity due to its influence on the surface-charge properties of the catalyst. Nevertheless, the interpretation of pH effects on photocatalytic activity is a difficult task. The difficulty is caused by the three possible reaction mechanisms of the degradation of pollutants that can take place, i.e. direct oxidation by positive hole,

hydroxyl radical attack, and direct reduction by the electron in the conduction band. Each mechanism depends on both the pH and substrate nature. Photocatalytic reactions taking place in acidic, neutral and alkaline conditions will not yield the same results. Differences in the pH of the solution change the charge of a photocatalyst particle and also shift the potential of catalytic reactions. pH affects the charge on the catalyst particle, the position of the conduction band and valence band, and the size of the aggregates (Kumar, 2017). Consequently, the adsorption of contaminants on a catalyst surface is altered, thereby changing the reaction rate. In summary, pH affects the degradation process in this way: the pH alters the electrical double layer of the solid electrolyte interface and consequently affects the sorption process and the separation of the photogenerated electron-hole pairs on the semiconductor surface (Kumar, 2017).

2.2.3.2 Size, surface area and structure of a photocatalyst

Surface morphology, including agglomerate size and particle size, is an important parameter to be considered in photocatalytic degradation activity because there exists a direct relationship between surface coverage of the catalyst material and organic compounds/pollutants (Kumar, 2017). Photocatalysts with a smaller particle size have higher efficiency; this is because smaller particles have a higher surface area than bigger particles. In photocatalytic reactions, a higher surface area allows for more molecules to be absorbed on a photocatalyst surface, thus increasing the degradation rate. In addition, a higher surface area has a greater number of active sites than materials with small surface area. The surface area can also be increased by suspending a photocatalyst made of fine particles either made into a porous film or in solvents. Nanostructured materials with the crystalline or grain size below 20 nm are usually the best to use as photocatalysts (Gbeddy *et al.*, 2020).

2.2.3.3 Reaction temperature

The reaction temperature has an effect on the way pollutant molecules interact with the catalyst surface. A high temperature encourages the recombination of charge carriers and discourages the adsorption of organic compounds on the surface of a photocatalyst (Qu *et al.*, 2020). Depending on the type of photocatalyst and other conditions of a reaction, a low temperature may result in the limited degradation of pollutants.

2.2.3.4 Nature and concentration of pollutants

The photocatalytic degradation process is influenced by the nature and concentration of the pollutants. Excessive concentration of contaminants in water saturate the photocatalyst surface and thus reduce the efficiency, which will eventually lead to deactivation of the photocatalyst. Generally, the efficiency of the degradation process or the rate at which pollutants are degraded decreases with the increasing quantity of the pollutant, provided the amount of the catalyst is kept constant. The explanation for this behaviour or relationship is that, as the concentration of the pollutants increases, more pollutants are adsorbed on the catalyst's surface, where fewer photons are present to reach

the catalyst surface and therefore fewer •OH radicals are generated, thus resulting in low degradation efficiency (Qu *et al.*, 2020). In addition, the chemical structures of target pollutants also influence the degradation performance of a catalyst. For instance, pollutants with complex structures take longer to degrade when compared to simple structured compounds. Photocatalytic reactions are more effective on light coloured particles than on non-transparent particles such as carbon black. If the natural form of the target pollutant in water is such that they stick to the catalyst material surface, the reaction would me more effective in degrading that particular pollutant (Qu *et al.*, 2020).

2.2.3.5 Catalyst loading

The amount of photocatalyst is directly proportional to the photocatalytic reaction rate. This can be explained on the basis that, as the amount of the catalyst increases, the number of active sites on the surface increase, thus causing an increase in the formation of •OH radicals that can take part in the actual degradation of the pollutant. However, this proportionality holds up to a certain level of photocatalyst amount. A photocatalyst can reach a saturation stage, where a light photo adsorption coefficient decreases readily, causing a reduction in the surface area of the photocatalyst exposed to irradiation (Rubio-Clemente *et al.*, 2014). This will therefore reduce the efficiency of the catalyst. It is important to note that, when a solution contains a certian amount of the photocatalyst, the solution becomes thicker and blocks the light radiation for the reaction to pass through.

2.2.4 Photocatalyst synthesis methods

There is great interest in the mass production of nanostructured photocatalytic materials that are bare or doped. This has been driven by the fact that nanostructured photocatalysts have the potential to address environmental challenges such as persistent toxic contaminants that are occupying the environment. It has been proven that preparation methods have an impact on the efficiency and physicochemical properties of photocatalysts. Depending on the end use of the product, photocatalysts may be developed in the form of fibers, powders , and thin films by different methods. These preparation methods include hydrothermal, direct oxidation, sol-gel processes, chemical vapour depositions, solvothermal, microwave, sonochemical, and electrodeposition methods (Medina-Ramírez *et al*., 2015). This section will only discuss the most popular methods. Selecting the appropriate method is important; it is also important to mention that the selection of synthesis method will depend on the cost, infrastructure available, the desired properties of the photocatalyst, as well as its application.

2.2.4.1 Sol-Gel method

The sol-gel method has become the most widely used technique for the synthesis of semiconductor photocatalysts. It is an excellent technique for synthesising metal oxides such that the material fits a particular application. Sol-gel allows for the regulation or manipulation of numerous variables such as the nature of a precursor, temperature, catalyst, pH, organic additives, time of reaction, the

amount of water added, catalyst concentration, and reagent concentration (Huang *et al.*, 2014). The main benefit for the sol-gel technique is the homogenous blending at the molecular level of metal ion, which promotes the production of polycrystalline particles with unique properties (Medina-Ramírez *et al.*, 2015). Furthermore, at some point of the preparation procedure, it is possible to integrate various types of dopants. By definition, the sol-gel process is a transformation of a precursor aqeous or non-aqeous solution into an inorganic solid through inorganic polymerisation reactions induced by water. Inorganic salts (chloride, sulphate, acetate, nitrate, etc.), alkoxides or aqueous are used as precursors. The sol-gel process follows these steps in order: (a) preparation of a homogenous solution, (b) conversion of homogenous mixture into a sol by treatment with an appropriate reagent (usually water with or without base or acid), (c) aging, (d) shaping, and (e) thermal treatment (Medina-Ramírez *et al.*, 2015). Precursors are converted to inorganic polymers made out of metal-oxide-metal (M-O-M) bonds via condensation and hydrolysis. To form a gel, further condensation takes place (Luan *et al.*, 2010). The produced gel needs to be dried at different conditions to produce different kinds of gel. When dried at hypercritical conditions, aerogels will be formed, and xerogel will form when dried at ambient conditions. Finally, the gel goes through thermal treatment in order to form the material of choice and desired forms of the material such as monosized powders, monoliths, fibers and films. Different synthesis conditions and thermal treatment temperatures yield different phases, namely rutile, anatase, or the brookie phase (Subbarao *et al.*, 2020). The sol-gel method is good because it does not require complex instrumentation and provides basic, simple processes for preparing doped nanosized particles.

2.2.4.2 Hydrothermal method

A hydrothermal reaction is referred to as any reaction with two or more phases taking place in the presence of mineralisers or aqueous solvents under high temperature and pressure conditions (Luan *et al.*, 2010). A hydrothermal reaction for the synthesis of photocatalysts commonly takes place in the steel pressure vessels known as autoclaves, with or without teflon liners inside, under controlled pressure and/or temperature, with the reaction in an aqueous solution (Gan *et al.*, 2020). The reaction temperature can be elevated such that it exceeds 100℃ (b.p. of water) and reaches the pressure of vapour saturation. The quantity of solution added in the autoclave and the operating temperature determine the internal pressure produced. If the autoclave is filled completely with solution and the temperature is too high, an explosion could occur. There are certain parameters that need to be considered when choosing a suitable autoclave; these include experimental pressure and temperature, resistance to corrosion at that particular pressure, and temperature range in a given solvent (Wang, 2020). In the event that the synthesis process is directly occuring in the autoclave, then corrosion resistance is the primary factor in selecting a vessel material. Hydrothermal reactions require materials that are resistant to corrosion and are alloys with high strength such as cobalt-based super alloys, austenitic stainless steel, nickel, iron, and titanium, together with alloys (Gan *et al.*, 2020). In hydrothermal methods, factors such as precursor type, reaction temperature

and duration, post-treatment (acid washing and calcination), and auxiliary methods influence the structure and shape of the particle.

2.2.4.3 Solvothermal technique

Solvothermal is basically derived from a hydrothermal method where the solvent is not an aqueous phase. Unlike the hydrothermal method, the reaction temperature in the solvothermal method can be increased to much higher levels because of the different solvents with a high boiling point that can be selected (Demazeau, 2014). Furthermore, in the solvothermal method, properties such as distribution, shape, crystallinity and particle size can be controlled better than in the hydrothermal technique. This technique has been found to be convenient in the development of a variety of materials with dispersity and narrow size distribution. Involving high pressure in the solvothermal reaction changes the physico-chemical behaviour properties of the solvent (Sam & John, 2020). As a result, using this method allows for the production of compounds, which cannot be achieved at standard conditions of temperature and pressure (Nunes *et al.*, 2019). Therefore, this method will be useful in a case where a certain photocatalyst needs to be modified to have a response in the visible region of the spectra.

2.2.4.4 Sonochemical method

This method involves the use of ultrasound potential in the synthesis of photocatalytic materials. Ultrasound techniques have been successfully applied in the preparations of a broad range of nanostructured materials, such as high surface area alloys, carbides, transition metals, colloids and oxides (Medina-Ramírez *et al*., 2015). When ultrasound is applied under some clearly specified conditions, it allows for the synthesis of nanocomposite materials in a shorter reaction time under moderate conditions, in the presence of air, and without heating to extremely high temperatures. The uniqueness of the sonochemical technique is the source that drives chemical reactions without extreme conditions (Jameel *et al*., 2020). It is one of the methods that represent an economical alternative way for saving energy in the process of synthesising nanoparticles.

2.2.4.5 Microwave method

The microwave (MW) method can be defined as a hydrothermal method assisted with radiation (Hoseinzadeh Hesas *et al.*, 2013). This method has been widely used in the production of several inorganic materials. Microwave radiation is used as a mechanism of activating energy to encourage chemical reactions to take place. Microwave aided chemical reactions rely highly on the ability of the reaction mixture to absorb MW energy, and this usually depends on the type of solvents selected for the reaction (Hoseinzadeh Hesas *et al.*, 2013 Medina-Ramírez *et al.*, 2015). Microwave methods have benefits such as energy and time saving, reaction temperature can be quickly raised and kept uniform for the duration of the reaction, various crystalline phases can be produced, and the kinetics of crystallisation is increased by one to two orders of magnitude compared to conventional methods.

2.2.5 Improving efficiency of photocatalytic materials

A wide range of photocatalysts have been created and have been seen as acceptable materials for the degradation of most contaminants. However, most of these photocatalysts have the disadvantages of inefficient charge separation and restricted range of light absorption, which prompt a high recombination process. It is because of this that various techniques have been explored or proposed to improve the capacity of catalysts to work in different conditions. Various endeavours have been made for the synthesis of new photocatalysts that can retain visible light with high catalytic activity. Oxides, for example, $InVO_4$, $BiVO_4$, $CaIn_2O_4$ and Bi_2MoO_6, are able to participate in visible-light driven catalytic reactions (Candal & Cruz, 2015). Alteration of photocatalysts to improve effectiveness can be accomplished through: doping with transition metals and non-metals, sensitisation, incorporation of two or more nanocrystalline semiconductors (coupling), and control of composition and particle size. The choice of modification method then relies on the photocatalyst to be improved and achieve the properties desired.

2.2.5.1 Ion-doped semiconductors

Doping semiconductors with transition metals and use as photocatalysts have been encouraged for the purpose of improving the physical properties of the semiconductor, i.e. the utilisation of transition metals narrows the energy band gap of the material (Ayodhya & Veerabhadram, 2018). This circumstance prompts the production of material with better photocatalytic activity. In fact, this application exploits the energy that is sourced from the visible light range of the solar spectrum. The development of semiconductor oxides doped with ions is simple, less expensive, and forms a large amount of material (Candal & Cruz, 2015). It has been demonstrated that doped semiconductors have a performance superior to pure semiconductors. The following materials have been doped with transition metals and demonstrated better performance: ZnO doped with Ce, HO, La^{3+}, Sm^{3+},WO_3 doped with mg^{2+}, Al^{3+},Fe^{3+}, Bi_2O_3 doped with Nb.

2.2.5.2 Non-metal doped materials

There are quite a number of semiconductors with the potential to be used in photocatalysis, such as ZnO, Ta_2O_5 and Nb_2O_5, which have the ability to allow visible light to pass through and are only activated with UV light. On the other hand, coloured semiconductors such as WO_3, Bi_2O_6 and $BiVO_4$ do not have enough range of light for activation as a photocatalyst (Candal & Cruz, 2015). In this manner, it is important to improve semiconductors with potential in photocatalysis application. Non-metal materials represent an alternative to improve photocatalytic efficiency for all these semiconductors, more particularly under visible light illumination. Non-metal materials, such as N, S, F, B and GO, have been utilised as dopants for most semiconductors (Karthikeyan *et al.*, 2020).

2.2.5.3 Dye-sensitised semiconductors

Most of the oxides' photocatalytic activities have been significantly improved by photocatalyst sensitisation in order to broaden the range in the solar spectrum, where it is able to assimilate light. This has encouraged the utilisation of semiconductor / organic-dye materials during wastewater treatment via photosensitisation mechanisms to tackle environmental issues. Photosensitisation in the degradation of pollutants is a process in which radiation energises electrons from the valence band, and then it is transferred to the conduction band of semiconductor oxide (Zhang *et al.*, 2019). Different types of substances have been suggested as powerful photosensitisers of a semiconductor. Many of these substances belong to the groups of inorganic sensitisers, dyes that contain carbon, and with complicated molecular structures and coordination metal complexes. Sensitisation can help decrease the band energy gap of semiconductors with poor photocatalytic activity (Candal & Cruz, 2015).

2.2.5.4 Coupled semiconductors

The incorporation of more than one nanocrystalline semiconductor improves the design of a photocatalyst. The primary aim of coupling semiconductors is to improve the photoresponse by associating a semiconductor with an enormous band gap with one that has a small band gap, and to further delay the recombination process of photogenerated charge carriers by infusing electrons in the conduction band of the semiconductor with a larger band gap (Candal & Cruz, 2015). There are two principal arrangements for associating two or more semiconductors, namely coupled and capped semiconductor heterostructure (Candal & Cruz, 2015). In coupled semiconductor systems, the particles are arranged in such a way that they are in close contact with one another, while the electrons and holes are always accessible for reduction or oxidation activities on the surface of various particles. In capped semiconductor systems, a charge amendment occurs, andonly one of the charge carriers can be reached at the surface, while the other charge carriers are caught inside the inner semiconductor (Akerdi & Bahrami, 2019). Coupling semiconductors with a large band gap and semiconductors with a small band gap allow for hole-electron separation without using a shorter wavelength, i.e. without using only UV light. Examples of some coupled semiconductor photocatalysts are: Sn/TiO_2, ZnO/SnO_2, and CdS/TiO_2. Each coupled material will yield a different enhanced photocatalytic activity.

2.2.5.5 Nanostructured semiconductors

The development of nanostructured photocatalysts provides materials with higher ratios of surface to volume with maintained bulk material physical properties (Bisquert *et al*., 2008). Methods including hydrothermal, sonochemical, microwave, coprecipitation and sol-gel have been effectively utilised in the development of nanostructured photocatalysts. The small sizes of particles of nanostructured photocatalysts reduce the pathway between the generation site of the electron-hole pair and the surface of the catalyst (Candal & Cruz, 2015). Nanostructured materials come with a bigger surface

area, which is desirable in photocatalysts on the grounds that it increases the mass of active surface sites where a contaminant can be attached to go through decomposition.

2.2.6 Photocatalyst characterisation techniques

There are wide ranges of analytical methods used to acquire physicochemical properties of photocatalytic materials readied as powders or meagre films. Physico-chemical properties of catalysts include composition, surface area, particle size and electronic properties. Different techniques are used to analyse for different properties. A photocatalyst can be analysed for its elemental compositions, surface area, topography, structure porosity, optical properties and vibrational properties (Bizarro & Rodil, 2015). This section will discuss in detail the most common techniques utilised in the analysis of the above-mentioned properties.

2.2.6.1 Elemental analysis

Analytical methods used for the purpose of measuring compositions or elements present in a photocatalyst can be characterised by the type of the test or probe used to analyse the material. Some techniques make use of ion, electrons or photons. Only the most common techniques will be discussed in detail. For elemental composition properties, X-ray photoelectron spectroscopy is the most notable technique and it will therefore be discussed in detail.

2.2.6.1.1 X-ray Photoelectron Spectroscopy, XPS

XPS, which is also commonly known as electron spectroscopy for chemical analysis (ESCA), is one of the techniques used for elemental composition analysis, and it uses photons to play the role of an incident beam. The photoelectric effect defined by Einstein was used as a phenomenon for photoelectron spectroscopy; in the phenomenon, the theory of the photon is applied to describe the discharge of electrons from the surface if the material when it is bombarded by the photons (Bizarro & Rodil, 2015). For XPS, Mg-kα (1253, 6 eV) or Al-kα (1486, 6 eV) cathodes provide photon energies as fundamental emissions. It should be noted that kα represents an energy produced by transmissions from n=2 and n=1 levels (n is the number of orbitals). The XPS technique does not work on all surfaces; it is surface-dependent because of the limited inelastic mean free path of the photoelectrons that are excited from the surface of the solid (Bizarro & Rodil, 2015). The energies of the photoelectrons departing the sample represent the characteristic of each element present in the sample. Each peak area indicates the number of atoms available in the material being analysed. In this technique, small changes can be made to binding energy and the shape of the peak, and by the emitting the chemical site of the atoms. As a result, XPS can give chemical bonding information as well. The binding energy of the discharged photoelectron is determined by using the following equation.

$$BE = h_v - KE - \emptyset \qquad \text{Equation 2-10}$$

Where (KE) is the kinetic energy of a photoelectron, (h_v) the incident photon energy, and (Ø) is the work function, which for each piece of equipment needs to be well defined (Sakamoto *et al.*, 2020). The analysis of the XPS spectrum allows for the determination of surface elemental composition through making a comparison between two materials, or through the use of XPS databases. The XPS analysis has a depth of about 1-10 nm, but the depth is highly dependent on the angle of collection, the kinetic energy of the electrons leaving the beam, and incidence energy of the photons. In XPS, samples to be analysed have to be assessed or analysed in dry conditions at all times; because this technique needs UHV conditions, the pressure range must be between 10^{-8} to 10^{-10} mbar. Some techniques are destructive and some non-destructive; XPS is a non-destructive technique.

2.2.6.2 Structure and topography

The photocatalytic reaction of a catalyst or semiconductor materials in general depends mainly on the intrinsic properties of the material, such as crystalline structure and the composition. Therefore, it is very important to know and identify the mixture of phases and the crystalline phase that are active in the photocatalytic material. The most common techniques used in the identification of crystalline phases in photocatalyst materials are transmission electron microscopy (TEM) and x-ray diffraction (XRD) (Bizarro & Rodil, 2015). Surface morphology or topography can be identified using both non-contacting and contacting methods. The most commonly used technique is the non-contacting method known as scanning electron microscopy (SEM).

2.2.6.2.1 X-ray Powder Diffraction

X-ray diffraction essentially measures the intensity of x-ray scatters from crystals. When waves are scattered at atoms at various positions, they will always arrive at the detector with a shift in the phase, forming destructive and constructive interference patterns, depending on the atomic position and angle. The easiest way to access structural information in the crystals is through the use of the Braggs equation (Drabavičius *et al.*, 2020) (Equation 2-11), which describes the XRD principle in terms of reflection of x-rays using sets of lattice planes. In the Braggs equation, (n) represents the sequence of diffraction, and it equates to the number of wavelengths in the path difference between rays that are scattered by the planes close to each other, (λ) represents the initial photon's wavelength, (θ) is the diffraction angle, and (d) is the interplanar distance. Lattice planes are called crystallographic planes made up of three indices (hkl).

$$n\lambda = 2dsin\theta \qquad \text{Equation 2-11}$$

Parallel planes always have the same indices and are equally distributed, separated by d_{hkl}. When the x-ray penetrates a material, several reflections occur at a thousand parallel planes. Finite crystalline size produces the Braggs peak of finite width. The Scherrer Equation (Equation 2-12) is used to estimate the Braggs peak finite width (Bizarro & Rodil, 2015). The (k) in the Scherrer

Equation relies on the shape of grain for for cubic-shaped grains k= 0.94 and ideal squares k= 0.89. The XRD analysis method is a non-destructive tool used for the identification of the crystalline sample phase (Bizarro & Rodil, 2015). Unlike other methods for elemental composition analysis, XRD technique does not provide elemental composition, but is able to distinguish different packing alternatives of the same set of elements. In other words, XRD can be used to determine the crystalline arrangement of elemental atoms in which they are disposed. The tetragonal structure (anatase and rutile) and orthorhombic structure (brookite) are structures that can be identified by XRD analysis.

$$L_{hkl} = \frac{K\lambda}{\beta_{hkl} cos\theta} \qquad \textit{Equation 2-12}$$

2.2.6.2.2 Transmission Electron Microscopy

TEM is a method that is used to extract and analyse the microstructure of materials with atomic scale; this technique utilises an electron beam with very high energy that penetrates a very slim sample (Bizarro & Rodil, 2015). TEM is a method that is based on the electron to electron interaction method; the incident electrons are moved at high voltages (100-1000 kV) to a velocity nearing the speed of light (Bizarro & Rodil, 2015). TEM consists of three modes. The imaging mode involves converting electron density to light-optical images (Falsafi *et al*., 2020). This mode allows for the determination of structure at the atomic level. The second is the diffraction mode, which allows for direct monitoring of the crystalline structure, and line and planar defects. Thirdly, in the microdiffraction mode, the incident electron beam is fixated to acquire the diffraction patterns from very tiny particles. This mode enables the identification of crystalline nanoparticles. Information that can be obtained from high-resolution TEM includes structure (shape) of materials, crystal interplanar spacing, and the structure (Bizarro & Rodil, 2015). The disadvantage of using TEM is that it requires the preparation of samples prior to analysis because a sample needs to be sufficiently slim to permit the transference of electrons with the least inelastic scattering. As a result, ion beam techniques are normally required before TEM analysis.

2.2.6.2.3 Scanning Electron Microscopy

Scanning electron microscopy is a non-contacting technique for determining morphological properties of a material (Kwiecinska, 1981). In SEM, an electron beam existing in the energy zone of 0.20 - 40 keV is fixated on the surface of the sample to make a spot with a size of about 0.4-5 nm, which is then scanned forming a two-dimensional image of the samples (Bizarro & Rodil, 2015). The secondary electron released by the conduction and valence bands, which has an intensity proportional to the morphology or surface topography, then forms an image. The contrast variations generated by the released electrons at various heights forms a 3D appearance in the image (Bizarro & Rodil, 2015). The SEM technique can yield information about both topography and composition if

the images are formed by elastically scattered electrons. The images obtained from SEM are no different from standard optical microscopes, except that SEM images have bigger depth of focus and therefore give an impression of a 3D image.

2.2.6.3 Porosity and surface

Porosity and surface area are also important parameters in photocatalytic materials. The standard method to determine surface area and porosity properties includes direct observation by electronic microscopy or optical, mercury porosimetry, gas adsorption and neutrons (SANS), or angle scattering x-rays (SAXS) (Bizarro & Rodil, 2015). Light dispersion techniques can be used to indirectly determine the surface area. The most commonly used technique for determining surface area and porosity is gas adsorption. This method involvesthe adsorption of non-reacting gas, mostly nitrogen, on the surface of a solid material. Gas adsorption takes place on the exterior surface of solid materials, and in the case of porous material, it occurs on the surface of pores (Bizarro & Rodil, 2015). This technique allows for the determination of the specific surface area (SSA). The most popular method for SSA determination is Brunauer, Emmett, and Teller (BET).

2.2.6.3.1 Brunauer, Emmett, and Teller

The BET method provides a precise SSA assessment by nitrogen multilayer adsorption, which is measured as a function of relative pressure using an analyser that is fully automated (Hidayu *et al.*, 2013). The development of gaseous molecules on the surface is utilised to find the SSA, while the principle of capillary condensation is used to evaluate the presence of pores, pore size distribution and pore volume (Bizarro & Rodil, 2015). This technique uses the combination of external and the area of the pores to find the total SSA in $m^2 g^{-1}$.

2.2.6.4 Vibrational spectroscopies

Vibrational spectroscopies are non-invasive and non-destructive tools that characterise material and provide data on the molecular composition and structure of the material. There are two analytical techniques that are used for vibrational properties, namely Infrared and Raman spectroscopy. These two methods measure vibrational energy levels that are linked to the chemical bonds in the sample (Bizarro & Rodil, 2015). The spectrum for this technique is unique. Hence, vibrational spectroscopies are used to characterise, identify, and monitor reactions and control the quality of the material. The Fourier transform infrared spectroscopy (FTIR) is the most popular to perform the above analysis.

2.2.6.4.1 Fourier Transform Infrared spectroscopy, FTIR

Infrared spectroscopy is a characterisation tool that is based on detecting the vibration of atoms found in a molecule by measuring how much the sample absorbs electromagnetic light (Bizarro & Rodil, 2015). It is useful in the determination of chemical bonds existing in the sample; therefore this method can confirm a certain structure. The infrared spectrum is usually attained by taking a sample and infrared radiation through it; this process is called transmission as well as finding the energy that

is adequate to absorb light. The IR energy ranging between 0.7 μm and 1 mm corresponds with energies required to stimulate fundamental modes of vibration and rotation in materials (Bizarro & Rodil, 2015). This explains why the incident IR signal absorption is a result of the excitation between excited vibrational and ground states. The reflection spectra display the definite vibrational nodes characteristic of each molecular structure and the mass of the atoms. IR spectroscopy is a non-destructive method that can be used in any type of sample (Dendisová *et al.*, 2018). It can be used in gaseous, liquid, solid, powder and fiber samples. It is very sensitive to the surface area and can sense a very tiny amount of particles, such as 10^{-5} monolayers.

2.2.6.5 Optical Properties

2.2.6.5.1 Photoluminescence spectroscopy

Photoluminescence(PL) spectroscopy is a method that provides data about the electronic structure from the excitation of light, and it examines the change between the state of very high energy (excited state) and the ground state (Bizarro & Rodil, 2015). The photo emission coming from this technique of analysis is usually estimated as fluorescence. When electrons in the conduction band and holes existing in the valence band recombine, fluorescence occurs; hence it is significant in the study of photocatalysts. This analytical technology can provide direct information about the kinetics of electron transfer during photocatalysis. The intensity in the PL spectrum can be used to make a comparison among combination rates for various photocatalytic systems, approximate the band gap via the band to band transitions, and detect faults and impurities in the sample (Bizarro & Rodil, 2015).

2.2.7 Photocatalytic materials for degradation

There are different forms of photocatalytic material, namely metal oxides, chalcogenides, ternary and quaternary materials. Among all the photocatalytic materials, simple binary metal oxides have been studied and used the most. Titanium oxide is mainly used in investigated metal oxide photocatalysts because of its water insolubility, nontoxicity, low cost, corrosion resistance, and stability (Hernández-Ramírez & Medina-Ramírez, 2015). Zinc oxide is also the most used metal oxide photocatalyst after TiO_2, owing to its excellent photochemical and optoelectronic catalytic properties, together with its non-toxic nature and lower cost (Hernández-Ramírez & Medina-Ramírez, 2015). A disadvantage of using TiO_2 is that it is only limited to UV light due to its wide band gap. ZnO has been found to have higher photocatalytic efficiency than TiO_2 because of its narrower band gap; however, its application is limited, since it is not resistant to corrosion and susceptible to dissolution at acidic conditions (Peng *et al.*, 2018). Other than metal oxides, chalcogenides are another example of semiconductor materials that have been widely investigated regarding their photoactivity; some examples include CdS and ZnS.

Chalcogenides have a low band gap energy, which takes advantage of solar energy (Hernández-Ramírez & Medina-Ramírez, 2015). Nevertheless, most chalcogenides experience challenges in terms of photo corrosion, toxicity in aqueous media, and their inability to oxidise water. Ternary and quaternary semiconductors are materials that are made up of two and three binary compounds, respectively. Ternary and quaternary semiconductors have been discovered to be good photocatalytic material that can be turned on with visible radiation. Ternary compounds such as bismutate, ferrites, vandates, niobates and molybdates, as well as quaternary (oxides, oxynitrides, oxysulfides and oxyhalides) are being progressively studied and prepared for photocatalytic application in both doped and pristine form due to their very high photocatalytic efficiency in the degradation of pollutants in water (Hernández-Ramírez & Medina-Ramírez, 2015). The properties of these semiconductors can be improved by doping them with non-metal materials. Ternary semiconductors are more common than quaternary materials; as a result, ternary materials will be discussed in detail, using Bi_2MoO_6 doped with graphene oxide (RGO) as an example.

Ternary mixtures, for example bismutate, ferrites, vandates, niobates, and molybdates, just as quaternary (oxides, oxynitrides, oxysulfides, and oxyhalides), are in effect progressively ready and arranged for photocatalytic application in both doped and immaculate structure, owing to their high photocatalytic productivity in the removal of toxins from water.

2.2.7.1 RGO-Bi_2MoO_6

Recently, a great focus has been placed on the synthesis of bismuth compounds (e.g. Bi_2MoO_6, $BiFeO_3$, Bi_2S_2, $BiWO_6$ and BiOBr), which have the potential of degrading organic pollutants under visible radiation (Hernández-Ramírez & Medina-Ramírez, 2015). Among various bismuth compounds, bismuth molybdate has been proven as able to participate in photocatalytic activities driven by visible light. A general chemical formula of bismuth molybdate is $Bi_2O_3.nMoO_3$, where n is equal to 1, 2 or 3, which corresponds to γ-Bi_2MoO_6, β-$Bi_2Mo_2O_9$ and α-$Bi_2Mo_3O_{12}$. Among the above three bismuth molybdate compounds, γ-Bi_2MoO_6 has been discovered to be an effective photocatalyst for water splitting, photodegradation of organic pollutants and carbon dioxide reduction under visible light irradiation (Bai *et al.*, 2017).

Bi_2MoO_6 is the simplest member of aurivillius oxide family, which is made up of $[Bi_2O_2]^{2+}$ layers combining with a corner-sharing structure of MoO_6 octahedral (Chen *et al.*, 2015). Some of its advantages include narrow band gap (2.5 – 2.8 eV) n-type semiconductor, low cost, corrosion resistance, non-toxicity and visible light response that extends to 500 nm. In addition, not only is this material used as a photocatalyst, it has applications such as super capacitors or energy storage devices (Kasinathan *et al.*, 2020). Bi_2MoO_6 may appear in different structures or morphologies, depending on the method of synthesis. Possible Bi_2MoO_6 morphologies include nanoparticles, nanosheets /nanoplates, hollow sphere, microtubes, microspheres, etc. (Shetty *et al.*, 2019; Wang *et al.*, 2016). Despite the advantages mentioned above, photocatalytic efficiency of Bi_2MoO_6 in the

degradation of contaminants is restricted by the rapid recombination rate of photogenerated holes and electrons.

Therefore, to overcome these challenges, some technological solutions have been developed to improve the photocatalytic activity of Bi_2MoO_6 and discourage the recombination of photogenerated carriers to increase the quantum yield of these materials. Technologies that have been developed include catalyst coupling (e.g NiO/TiO_2 andCu_2O/Bi_2MoO_6), doping with a precious metal, such as Ag and Pd, and synthesising composites that are carbon based, like reduced graphene oxide (RGO), carbon nanotubes, graphitic nitrite, carbon fiber, quantum dots, etc. (Singh *et al.*, 2020). Among these materials, graphene has attracted great interest due to its exceptional properties such as extremely high specific surface area (2630 m^2/g), structure flexibility, thermal flexibility, two-dimensional sp2 hybridised carbon structure, and excellent mechanical flexibility. These distinctive physicochemical properties indicate that graphene has high potential for yielding new methods and powerful improvements in the field of photocatalysis. Graphene is a two-dimensional thin material with zero band gap and possesses a higher surface area compared to other carbonaceous materials such as activated carbon (Xiao *et al.*, 2018). Graphene is utilised as reduced-graphene oxide (RGO), which is basically a derivation of graphene, retaining its remarkable properties (Singh *et al.*, 2020). RGO is the most recently discovered support of Bi_2MoO_6 and can be easily produced from graphite, which is cheaper and naturally sufficient (Wang *et al.*, 2012). The high surface area in graphene improves interfacial interactions with other inorganic/organic compounds and also disfavours the aggregation of metal oxides immobilised on its surface (Wang *et al.*, 2016). Graphene-based nanocomposites such as RGO-Bi_2MoO_6 have advantages such as good water dispersion and easy functionalisation by chemical reactions. Moreover, graphene-based nano-composites are weak oxidants and therefore not expected to produce disinfection by-products (DBPs) (Yang *et al.*, 2015). When RGO is incorporated in Bi_2MoO_6, it limits restacking, reduces aggregation, provides mechanical strength, increases surface area, supports material, inhibits electron scavengers, corrosion and leaching, and acts as a photosensitiser (Zhang *et al.*, 2013).

References

Abdel-Shafy, H.I. & Mansour, M.S.M. 2016. A review on polycyclic aromatic hydrocarbons: Source, environmental impact, effect on human health and remediation. *Egyptian Journal of Petroleum,* 25(1):107-123.

Akerdi, A.G. & Bahrami, S.H. 2019. Application of heterogeneous nano-semiconductors for photocatalytic advanced oxidation of organic compounds: A review. *Journal of Environmental Chemical Engineering*, 7(5):103283.

Alegbeleye, O.O., Opeolu, B.O. & Jackson, V.A. 2017. Polycyclic Aromatic Hydrocarbons: A Critical Review of Environmental Occurrence and Bioremediation. *Environmental Management*, 60(4):758-783.

Ayodhya, D. & Veerabhadram, G. 2018. A review on recent advances in photodegradation of dyes using doped and heterojunction based semiconductor metal sulfide nanostructures for environmental protection. *Materials Today Energy*, 9:83-113.

Bai, J., Li, Y., Li, X. & Liu, L. 2017. Facile preparation of 2D Bi_2MoO_6 nanosheets–RGO composites with enhanced photocatalytic activity. *New Journal of Chemistry*, 41(15):7783-7790.

Bisquert, J., Fabregat-Santiago, F., Mora-Seró, I., Garcia-Belmonte, G., Barea, E.M. & Palomares, E. 2008. A review of recent results on electrochemical determination of the density of electronic states of nanostructured metal-oxide semiconductors and organic hole conductors. *Inorganica Chimica Acta*, 361(3):684-698.

Bizarro, M. & Rodil, S. 2015. Physicochemical Characterization of Photocatalytic Materials. 103-153.

Candal, R. & Cruz, A.M.-d.l. 2015. New Visible-Light Active Semiconductors. In Hernández-Ramírez, A. & Medina-Ramírez, I., eds. Photocatalytic Semiconductors: Synthesis, Characterization, and Environmental Applications. Cham: Springer International Publishing. 41-67.

Chen, C.-F., Ju, Y.-R., Su, Y.-C., Lim, Y.C., Kao, C.-M., Chen, C.-W. & Dong, C.-D. 2020. Distribution, sources, and behavior of PAHs in estuarine water systems exemplified by Salt River, Taiwan. *Marine Pollution Bulletin*, 154:111029.

Chen, X., Yang, L., Myneni, S.C.B. & Deng, Y. 2019. Leaching of polycyclic aromatic hydrocarbons (PAHs) from sewage sludge-derived biochar. *Chemical Engineering Journal*, 373:840-845.

Chen, Y., Tian, G., Shi, Y., Xiao, Y. & Fu, H. 2015. Hierarchical MoS2/Bi2MoO6 composites with synergistic effect for enhanced visible photocatalytic activity. Applied Catalysis B: *Environmental*, 164:40-47.

Demazeau, G., 2014. Solvothermal Processes: Definition, Key Factors Governing. Zeitschrift für Naturforschung B, 65:999 – 1006.

Dendisová, M., Jeništová, A., Parchaňská-Kokaislová, A., Matějka, P., Prokopec, V. & Švecová, M. 2018. The use of infrared spectroscopic techniques to characterize nanomaterials and nanostructures: A review. *Analytica Chimica Acta*, 1031:1-14.

Dobaradaran, S., Schmidt, T.C., Lorenzo-Parodi, N., Kaziur-Cegla, W., Jochmann, M.A., Nabipour, I., Lutze, H.V. & Telgheder, U. 2020. Polycyclic aromatic hydrocarbons (PAHs) leachates from cigarette butts into water. *Environmental Pollution*, 259:113916.

Drabavičius, A., Naujokaitis, A., Stalnionis, G., Giraitis, R., Mockus, Z., Kanapeckaitė, S., Kalinauskas, P., Nedzinskas, R., Niaura, G. & Juškėnas, R. 2020. Photoelectrochemical, Raman spectroscopy, XRD and photoluminescence study of disorder in electrochemically deposited kesterite thin film. *Journal of Alloys and Compounds*, 824:153853.

Falsafi, S.R., Rostamabadi, H., Assadpour, E. & Jafari, S.M. 2020. Morphology and microstructural analysis of bioactive-loaded micro/nanocarriers via microscopy techniques; CLSM/SEM/TEM/AFM. *Advances in Colloid and Interface Science*, 280:102166.

Fosso-Kankeu, E. 2019. Coal tar production processes and potential of PAHs release into the environment. 17th Johannesburg International Conference on Science, Engineering, Technology and Waste Management (SETWM-19) At: Johannesburg, South Africa

Gan, Y. X. et al., 2020. Hydrothermal Synthesis of Nanomaterials. *Hindawi Journal of Nanomaterials*,2020:1-3

Gbeddy, G., Goonetilleke, A., Ayoko, G.A. & Egodawatta, P. 2020. Transformation and degradation of polycyclic aromatic hydrocarbons (PAHs) in urban road surfaces: Influential factors, implications and recommendations. *Environmental Pollution*, 257:113510.

Gitipour, S., Sorial, G.A., Ghasemi, S. & Bazyari, M. 2018. Treatment technologies for PAH-contaminated sites: a critical review. *Environ Monit Assess*, 190(9):546.

Guo, X., Tang, Y., Eble, C.F., Wang, Y. & Li, P. 2020. Study on petrographic characteristics of devolatilization char/coke related to coal rank and coal maceral. *International Journal of Coal Geology*, 227:103504.

Hernández-Ramírez, A. & Medina-Ramírez, I. 2015. Semiconducting Materials. (In Hernández-Ramírez, A. & Medina-Ramírez, I., eds. Photocatalytic Semiconductors: Synthesis, Characterization, and Environmental Applications. Cham: Springer International Publishing. 1-40.

Hidayu, A.R., Mohamad, N.F., Matali, S. & Sharifah, A.S.A.K. 2013. Characterization of Activated Carbon Prepared from Oil Palm Empty Fruit Bunch Using BET and FT-IR Techniques. *Procedia Engineering*, 68:379-384.

Hoseinzadeh Hesas, R., Wan Daud, W.M.A., Sahu, J.N. & Arami-Niya, A. 2013. The effects of a microwave heating method on the production of activated carbon from agricultural waste: A review. *Journal of Analytical and Applied Pyrolysis*, 100:1-11.

Huang, Y., Sui, Q., Lyu, S., Wang, J., Huang, S., Zhao, W., Wang, B., Xu, D., Kong, M., Zhang, Y. & Yu, G. 2020. Tracking emission sources of PAHs in a region with pollution-intensive industries, Taihu Basin: From potential pollution sources to surface water. *Environmental Pollution*, 264:114674.

Jameel, M.S., Aziz, A.A. & Dheyab, M.A. 2020. Comparative analysis of platinum nanoparticles synthesized using sonochemical-assisted and conventional green methods. *Nano-Structures & Nano-Objects*, 23:100484.

Karthikeyan, C., Arunachalam, P., Ramachandran, K., Al-Mayouf, A.M. & Karuppuchamy, S. 2020. Recent advances in semiconductor metal oxides with enhanced methods for solar photocatalytic applications. *Journal of Alloys and Compounds*, 828:154281.

Kasinathan, M., Thiripuranthagan, S., Sivakumar, A., Ranganathan, S., Vembuli, T., Kumaravel, S. & Erusappan, E. 2020. Fabrication of novel Bi2MoO6/N-RGO catalyst for the efficient photocatalytic degradation of harmful dyes. *Materials Research Bulletin*, 125:110782.

Kim, K.-H., Jahan, S.A., Kabir, E. & Brown, R.J.C. 2013. A review of airborne polycyclic aromatic hydrocarbons (PAHs) and their human health effects. *Environment International*, 60:71-80.

Kumar, A. 2017. A Review on the Factors Affecting the Photocatalytic Degradation of Hazardous Materials. *Material Science & Engineering International Journal*, 1(3):106-114..

Kuppusamy, S., Thavamani, P., Venkateswarlu, K., Lee, Y.B., Naidu, R. & Megharaj, M. 2017. Remediation approaches for polycyclic aromatic hydrocarbons (PAHs) contaminated soils: Technological constraints, emerging trends and future directions. *Chemosphere*, 168:944-968.

Kwiecinska, B.K. 1981. Scanning electron microscopy, Volume 1978-I: An international review of advances in instrumentation. Techniques, theory and physical applications of the scanning electron microscope. Volume 1979-I: An international review of advances in techniques and applications of the SEM. Volume 1979-II: An international review of advances in techniques and applications of the SEM, volume 1980-I: An international journal of SEM, related techniques and applications: All four volumes edited by O. Johari. Published by Scanning Electron Microscopy Inc., Ill., U.S.A. Vol. 1978-I, xiv + 898 pp.; Vol. 179-I, x + 598 pp.; Vol. 1979:II, xvii + 910 pp.; Vol. 1980-I; xiv + 608 pp. *International Journal of Coal Geology*, 1(2):169-171.

Laursen, S. & Poudyal, S. 2015. Chapter 8 - Photo- and Electro-Catalysis: CO_2 Mitigation Technologies. In Shi, F. & Morreale, B., eds. Novel Materials for Carbon Dioxide Mitigation Technology. Amsterdam: Elsevier. p. 233-268.

Lawal, A.T. 2017. Polycyclic aromatic hydrocarbons. A review. *Cogent Environmental Science*, 3(1):1339841.

Luan, J. et al., 2010. Research on Different Preparation Methods of New Photocatalysts. Current Organic Chemistry, 683-698.

Mahmoudi, N., Slater, G.F. & Juhasz, A.L. 2013. Assessing Limitations for PAH Biodegradation in Long-Term Contaminated Soils Using Bioaccessibility Assays. *Water, Air, & Soil Pollution*, 224(2):1411.

Medina-Ramírez, I., Hernández-Ramírez, A. & Maya-Treviño, M.L. 2015. Synthesis Methods for Photocatalytic Materials. In Hernández-Ramírez, A. & Medina-Ramírez, I., eds. Photocatalytic Semiconductors: Synthesis, Characterization, and Environmental Applications. Cham: Springer International Publishing. p. 69-102.

Nunes, D. et al., 2019. Synthesis, design, and morphology of metal oxide nanostructures. *Metal Oxide Nanostructures*, 1:21-57.

Peng, X., Xu, P.F., Du, H., Tang, Y., Meng, Y., Yuan, L. & Sheng, L.P. 2018. Degradation of polycyclic aromatic hydrocarbons: A review. *Applied Ecology and Environmental Research*, 16:6419-6440.

Qiu, Y.-Y., Gong, Y.-X. & Ni, H.-G. 2019. Contribution of soil erosion to PAHs in surface water in China. *Science of the Total Environment*, 686:497-504.

Qu, Y., Gong, Y., Ma, J., Wei, H., Liu, Q., Liu, L., Wu, H., Yang, S. & Chen, Y. 2020. Potential sources, influencing factors, and health risks of polycyclic aromatic hydrocarbons (PAHs) in the surface soil of urban parks in Beijing, China. *Environmental Pollution*, 260:114016.

Rubio-Clemente, A., Torres-Palma, R.A. & Peñuela, G.A. 2014. Removal of polycyclic aromatic hydrocarbons in aqueous environment by chemical treatments: A review. *Science of The Total Environment*, 478:201-225.

Sakamoto, K., Hayashi, F., Sato, K., Hirano, M. & Ohtsu, N. 2020. XPS spectral analysis for a multiple oxide comprising NiO, TiO_2, and $NiTiO_3$. *Applied Surface Science*, 526:146729.

Sam, S.R. & John, F. 2020. Optical properties of pure and doped CdS nanoparticles under solvothermal method. Materials Today. AIP Conference Proceedings 2270, 110006 Seo, M.W., Jeong, H.M., Lee, W.J., Yoon, S.J., Ra, H.W., Kim, Y.K., Lee, D., Han, S.W., Kim, S.D., Lee, J.G. & Jeong, S.M. 2020. Carbonization characteristics of biomass/coking coal blends for the application of bio-coke. *Chemical Engineering Journal*, 394:124943.

Shen, J.-H., Chuang, H.-Y., Jiang, Z.-W., Liu, X.-Z. & Horng, J.-J. 2020. Novel quantification of formation trend and reaction efficiency of hydroxyl radicals for investigating photocatalytic mechanism of Fe-doped TiO_2 during UV and visible light-induced degradation of acid orange 7. *Chemosphere*, 251:126380.

Shetty, M., M, M., Shastri, M., M, S., H P, N., Shivaramu, P. & Rangappa, D. 2019. Hydrothermal synthesized of Bi_2MoO_6/Reduced Graphene Oxide composite as anodes for lithium-ion batteries. *Ceramics International*, 45 (18): 24965-24970

Singh, P., Shandilya, P., Raizada, P., Sudhaik, A., Rahmani-Sani, A. & Hosseini-Bandegharaei, A. 2020. Review on various strategies for enhancing photocatalytic activity of graphene based nanocomposites for water purification. *Arabian Journal of Chemistry*, 13(1):3498-3520.

Srinivasa Subbarao, P., Aparna, Y. & Chitturi, K.L. 2020. Synthesis and characterization of Ni doped SnO_2 nanoparticles by sol-gel method for novel applications. Materials Today: Proceedings, 26: 1676-1680.

Theerakarunwong, C.D. & Phanichphant, S. 2018. Visible-Light-Induced Photocatalytic Degradation of PAH-Contaminated Soil and Their Pathways by Fe-Doped TiO_2 Nanocatalyst. *Water, Air, & Soil Pollution*, 229(9):291.

Wang, C. 2020. Triethylamine sensing properties of ZnO nanostructures prepared by hydrothermal method at different pH values. *Chemical Physics Letters*, 749:137471.

Wang, D., Shen, H., Guo, L., Wang, C. & Fu, F. 2016a. Porous BiOBr/Bi2MoO6 Heterostructures for Highly Selective Adsorption of Methylene Blue. *ACS Omega*, 1(4):566-577.

Wang, P., Ao, Y., Wang, C., Hou, J. & Qian, J. 2012. A one-pot method for the preparation of graphene–Bi2MoO6 hybrid photocatalysts that are responsive to visible-light and have excellent photocatalytic activity in the degradation of organic pollutants. *Carbon*, 50(14):5256-5264.

Wang, Y., Niu, C.-G., Zhang, L., Wang, Y., Zhang, H., Huang, D.-W., Zhang, X.-G., Wang, L. & Zeng, G.-M. 2016b. High-efficiency visible-light AgI/Ag/Bi2MoO6 as a Z-scheme photocatalyst for environmental applications. *RSC Advances*, 6(13):10221-10228.

Xiao, J., Zhang, J., Liu, W., Huang, T., Qu, Y., Chen, H. & Lin, Z. 2018. Construction of RGO/Bi2MoO6 2D/2D nanocomposites for enhancement visible light-driven photocatalytic reduction of Cr (VI). *Materials Research Express*, 5

Yang, J., Wang, X., Zhao, X., Dai, J. & Mo, S. 2015. Synthesis of Uniform Bi2WO6-Reduced Graphene Oxide Nanocomposites with Significantly Enhanced Photocatalytic Reduction Activity. *The Journal of Physical Chemistry C*, 119(6):3068-3078.

Zhang, S., Ye, H., Hua, J. & Tian, H. 2019a. Recent advances in dye-sensitized photoelectrochemical cells for water splitting. *EnergyChem*, 1(3):100015.

Zhang, Y., Zhang, L., Huang, Z., Li, Y., Li, J., Wu, N., He, J., Zhang, Z., Liu, Y. & Niu, Z. 2019b. Pollution of polycyclic aromatic hydrocarbons (PAHs) in drinking water of China: Composition, distribution and influencing factors. *Ecotoxicology and Environmental Safety*, 177:108-116.

Zhang, Y., Zhu, Y., Yu, J., Yang, D., Ng, T.W., Wong, P.K. & Yu, J.C. 2013. Enhanced photocatalytic water disinfection properties of Bi2MoO6–RGO nanocomposites under visible light irradiation. *Nanoscale*, 5(14):6307-6310.

Zhao, G., Chang, W., Yan, J., Li, X., Tong, D., Zhao, R., David, S.J. & Tai, P. 2017a. Spatial distribution and sources identification of polycyclic aromatic hydrocarbons in Wolong Lake, Northeast China. *Chinese Geographical Science*, 27(6):1003-1012.

Zhao, Z., Qin, Z., Cao, J. & Xia, L. 2017b. Source and Ecological Risk Characteristics of PAHs in Sediments from Qinhuai River and Xuanwu Lake, Nanjing, China. *Journal of Chemistry,* 2017:3510796.

CHAPTER 3: PAPER 1

PAH profile of coal tars generated from coke production process and their toxicity

Shelter Maswanganyi, Elvis Fosso-Kankeu, Neeraj Kumar, Frans Waanders, John Bunt, Suprahkas Sinha Ray

ABSTRACT

Coke is the material left when water, coal gas, and coal tar are driven off during the carbonisation of coal at temperatures around 1100 ^{o}C in an air-tight oven, a process referred to as coke making or coking. Coal tar is produced during the coking process, although often considered for reuse in some other processes; a considerable amount of coal tar is eventually released into the environment. Coal tars are among the biggest sources of polyclic aromatic hydrocarbons (PAHs) that are carcinogenic and toxic to humans. PAHs are of major concern, as they have the ability to leach into the environment during rain runoff. In this study, coal tar received from a steel company in South Africa was characterised using GCXGC-TOFMS to determine the PAH profile. It was found that the coal tar sample contained more than 100 PAHs, among which were naphthalene and benzo[a]pyrene, which exhibited the highest abundance and toxicity equivalent factor (TEF), respectively.

Keywords: Coal Tars, Coking, PAHs, Toxicity

3.1 Introduction

South Africa obtains about 70% of its energy from coal (Fosso-Kankeu *et al.*, 2017). The conversion of coal to energy is achieved through the combustion of coal. Besides energy production, coal is also intensively used in steel, oils and coke making (Jin *et al.*, 2019). Industrial processing such as gasification of biomass, coal combustion, coking and pyrolysis can result in tar formation, which is generated as a by-product. Coking is simply an extreme pyrolysis of coal, where coal is heated at temperatures around 1100 ^{o}C. The process takes place in an oven battery, which is composed of many coke ovens stacked in rows and often located at or near an integrated steel mill. In South Africa, coking is one of the largest sources of coal tar. It is estimated that around 109000 tonnes of tar was produced in 2013; this creates an environmental concern, as a total of 1.65 m tonnes of by-products produced in the same period needed space to be disposed of, with 290 hectares of land under restoration (Arcelor Mittal, 2014). Coal tar is material driven off as a by-product during the production of coke. Coal tar is defined as complex and valuable mixtures of phenols, PAHs and heterocyclic compounds (Jin *et al.*, 2019). Coal tars are classified according to their hydrocarbon chains and boiling points. The ones with short rings are referred to as phenols, and the larger ones are called polycyclic aromatic hydrocarbons (PAHs) (Abdel-Shafy & Mansour, 2016). The transition of tars from lower to higher hydrocarbons is a function of temperature. Tar is considered a threat to the environment when disposed of, as it is known to be the largest source of PAHs, with the potential of being carcinogenic, mutagenic and toxic (Mulder *et al.*, 2001).

PAHs are an important group of compounds of major environmental concern (Gupta & Gupta, 2015). They are compounds with two or more aromatic hydrocarbons (benzene) rings. PAHs have been reported to be highly carcinogenic and mutagenic in humans; hence, they are considered an environmental hazard when in contact with water. There are several sources of these aromatic hydrocarbons; some can be natural and some are due to anthropogenic activities. Anthropogenic sources are, however, considered the biggest contributor of PAHs to the environment (Bergendahl, 2007). Among the anthropogenic sources, petrogenic and pyrolytic sources are considered to be the most important. PAHs are also called secondary tars, as they start forming at a temperature of at least 800 ℃ and decompose at a temperature above 1000℃. Naphthalene, phenanthrene, pyrene and benzopyrene are examples of PAHs (Roetsa *et al.*, 2014). Due to the fact that PAHs have the potential of being easily transported by rainwater to nearby water sources, polluting the limited water sources (Fosso-Kankeu *et al.*, 2008; Fosso-Kankeu *et al.*, 2019); it is therefore important to assess their toxicity. PAHs that end up in rivers may lead to an increased risk to human beings and aquatic life. The interest in this study is only to predict the overall toxicity of the coal tar related to its PAH content. The 16 EPA (Environmental Protection Agency) priority PAHs will therefore be used as indicators of the toxicity of coal tar, since they have been widely studied. According to the literature, 80% of the total PAH contribution to health and environmental concerns could be ascribed to the 16

EPA priority PAHs (Zhang *et al.*, 2019). In this study, the PAH profile was studied using coal tar from the Arcelor Mittal coking process, Newcastle. The gas chromatography (GC) analytical technique using a Gas Chromatograph X Gas Chromatograph Time Of-Flight Mass Spectrometry (GCXGC-TOFMS) was used to generate the PAH profile; the toxicity potential of identified PAHs was determined by calculating the toxicity equivalent factors.

3.2 Experimental section

3.2.1. Materials and methods

The tar collected was sent to an external laboratory for analysis. Tar sample profiles were determined through a two-dimensional gas chromatography (GC) analytical technique using a Gas Chromatograph X Gas Chromatograph Time-Of-Flight Mass Spectrometry (GCXGC-TOFMS) coupled with MS for the relative quantification (area%) and identification of PAHs. The two-dimensional gas chromatography (GCXGC) utilises a high frequency modular to divert the entire one-dimensional effluent onto a second-dimensional column. The chromatographic separation space is dramatically increased compared to a conventional 1D-GC analysis, yielding a big leap in potential peak capacity. Samples for GCXGC-TOFMS analysis were prepared by dissolving tar into superior grade hexane (diluting 0.03 – 1 mL of sample into 10 mL volumetric flask). An auto-sampler was utilised for injection, and the sample sizes varied from 0.2 – 1 µL per injection. The setting of the GCXGC-TOFMS was done according to the basic set-up recommended by the supplier.

3.3 Results and discussion

3.3.1 PAH Profile for the Newcastle tar

PAHs have been reported as major components of coal-derived products and thermally cracked petroleum oils (Nishioka *et al.*, 1986); PAHs are toxic and/or mutagenic in biological systems and must therefore be seriously considered in coal tar. The coal tar PAH composition was determined using GCXGC-TOFMS, and the results are shown in Table 3-1. A variety of PAHs were observed in the coal tars from the coking process at Arcelor Mittal South Africa, with a dominance of naphthalene. The toxicities of PAHs have been reported to be related to specific structures and positions of ring substitution (Nishioka *et al.*, 1986). More than 100 PAHs were identified in tars from the coking process, but only the PAHs listed among the 16 EPA priority PAHs will be considered in this study. Among the PAHs identified, 10 EPA priority PAHs were detected in the tar from the coking process; of these EPA priority PAHs, four have been classified as having the potential to cause cancer to humans. The complete EPA list has seven carcinogenic PAHs. Cancer-causing PAHs are classified as either group 1, 2A or 2B. The description of the classification numbers is presented in Table 3-2. Many studies have reported that these seven PAHs cause lung and skin cancer in humans.

Table 3-1: Newcastle coal tar characteristics

PAHs names	Number of rings	IARC classification	Structure
Naphthalene	2	2B	linear
Acenaphthene	3	N/A	clustered
Acenaphthylene	3	3	clustured
Fluorene	3	3	linear
Phenanthrene	3	3	angular
Anthracene	3	3	linear
Pyrene	4	2A	clustered
Benzo(k)anthracene	4	2B	angular
Benzo(k)fluoranthene	5	2B	angular
Benzo(a)pyrene	5	1	clustered

Table 3-2: Classification of PAHs

IARC classification	Definition
Group 1	Carcinogenic to humans
Group 2A	Probably carcinogenic
Group 2B	Possibly carcinogenic
Group 3	Not classifiable

PAHs have also been classified by IARC and DHHS as carcinogenic in animals, in which they cause bladder, liver and stomach cancer (Rengarajan *et al.*, 2015). The coking tar contains benzo(a)pyrene, which has been identified as the environmental indicator of PAHs (Nisbet & LaGoy, 1992). Therefore, the Newcastle coking tar has the potential of threatening the health of humans and animals when it comes into contact with them either by direct handling of tar or through exposure to contaminated surface water or ground water. Although the coal tar analysis did not give the exact concentration level of the PAHs in the tar, the areas under a peak that is proportional to the concentration of PAHs in coal tars could be obtained (Figure 3-1).

The size of the area therefore reflects the abundance of the PAHs in the tar; PAHs with high areas are more abundant. Different concentration levels of the PAHs may depend on the type of tar

production process, coal rank, operating conditions and other factors. The abundance of PAH is well presented by the bar graph in Figure 3-1. It can be seen that naphthalene has the highest area for both tars and therefore is the most abundant PAH. More PAHs with higher concentrations may be found in the tar produced at temperatures lower than 1200 ˚C because the formation of PAH mixtures is a function of temperature (Jin *et al.*, 2019). The decomposition of PAHs is likely to take place at temperatures higher than 1000 ˚C.

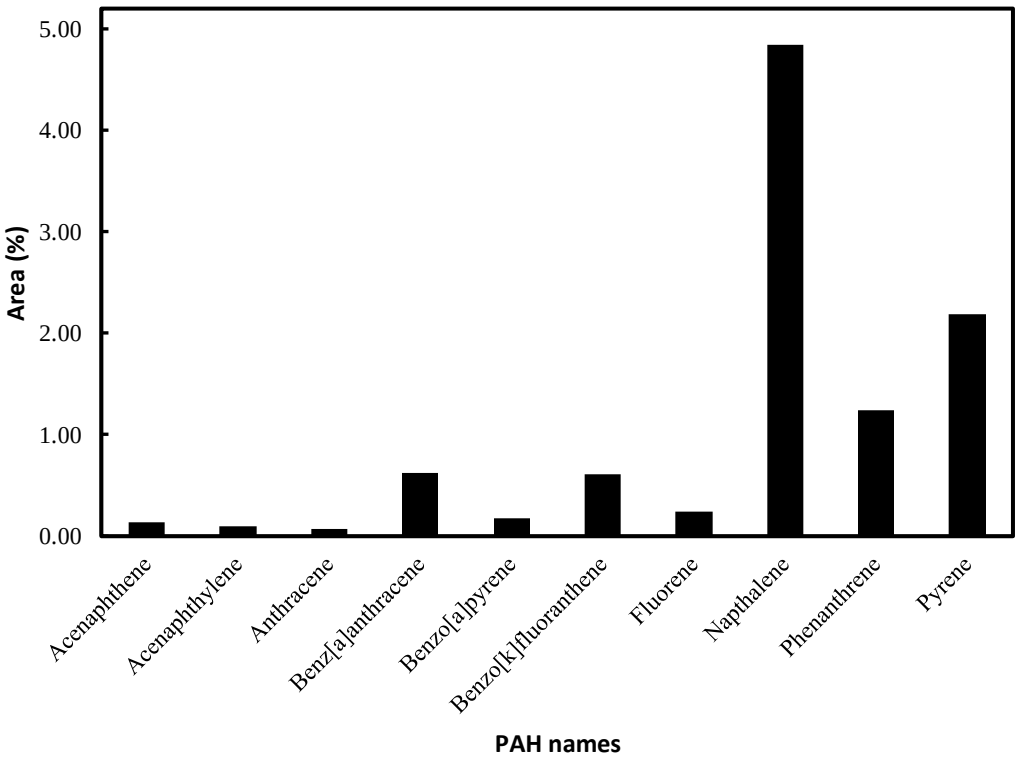

Figure 3-1: Abundance of PAHs in coal tar

3.3.2 Toxicity of PAHs and risk of exposure

PAHs can be carcinogenic, genotoxic, mutagenic and teratogenic. However, not all toxic PAHs are carcinogenic (Rengarajan *et al.*, 2015). The toxicity of the seven PAHs identified as carcinogens by the EPA is not of the same extent. Benzo[a]anthracene, benzo[a]pyrene, naphthalene, and benzo[k]fluoranthene are the carcinogens that have been identified in this study. However, not all of them have the same carcinogenic potency. The carcinogenic or toxicity potency of the PAHs is related with the complexity of the molecule and the structural characteristics (Guo *et al.*, 2011). A compound with a more complex structure is usually the more potent (Abdel-Shafy & Mansour, 2016). The number of benzene rings or the molecular weight of PAHs is one of the examples of structural features that can affect the carcinogenic potency. PAHs have benzene rings bonded in a linear, angular or clustered arrangement (Larsson *et al.*, 2017). The difference in the arrangement of the rings results in PAHs having different carcinogenic effects.

Figure 3-2 shows the chemical structures of some of the most studied PAHs. PAHs with clustered or angular arrangements have higher carcinogenic potency than linear PAHs (Qu *et al.*, 2020). Also, larger PAHs (more than six rings) are more potent than smaller PAHs (two to five rings) (Abdel-Shafy & Mansour, 2016). Benzo[a]anthracene is more toxic than naphthalene because it has a more complex structure and more rings than naphthalene. Although benzo[a]pyrene and benzo[k]fluoranthene have the same number of rings, their ring arrangement is different. Benzo[a]pyrene has a more complex structure than benzo[k]fluoranthene; hence it is more toxic. Of all the PAHs found in both coal tars, naphthalene is the least toxic PAH because it has the lowest number of rings (i.e. two rings), and it possesses a linear arrangement. In contrast, benzo[a]pyrene has five rings with a clustered arrangement; therefore it is the most toxic. However, benzo[a]pyrene cannot be the only PAH considered when investigating the dangers related to the exposure to coal tars. The risks related to contact with PAHs could never be related to single PAHs. The toxicity of PAHs is higher for mixtures than for single PAHs, and the health effects of individual PAHs are not the same as those of PAH mixtures (Abdel-Shafy & Mansour, 2016). Therefore, understanding the mixtures of PAHs instead of single PAHs give precise assessment of their dangers. Nontoxic PAHs may still show adverse effects on humans and animals when they appear in mixtures, due to different factors such as the mechanism of metabolism, age and pre-existing health effects (Gbeddy *et al.*, 2020). Owing to the fact that PAHs require the activation of electrophilic metabolites to evoke their cancer-causing effects, in other words, PAHs must be metabolised to their diol epoxide or metabolites (Abdel-Shafy & Mansour, 2016; Gitipour *et al.*, 2018). In mixtures, weaker or smaller PAHs may increase the rate of metabolism, which will increase the toxicity effect. According to occupational studies on workers exposed to PAHs, it was found that mixtures of PAHs cause cancer in humans (Adeniji *et al.*, 2018). Therefore, anthracene , acenaphthylene, acenaphthene, fluorene, phenanthrene, and pyrene cannot be overlooked because exposure to mixtures containing these PAHs may also cause adverse health effects. These non-carcinogenic PAHs have reactive metabolites such as epoxides and dihydroidiols that can bind to cellular proteins and DNA (Rengarajan *et al.*, 2015). The resulting biochemical disturbances and damaged cells lead to mutations and development of malformations and tumors (Gitipour *et al.*, 2018).

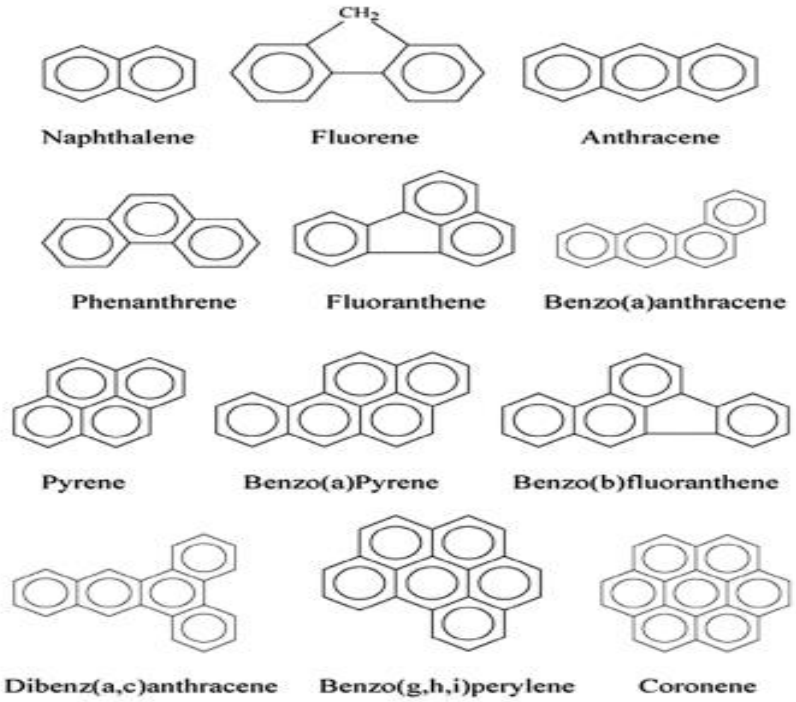

Figure 3-2: Chemical structure of some of the common PAHs

3.3.3 Toxic equivalency factors

The International Agency for Research on Cancer (IARC) classification criteria do not indicate more potent and less potent PAHs (Nisbet & LaGoy, 1992). To conduct a reasonable risk assessment, the potency of individual PAHs have to be known, and this is determined by assigning toxic equivalency factors (TEFs) (Halek *et al.*, 2008). Only limited numbers of PAHs have been extensively studied for provision of toxicity criteria. The risks posed by PAH mixtures have been investigated by the EPA, making an assumption that all carcinogenic PAHs are as potent as benzo[a]pyrene (Ba[a] P), one of the most potent PAHs (Richter-Brockmann & Achten, 2018). The available information that has been collected recently suggests that most are considerably less potent than Ba[a] P, and therefore, the EPA approach is likely to overestimate risks (Fang *et al.*, 2002). The basis of risk assessment considered by the EPA consisted of dividing the PAHs into two subclasses of carcinogenic (TEF=1) and non-carcinogenic (TEF=0) PAHs (Fang *et al.*, 2002). A new TEF approach by Nisbet and LaGoy (1992) has been adopted to yield a set of TEFs that will assist in accurately predicting risks associated with the different PAHs based on the current knowledge (Nisbet & LaGoy, 1992). The approach assigns TEFs to individual PAHs based on the data from previous studies and elevated tumor incidences (Halek *et al.*, 2008). Furthermore, this approach assigns TEFs to PAHs determined to be non-carcinogenic by the IARC or the EPA. PAHs are assigned 1, 0.1, 0.01, or 0.001 (Halek *et al.*, 2008) . A TEF of 1 is assigned to PAHs with high cancer potency, 0.1 to carcinogenic PAHs with low potency, 0.01 to PAHs with limited carcinogenic potency and finally 0.001 to PAHs with little if any cancer potency,see Table 3-3 for TEFs.

For the evaluation of the toxicity of known PAHs, toxic equivalents (TEQ) are calculated as the product of the individual PAH concentration and its corresponding TEF (Meng *et al.*, 2019). In this case, the toxicity was estimated using an area that is proportional to the concentration. Figure 3-3 shows the toxic potential of individual PAHs. It is evident from the graph that benzo[a]pyrene is the most toxic, followed by benzo[a]anthracene. From this graph, it can be concluded that, although the benzo[a]pyrene content in the coal tar is relatively low, the estimated toxicity may be of serious concern. On the other hand, all other PAHs can exhibit high toxicity if their content in the coal tar is increased.

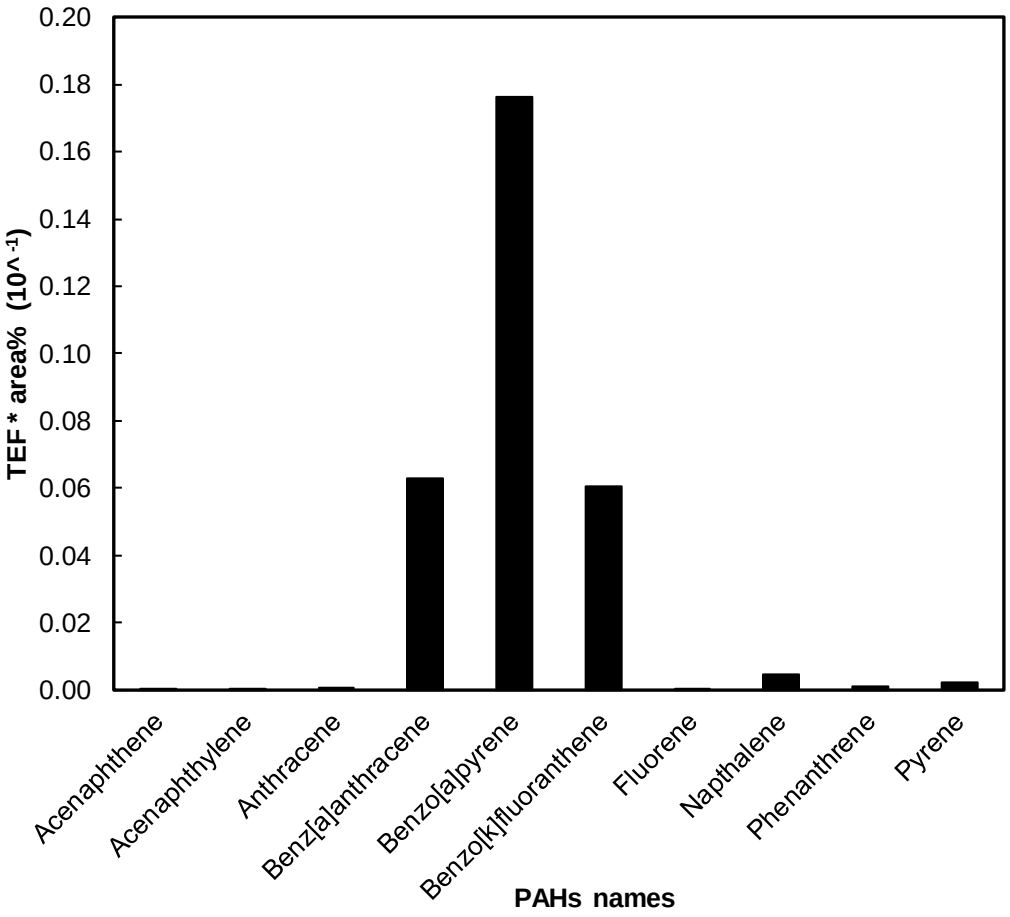

Figure 3-3: Approximate TEQs of individual PAHs in coal tar

Table 3-3: Toxic equivalent factors of PAHs

	Toxic Equivalent factors(TEQ)	
PAH compound	EPA	Nisbtet and LaGoy
Dibenz(a,h)anthracene	1	1
Benzo(a)pyrene	1	1
Benzo(a)anthracene	1	0.1
Benzo(b)fluoranthene	1	0.1
Benzo(k)fluoranthene	1	0.1
Indeno(123-cd)pyrene	1	0.1
Anthracene	0	0.01
Benzo(g,h,i)perylene	0	0.01
Chrysene	1	0.01
Acenaphthene	1	0.001
Acenaphthylene	0	0.001
Fluoranthene	0	0.001
Fluorene	0	0.001
2-methylnaphthalene	0	0.001
Naphthalene	0	0.001
Phenanthrene	0	0.001
Pyrene	0	0.001

3.3.4 Toxicity Of non-EPA PAHs

There are some toxic PAHs not included on the EPA list. As mentioned above, the determination of the exact health effects of a given PAH during epidemiological studies will be quite challenging , since most exposures are to PAH mixtures. Recent studies have discovered that 7, 12-dimethylbenzo anthracene (DMBA), which is a non-EPA PAH, has the potential of increasing the risk of breast cancer in animals through a variety of mechanisms (Lawal, 2017). DMBA tends to accumulate and persists in the adipose tissue of the mammarian gland due to the fact that it is a fat soluble compound; this eventually contributes to increase the exposure of mammary epithelium to this chemical carcinogen (Alegbeleye *et al.*, 2017). This PAH has shown its carcinogenicity effects on

experimental rats, and it is an indirect carcinogen, requiring metabolic activation to yield its ultimate carcinogenic form (Rengarajan *et al.*, 2015).

3.4 Conclusion and recommendations

The PAHs profile of coal tars from the coking process at Arcelor Mittal was determined using gas chromatography and showed that Newcastle tar contained a host of different PAHs, but the focus was mainly placed on those classified by the United States Environmental Protection Agency (US-EPA) as priority pollutants. Among the selected PAHs, naphthalene was found to be the most abundant in both tars; however, based on the toxic equivalent factor that gives an indication of the potency of individual PAHs, benzo[a]pyrene was the most toxic PAH, followed by benzo[a]anthracene and benz[k]fluoranthene, which all occurred in the tar from the coking process. These PAHs have been reported to be related to elevated tumor incidences, and therefore have high cancer potency. However, it is also important to note that the mixture of less potent PAHs increases their toxicity effects on humans. Therefore, the discharge of all these coal tars in the environment is likely to pose significant risks to the ecosystems once the PAHs are naturally leached into surface and groundwater and dispersed into the water network. It is therefore important to carry out further study to understand the susceptibility of PAH release from coal tar and develop suitable photocatalytic methods for their degradation in aqueous solutions.

References

Abdel-Shafy, H.I. & Mansour, M.S.M. 2016. A review on polycyclic aromatic hydrocarbons: Source, environmental impact, effect on human health and remediation. *Egyptian Journal of Petroleum*, 25(1):107-123.

Adeniji, A., Oluranti Okoh, O. & Ifeanyi Okoh, A. 2018a. Analytical Methods for Polycyclic Aromatic Hydrocarbons and their Global Trend of Distribution in Water and Sediment: A Review.

Alegbeleye, O.O., Opeolu, B.O. & Jackson, V.A. 2017. Polycyclic Aromatic Hydrocarbons: A Critical Review of Environmental Occurrence and Bioremediation. *Environmental Management*, 60(4):758-783.

Arcelormittal South Africa, Parliament colloquium on beneficiation, 24 August 2014. Available: https://www.thedti.gov.za/parliament/2014/ArcelorMittal.pdf

Bergendahl, J. 2007. Batch Leaching Tests: Colloid Release and PAH Leachability. Soil & Sediment Contamination, *an International Journal*, 14(6):527-543.

E Fosso-Kankeu, R Weideman, D Moyakhe, FB Waanders, M Le Roux, QP Campbell. 2019. Hydrothermal preparation of biochar from spent coffee grounds, and its application for the removal of cadmium from coal tailings leachate. *The Journal of the Southern African Institute of Mining and Metallurgy*, 119: 607-612.

Fang, G.-C., Chang, K.-F., Lu, C. & Bai, H. 2002. Toxic equivalency factors study of polycyclic aromatic hydrocarbons (PAHs) in Taichung City, Taiwan. *Toxicology and Industrial Health*, 18(6):279-288.

Fosso-Kankeu, E., Jagals, P., Du Preez, H. 2008. Exposure of rural households to toxic cyanobacteria in container-stored water. *Water SA*, 34:631-636.

Gbeddy, G., Goonetilleke, A., Ayoko, G.A. & Egodawatta, P. 2020. Transformation and degradation of polycyclic aromatic hydrocarbons (PAHs) in urban road surfaces: Influential factors, implications and recommendations. *Environmental Pollution*, 257:113510.

Gitipour, S., Sorial, G.A., Ghasemi, S. & Bazyari, M. 2018. Treatment technologies for PAH-contaminated sites: a critical review. *Environ Monit Assess*, 190(9):546.

Guo, Y., Wu, K.-S., Huo, X. & Xu, X. 2011. Sources, Distribution, and Toxicity of Polycyclic Aromatic Hydrocarbons. *Journal of Evironmental Health*, 73:22-25.

Gupta, H. & Gupta, B. 2015. Photocatalytic degradation of polycyclic aromatic hydrocarbon benzo[a]pyrene by iron oxides and identification of degradation products. Elsevier *Chemosphere*, 138: 924-931.

Halek, F., Nabi, G. & Kavousi, A. 2008. Polycyclic aromatic hydrocarbons study and toxic equivalency factor (TEFs) in Tehran, IRAN. *Environmental Monitoring and Assessment*, 143(1):303-311.

Jin, L., Zhao, H., Wang, M., Wei, B. & Hu, H. 2019. Effect of temperature and simulated coal gas composition on tar production during pyrolysis of a subbituminous coal. *Fuel*, 241:1129-1137.

Khethane, T. C., Fosso-Kankeu, E., Waanders, F. & J.J. 2017. PAHs Content of Tar Produced from Fischer Assay of Medium Rank C Bituminous South African Coal. Science, Engineering, Technology & Waste Management, 9th Int'l Conference on Advances in Science, Engineering, Technology & Waste Management (ASETWM-17). November 2017, Parys, South Africa. Editors: F. Waanders, E. FossoKankeu, B. Topcuoglu, M. Plaisent, Y. Thaweesak. ISBN: 978-81-934174-6-1, 27-28.

Larsson, M. *et al*. 2017. Occurrence and leachability of polycyclic aromatic compounds in contaminated soils: Chemical and bioanalytical characterization. s.l.: *Science of the Total Environment*, 1:622-62

Lawal, A.T. 2017. Polycyclic aromatic hydrocarbons. A review. *Cogent Environmental Science*, 3(1):1339841.

Meng, Y., Liu, X., Lu, S., Zhang, T., Jin, B., Wang, Q., Tang, Z., Liu, Y., Guo, X., Zhou, J. & Xi, B. 2019. A review on occurrence and risk of polycyclic aromatic hydrocarbons (PAHs) in lakes of China. *Science of the Total Environment*, 651:2497-2506.

Mulder, E., Brouwer, J. P., Blaakmeer, J. & FreÂnay, J. W. 2001. Immobilisation of PAH in waste materials. *Waste Management*, 21: 247-253.

Nisbet, I.C.T. & LaGoy, P.K. 1992. Toxic equivalency factors (TEFs) for polycyclic aromatic hydrocarbons (PAHs). *Regulatory Toxicology and Pharmacology*, 16(3):290-300.

Nishioka, M., Campbell, R.M., Lee, M.L. & Castle, R.N.Isolation of sulphur heterocycles from petroleum and coal-derived materials by ligand exchange chromatography, *Fuel* 65: 270-273, 1986.

Qu, Y., Gong, Y., Ma, J., Wei, H., Liu, Q., Liu, L., Wu, H., Yang, S. & Chen, Y. 2020. Potential sources, influencing factors, and health risks of polycyclic aromatic hydrocarbons (PAHs) in the surface soil of urban parks in Beijing, China. *Environmental Pollution*, 260:114016.

Rengarajan, T., Rajendran, P., Nandakumar, N., Lokeshkumar, B., Rajendran, P. & Nishigaki, I. 2015. Exposure to polycyclic aromatic hydrocarbons with special focus on cancer. *Asian Pacific Journal of Tropical Biomedicine*, 5(3):182-189.

Richter-Brockmann, S. & Achten, C. 2018. Analysis and toxicity of 59 PAH in petrogenic and pyrogenic environmental samples including dibenzopyrenes, 7H-benzo[c]fluorene, 5-methylchrysene and 1-methylpyrene. *Chemosphere*, 200:495-503

Roetsa, L., Bunta, J.R., Neomagusa, H.W. & Van Niekerk B.D. 2014. An evaluation of a new automated duplicate-sample Fischer Assay setup according to ISO/ASTM standards and analysis of the tar fraction. *Journal of Analytical and Applied Pyrolysis*, 106:190-196.

Zhang, Y., Zhang, L., Huang, Z., Li, Y., Li, J., Wu, N., He, J., Zhang, Z., Liu, Y. & Niu, Z. 2019. Pollution of polycyclic aromatic hydrocarbons (PAHs) in drinking water of China: Composition, distribution and influencing factors. *Ecotoxicology and Environmental Safety*, 177:108-116

CHAPTER 4: PAPER 2

Mobilisation of PAHs from coal tar by various environmental aqueous solutions

Shelter Maswanganyi, Elvis Fosso-Kankeu, Neeraj Kumar, Frans Waanders, John Bunt, Suprahkas Sinha Ray

ABSTRACT

In this study, coal tar from the coking process was exposed to real environmental solutions (river and normal water) and simulated environmental solutions (synthetic rain water) at various solid/liquid ratios, temperatures, pH and time. It was found that, among all the solutions, river water was the most effective for the mobilisation of PAHs; a mass/volume ratio of 5/95 was found suitable for maximum mobilisation of PAHs. Although there was no consistent trend of the effect of temperature, it was evident that better mobilisation of PAHs was achieved above room temperature (25°C). Acid and moderate alkaline pH promoted better mobilisation of PAHs; the maximum mobilisation of PAHs was achieved after four weeks of exposure, while it was observed that more time was required to mobilise heavy PAHs (five to six benzene rings) compared to light PAHs (two to three benzene rings), which were mostly mobilised after the first week. Naphthalene was the most abundant PAH in the leachate, while compared to other solutions; river water was most effective in mobilising benzo (a) pyrene, which is one of the most toxic PAHs. It is therefore proven in this study that the extent of mobilisation of PAHs from coal tar in receiving water, and hence the impact on the environment, will depend on the physico-chemical properties of the water; acidic and environmental waters are most likely to mobilise PAHs and promote their dispersion in the environment.

Keywords: Coal tar, PAHs, mobilisation, river water, rainwater

4.1 Introduction

Globally, coal plays a vital role in securing energy demand and is anticipated to stay the second-largest primary source of energy until 2030 (Shafiee & Topal, 2008; Wolde-Rufael, 2010). As from 2008, the global coal reserve was estimated to be around 861 billion tonnes; however, coal of high quality is rapidly depleting because of increasing demand, especially from the most prominent consumers such as China and the USA (WEC, 2010). South Africa mines around 220 Mt of coal per annum and is considered the sixth largest producer in the world, after countries like China and the USA. Coal is the primary source of energy in South Africa, accounting for 72% of total primary energy supply in the country in 2005, while contributing to approximately 95% of the electricity generated. It is reported that, coal in South African is also locally used as a feedstock for the production of large amount of the liquid fuels (Hancox & Gotz, 2014). The South African Synthetic Oil Limited (Sasol) is reported as the fastest-growing consumer of coal, using 29% of locally produced coal to feed Sasol Chemical Industries (SCI) gasifiers at Sasolburg and Sasol Synthetic Fuels (SSF) gasifiers at Secunda for conversion into crude syn-gas (Blignaut & Hassan, 2002; Hancox & Gotz, 2014). According to current practices, more than half of South Africa's mined coal considered as low-grade coal is used by the electricity and petrochemical industries; the latter is relying on gasification processes to produce fuel and synthetic chemicals.

However, with the rapidly growing consumption of coal, researchers forecast that the extreme reliance of the country on coal for electricity supply and power generation will result in a peak of the production rate at approximately 284 Mt/year in 2020, contributing to the exhaustion of at least half (12 Gt) of the total reserve (23 Gt), which will compel consumers to mostly depend on or develop processes suitable for low-grade coal (Hartnady, 2010). It is, for example, estimated that processes such as underground coal gasification (UCG) may eventually make marginal coal reserves accessible (Heinberg & Fridley, 2010). The major environmental problem associated with such processes is the coal tar generated as by-product, which may be challenging to handle and has the potential to release carcinogenic compounds such as PAHs into the receiving waters. The rapid decline of quality coal is likely to contribute to the increasing use of technologies that can be effectively operated with low-quality coal such as gasification for the production of energy, chemicals and other products. These technologies are more prone to the generation of tar as a by-product. The technologies include gasification processes (the Sasol-Lurgi gasification process and the underground coal gasification) and coking of coal.

The Sasol gasifiers are very tolerant of changes in feedstock quality and capable of gasifying coal with ash content as high as 35% (Quass & Skinner, 1987); it is estimated that > 30 million tons per annum of bituminous coal of domestically produced coal is consumed by Sasol in the gasification process. During raw gas cooling, unreacted gasification steam and water formed in some of the gasification reactions condense; these wastewater streams contain a number of contaminants, including tar, oil and phenols that must be removed prior to reuse and discharge.

Currently, the mining of coal via underground coal gasification (UCG) technology appears to be both technically and economically feasible (Walker, 1999). UCG makes possible the exploitation of marginal coal reserves that could not be recovered using the conventional method; therefore, offering the prospect of increasing the world's usable coal reserves by a factor of no less than three. Inaccessible and low grade coal can be competitively converted by UCG to syngas that will eventually be used for power generation and production of chemicals (Bhutto *et al*., 2013). UCG syngas has been produced at Majuba power plant in South Africa since 2007; the project is considered as the longest UCG running trial in the western world, contributing about 3 MW to the overall output of 650 MW at that plant. The facilities are to be expanded shortly to an output of 1200 MW; the syngas will contribute to around 30% of the plant fuel (Bhutto *et al*., 2013). Krzysztof and Kapusta (2011 conducted a study on the pollution of water during the process of UCG. Typical pollutants identified in ground water nearby the UCG process include benzene, phenols and its derivatives, PAHs, heterocyclics and inorganic pollutants, mainly sulphate, chloride and ammonium (Stuermer *et al*., 1982; Lindblom & Smith, 1993; Covell & Thomas, 1996; Shu-qin *et al*., 2007; Kapusta & Stanczyk, 2011).

Coke is the material left over when water, coal gas and coal tar are driven off during the carbonisation of coal at temperatures around 1100°C in an air-tight oven, a process referred to as coke making or coking (Bieda *et al*., 2015). Arcelor Mittal South Africa operates five coke batteries; during this process gas and other by-products, including tar, are formed. It is estimated that around 109000 tonnes of tar was produced in 2013. This creates an environmental concern, as a total of 1.65 m tonnes of by-product produced in the same period needs space to be disposed of, with 290 ha of land under restoration (Arcelor Mittal South Africa, 2014).

Millions of tonnes of coal tar are discharged into the environment throughout the world every year without proper management; the risks of PAH release from such coal tar and the potential impact on the environment have often been overlooked, while the deleterious effects continue to cause a lot of health issues among humans and other biological systems. PAHs are reported to have mutagenic and carcinogenic properties. Owing to their persistence in water and carcinogenic and mutagenic potential, they have been categorised as priority contaminats by the United States Environmental Protection Agency (US-EPA) and also by the European Environment Agency (Haritash & Kaushik, 2009; USEPA, 2009). It is therefore important for future research to focus on the environmental risks related to coal tar.

4.2 Experimental procedure

4.2.1 Chemicals and reagents

- Suphuric acid
- Nitric acid

4.2.2 Sample collection

Water samples consisted of river water, demin water, and simulated rainwater (S. rain). River water was collected near Sasol in Secunda, Mpumalanga, South Africa. Water samples were collected in 500 mL polypropylene plastic bottles, and physico-chemical parameters such as pH, oxido-redox potential (ORP), electrical conductivity, and temperature were measured in-situ using a portable Lovibond SensoDirect 150 multi-parameter water quality meter. The coal tar was received in a 5 L container at Arcellor Mittal Vanderbijlpark; the tar sample derives from the coking process.

4.2.3 Sample preparations

4.2.3.1 Preparation of synthetic rain (S.rain)

Rainwater was prepared to simulate the acidic rain in the Mpumalanga area. The pH of the rainwater in Mpumalanga is below 4.3 due to the high release of sulphur dioxide in the area. S. Rain was made by mixing 1 L of deionised water with 0.911 µL of H_2SO_4 and 2.86 µL of HNO_3 to achieve a pH of 4.3, according to the previous protocol (Fosso-Kankeu *et al*., 2017)

4.2.4 Leaching experiments

4.2.4.1 Batch Leaching

4.2.4.1.1 Optimum solid to liquid ratio

This study aimed to test the leachability of PAHs from coal tar into water sources. Before investigating other factors that can enhance the release of PAHs from coal tar, it is of importance to first determine how the leaching solution volume affects the process. An optimum ratio of coal tar to leaching lixiviant obtained was used for the rest of the experiments. To determine an optimum ratio, the ratio of coal tar to leaching solution was varied in this way: first, a ratio of 5/95 weight per cent (wt. %) was used, and then 10/90 wt. %, and finally 15/85 wt. %. Samples with different masses,which were 5 g, 10 g, and 15 g of tar, were weighed and transferred into three different 250 mL sealable jars with different lixiviants (water, S. rain and river water),represented in Figure 4-1. Each lixiviant was used for all three ratios. The experiments were carried out in duplicate; therefore a total of 18 jars were prepared. All these samples were placed in the platform shaker for 12 h. The shaker speed and temperature were set at 250 rpm and 55°C, respectively. The ratio that resulted in a higher amount of PAHs in the leachate was taken as the optimum ratio.

A batch test utilising S. rain, river and demin water as leaching solutions was used in this study. Coal tar and leaching solution were added into a 250 mL sealed jar. Five grams of coal tar was weighed in a 250 mL sealable jar, and 95 mL of lixiviant was added into the jar. The sealed jars were placed in a platform shaker at 250 rpm. Jars in the shaker were allowed to shake for different times. The shaking times of jars were varied in this way: 0.5, 1.5, 3 and 6 hrs. The resultant leachate was collected at each time interval. This step was carried out while also changing the temperature of the platform shaker. The experiment was run at 25°C, 35°C, 45°C, and 55°C. Each experimental run was carried out in duplicate. The control samples consisted of demin water as leaching solution. The

control samples were prepared by weighing 5 g of coal tar in a jar and adding 95 mL of demin water. All the leachate samples were kept in the fridge at a temperature of 0-6°C before analysisTo investigate the effect of pH on the leachability of PAHs, similar steps as the above were followed, except that the solid to liquid ratio, time, and temperature were not varied. The ratio of 5/95 wt. % of coal tar/water was used, the temperature was kept at 45°C, and the leaching period was kept at 1 and a half hour. These parameters were the optimum conditions found in the previous experiments. The pH of the water was varied from 2.2 to 10.3 ±0.1. The pH of the solution was varied by adding drops of HCl or NaOH to reduce or increase the pH, respectively. The test was conducted in triplicate. The resulting leachates from all the experiments were collected from the jar using a syringe and filtered through 0.45 µm pore syringe filter to remove suspended particles in the leachate.A filtered leachate of 80 mL was stored in plastic bottles and kept in the fridge until sent for analysis at an accredited laboratory,as represented in Figure 4-2.

Figure 4-1: 250 mL jars used for batch leaching tests

Figure 4-2: Leachate storage bottles

4.2.5 Column leaching

The column leaching test was performed using a glass column of 300 cm length and 8 cm internal diameter. The setup is displayed in Figure 4-3. Five grams of coal tar was weighed and transferred in each column, as in Fig 4-3. Similar to batch leaching river water, S. Rain and demin water were used as leaching solutions. Columns were filled with 300 mL of lixiviant. The experimental run was carried out in triplicate. All columns were placed at room temperature conditions and away from light to prevent photodegradation of PAHs to takeplace. To ensure proper interaction between the tar and water, the columns were inverted up and down once daily for few weeks. The leachate amount of

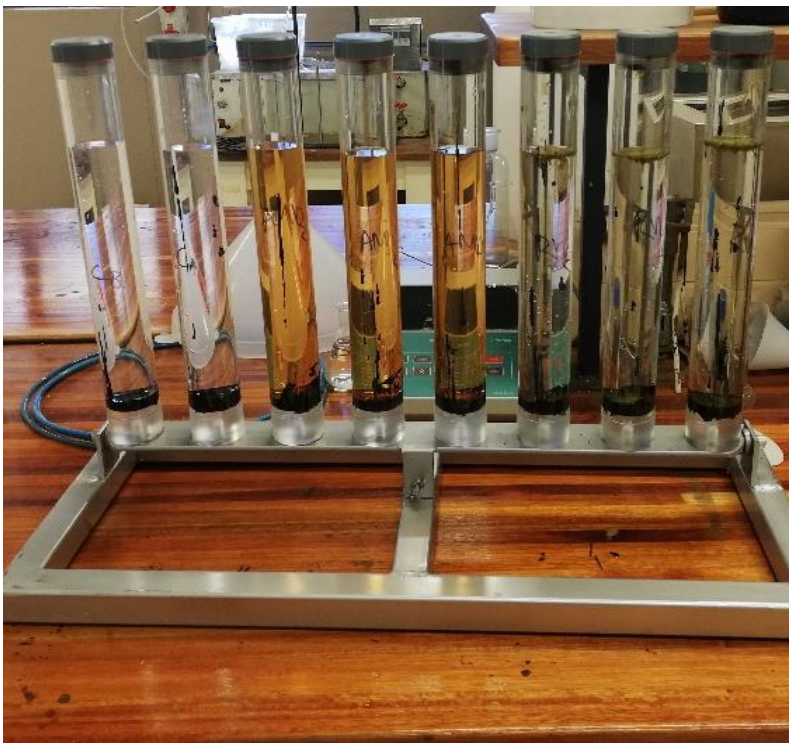

Figure 4-3: Leaching colunm set-up

25 mL from each column was collected weekly in a period of 4 weeks. The leachate was collected using a 5000 µL pipette and filtered with similar filters used in the batch test.

4.3 Results and discussion

In this chapter, the results obtained during experimentation are presented, and relevant interpretations are given. The section is subdivided into:

- Batch leaching
- Column leaching

In this study, both batch and column leaching tests were studied to investigate the leachability of PAHs from coal tar. Batch tests often lead to enhanced mobilisation of PAHs due to agitation and the large diameter of bottles/containers used (Kruger *et al.*, 2012). Constant agitation in batch leaching results in the viscosity of coal tar decreasing. As a result, the eluate contains a large amount of coal tar that has to be filtered out when collecting the leachate solution to avoid an overestimation of PAH contamination. To simulate an almost realistic leaching process, the column test was used. Column leaching makes use of smaller diameter columns, and no constant agitation is done. In this way, the mobility of PAHs is not enhanced by any external factors. Note that all the values plotted in the graphs are average values.

4.3.1 Data analysis

Analysis of river samples was done at the Water Lab in Pretoria, South Africa. General water quality parameters obtained from the analysis are shown in Table 4.1. The collected leachate from both

batch and column leaching was analysed for PAH content at the UIS organic laboratory using the UISOL-T-020 method.

Table 4-1: River water characteristics

Variable	River Water (mg L^{-1})
Total Acidity as $CaCO_3$	<5
Total Alkalinity as $CaCO_3$	136
Chloride as Cl	23
Sulphate as SO_4	18
Fluoride as F	0.3
Nitrate as N	<0.1
Nitrite as N	<0.05
Ortho Phosphate as P	0.2
pH	7.6

4.3.2 Batch leaching

4.3.2.1 Effect of solid to liquid ratio on leaching

The effect of the solid to liquid ratio on the mobility of PAHs is a vital parameter to assess, given the variation of such parameters in the environmental scenario. Figure 4-4 displays the leachability behaviour of PAHs when the solid to liquid ratio is varied. From the observation on Figure 4-4, the leaching volume does influence the mobility of PAHs. The maximum leaching was achieved in the presence of a larger volume of liquid. This behaviour was observed for all the leaching lixiviants. The total concentration of PAHs leached at 5/95 wt.% for demin water and river water was 1747.8 and 840.9 µg L^{-1}, at 10/90 wt.%, it was 1234.3 and 631.3 µg L^{-1}, and at 15/85 wt.% , it was 1603 and 802.4 µg L^{-1}, respectively. However, at 15/85 wt. %, the total concentration of PAHs in the leachate was higher than that of 10/90 wt. % for demin water. This discrepancy was caused by polarity/higher insolubility of coal tar in pure water. Therefore, a decrease in the ratio may not necessarily mean an increase in the leachability of pollutants when using demin water as a leaching solution. Similar results were found in the study done by Cai *et al.* (2019).

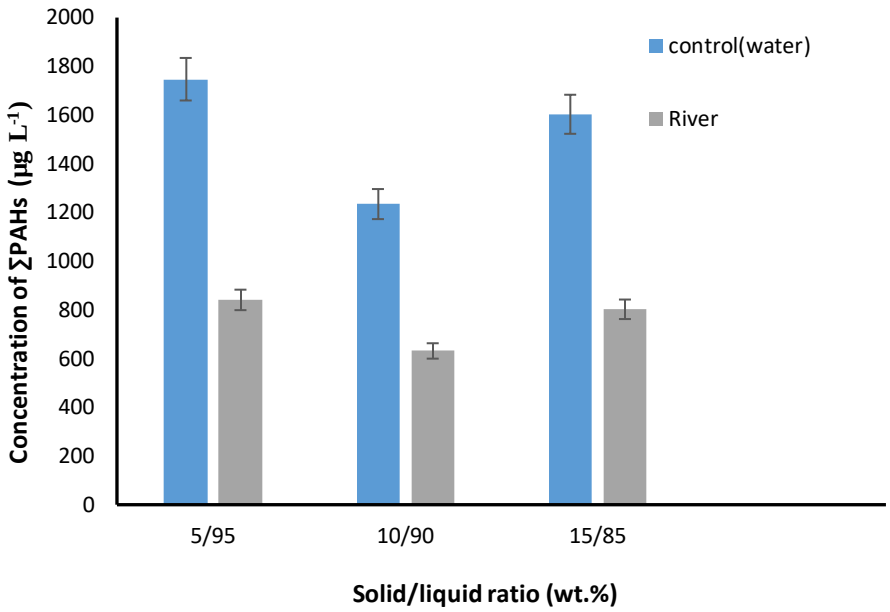

Figure 4-4: Effect of solid to liquid ratio on leachability of PAHs. Fixed conditions: Shaking speed=250 rpm, temperature= 55 °C

4.3.2.2 Effect of time, temperature and lixiviant type

The effect of time, temperature and the type of leaching lixiviant can be observed in Figure 4-5. The highest total concentration of PAHs leached was observed when the leaching time was 1.5 hr. The highest concentration of PAHs in the leachate was 12777 µg L^{-1} when using river water at 45°C; from the above observation, it could be said that more PAHs were leached at 1 hour 30 mins because there was just enough interaction between the coal tar and the lixiviant for the mobilisation of PAHs, and no tar was floating in the solutions, so this means that the PAHs were freely available in the aqueous phase. There was no linear relationship between the concentration of PAHs and temperature. As can be seen from all the graphs in Figure 4-5, a high leaching temperature does not correlate with a higher concentration of PAHs in the leachate. For instance, after 3 hours of exposure, high PAH content was recorded in the river water leachate at 25°C. The temperature influence may be affected by other factors such as the repartition of PAHs in the various phases, including the entrapment on the flask/column wall that may lead to some inconsistency.

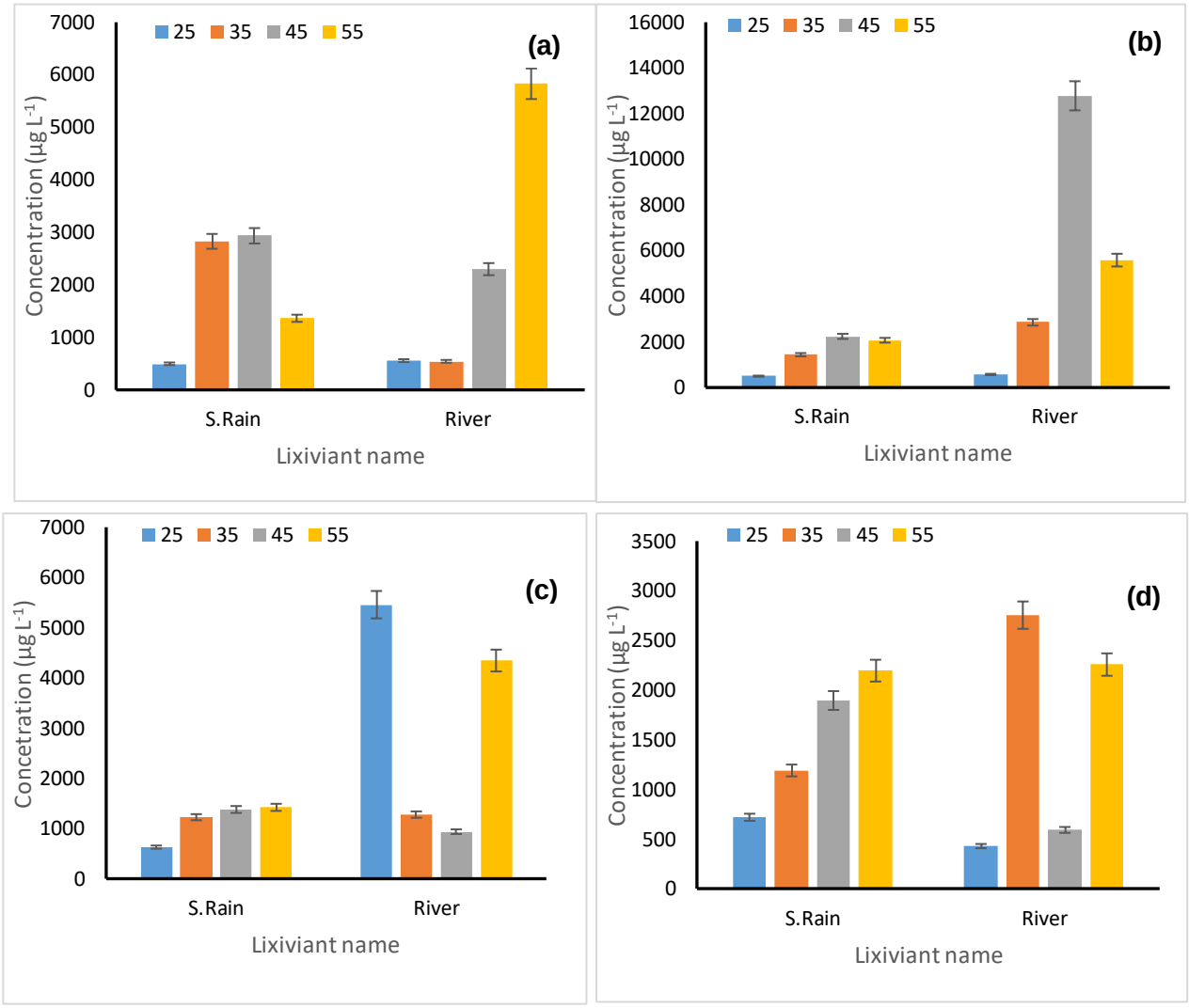

Figure 4-5: The effect of time, temperature and leaching solution on the leachability of PAHs. For a period of (a) 0.5 h, (b) 1.5 h, (c) 3 h, (d) 6 h. Fixed conditions: shaking speed= 250 rpm.n= 3,RSD

4.3.2.3 Individual PAHs concentration

It should be noted that it is very important to understand the leaching behaviour of an individual PAH to study the environmental risks of PAHs. Mixtures of PAHs and individual PAHs have a different impact on the environment due to the difference in their interactions. The concentration of individual PAHs leached after 6 hours at different temperatures is shown in Figure 4-6. For the comparison of the leachability of individual PAHs at different temperatures and types of lixiviants used, an exposure time of 6 h was considered, becauseat this time, almost all the 16 priority PAHs were leached out. A log-scale was used for a better representation of PAHs with a very low concentration in the leachate. Naphthalene was the most abundant PAH released from coal tar, as it is present in high

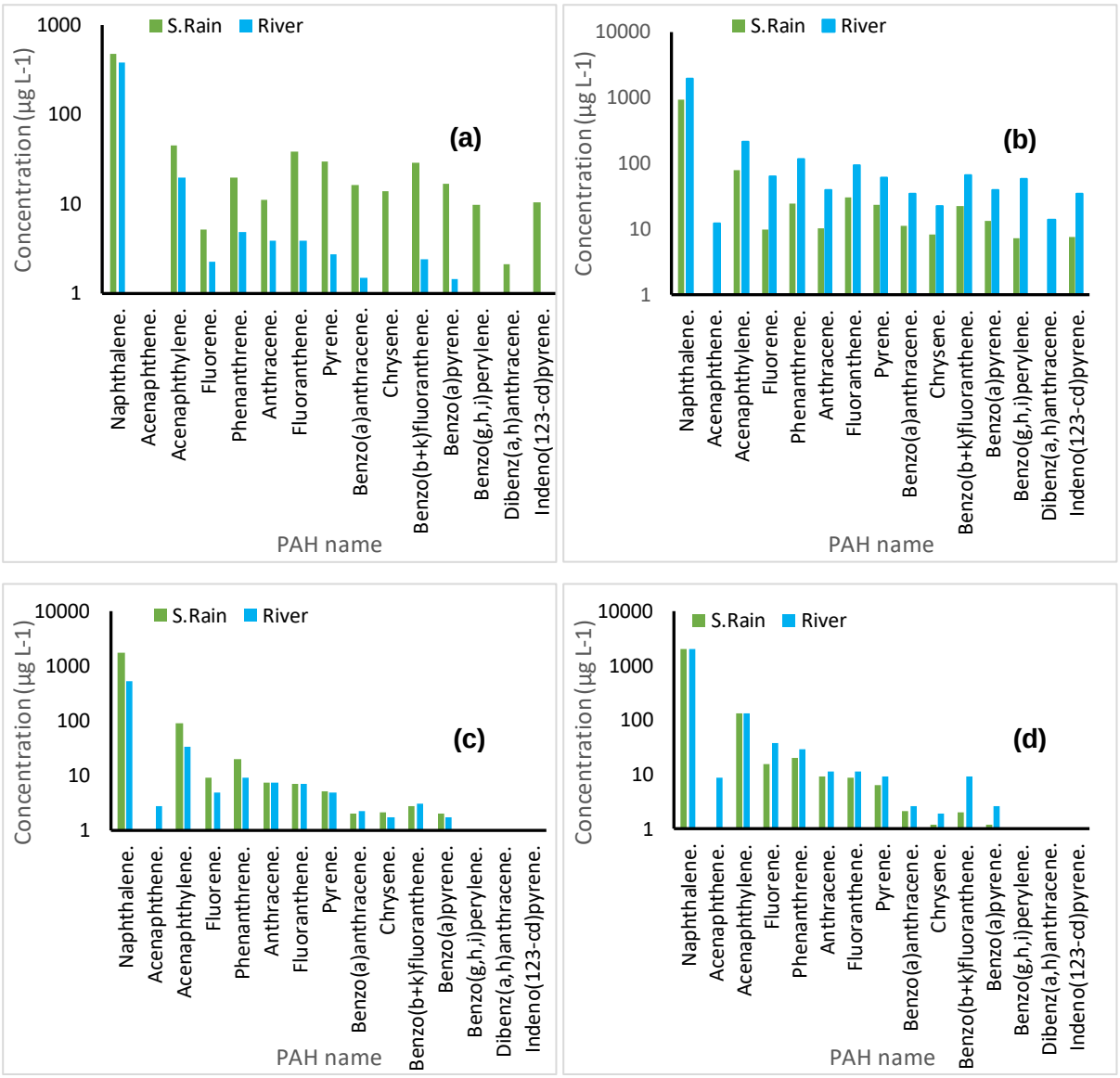

Figure 4-6: Effect of temperature on individual PAHs, at temperature, (a) 25 °C, (b) 35°C,(c) 45°Cand (d) 55°C. Fixed conditions: time= 6h,shaking speed=250 rpm. n=3, RSD

concentrations in all the leachates. Temperature plays a role in enhancing the mobility of PAHs; however, it was difficult to clearly define its impact. It can be seen that the lowest concentration of naphthalene leached is at 25°C. However, it does not mean there was a positive correlation between the concentration of PAHs leached and temperature. What can be deduced is that the leaching process occurring at temperatures above room temperature will likely result in a higher concentration of PAHs in the leachate.

The data represented in Table 4-2 show the results obtained from the analysis of leachate from the samples that were used as control. These samples were put at room temperature, where no agitation took place. Unlike the other batch leaching experiments, these two samples were not placed in the shaker. The results show that almost no PAHs were detected in the control samples. Therefore, it

can be concluded that batch leaching of coal tar in demineralised water mobilises very little PAHs, or it was slow when there are no external factors to enhance the process of leaching.

Table 4-2: Concentration of PAHs samples used as control

PAHs	Water sample 1 concentration ($\mu g\ L^{-1}$)	Water sample 2 concentration ($\mu g\ L^{-1}$)
Naphthalene	<10	<1
Acenaphthene	<10	<1
Acenaphthylene	<10	<1
Fluorene	<10	<1
Phenanthrene	<10	<1
Anthracene	<10	<1
Fluoranthene	<10	<1
Pyrene	<10	<1
Benzo(a)anthracene	<10	<1
Chrysene	<10	<1
Benzo(b+k)fluoranthene	<10	<1
Benzo(a)pyrene	<10	<1
Benzo(g,h,i)perylene	<20	<2
Dibenz(a,h)anthracene	<20	<2
Indeno(123-cd)pyrene	<20	<2

4.3.2.4 Effect of pH

Coal tar may be exposed to water sources with different pH values in different areas. Therefore, it is important to assess the effect of pH on the release of PAHs from coal tars. Figure 4-7 shows the relationship between PAH concentration levels in the leachate and the pH of water. When the pH was less than 6.3,concentration of PAHs in the leachate would decrease as the pH of the solution approaches 6.3. This observation implies that decreasing the pH of the lixiviant (i.e. making the solution more acidic) increases the solubility of PAHs in water and thus increases their mobility. A drastic increase in PAH content in the leachate is observed at pH 8.4, while a further increase of pH (10.3) resulted in a decrease of PAH concentrations. This means that alkaline (moderate) water has the potential of increasing the mobility of PAHs. Even though acidic solutions have shown an appreciable amount of PAHs leached, it does have the same ability to leach as the moderate alkaline solutions (pH 8.4). Lighter molecular weight (LMW) PAHs were more easily leached by both acidic and alkaline solutions than heavy molecular weight (HMW) PAHs.

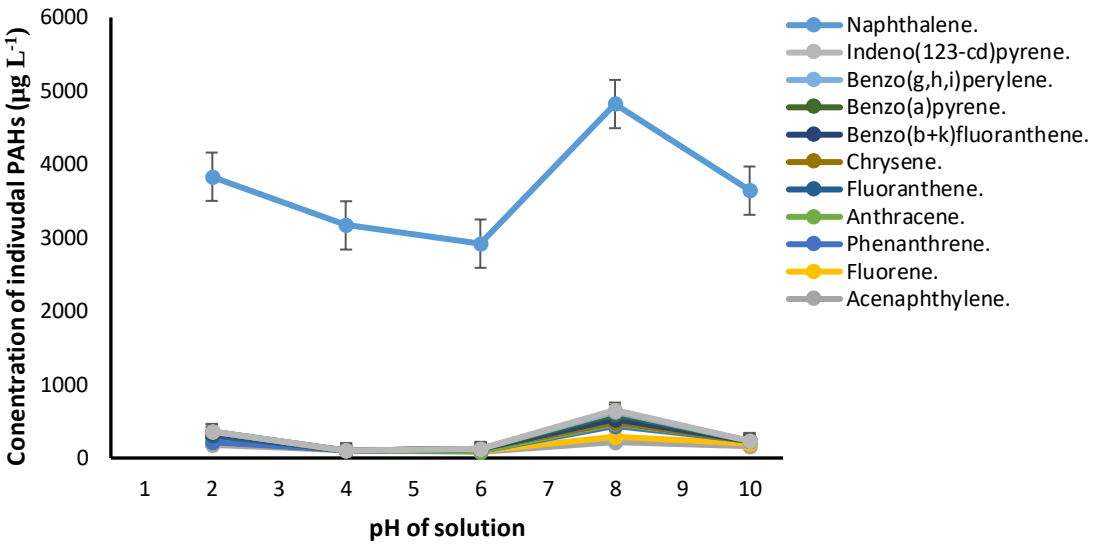

Figure 4-7: Effect of pH on the leachability of individual PAHs. Fixed conditions: shaking speed=250 rpm,temperature= 45°C

When the alkalinity of a solution was extreme (above 8.4), PAH content in the leachate drops. This behaviour is consistent with the findings by Xiaoxing *et al.* (2013) on the influence of pH on the extraction of PAHs from environmental water. In the study by Xiaoxing *et al.* (2013), more PAHs were extracted at pH 6, and a sharp decrease was seen at a pH above 6. Therefore, the optimum pH was 6; in this study, the optimum pH was 8.4. The effect of pH on the release of PAHs cannot therefore be generalised. Besides the pH, the leachability was influenced by factors such as the source of PAHs as well as the pyrolysis temperature. The leachability of PAHs from different sources was likely to show a different trend, depending of the pH of the solution. For the coal tar from the coal coking process to ensure that the leaching of PAHs into the environment is minimised, contact with an excessively acidic solution and moderate alkaline solutions should be avoided.

4.3.3 Column leaching

4.3.3.1 Influence of time and lixiviants on the leaching process

The total concentration of PAHs leached from coal tar into the leaching solution decreases from week 1 to week 2 and then increases from week 2 to week 4, and the total concentration in the leachate in week 4 is always higher than the total concentration in week 1, as evident from Figure 4-8. It should be noted that this trend is observed for all three leaching lixiviants, except for demin water. There was a slight decrease in the sum of the concentration of the PAHs leached for demin water from week 2 to week 3, and there was an increase in a total concentration of PAHs from week 3 to week 4. Even though there was an increase of PAH content in the water from week 3 to week 4, the increase in the concentration was almost equal to the decrease recorded from week 1 to week 2. As can be seen from Figure 4-9, the total concentration of PAHs in week 1 and 4 was almost equal

for the demin water lixiviant. In week 1, the total concentration leached was 964 µg L^{-1}, and in week 4, the concentration was 950.4 µg L^{-1}. The valuable explanation that can be given is that, at week 1, loose PAHs were released in the water. In contrast, from the second week to the fourth week, the increase recorded corresponds to the effect of lixiviants that interact with the coal tar to mobilise the PAHs into solution.

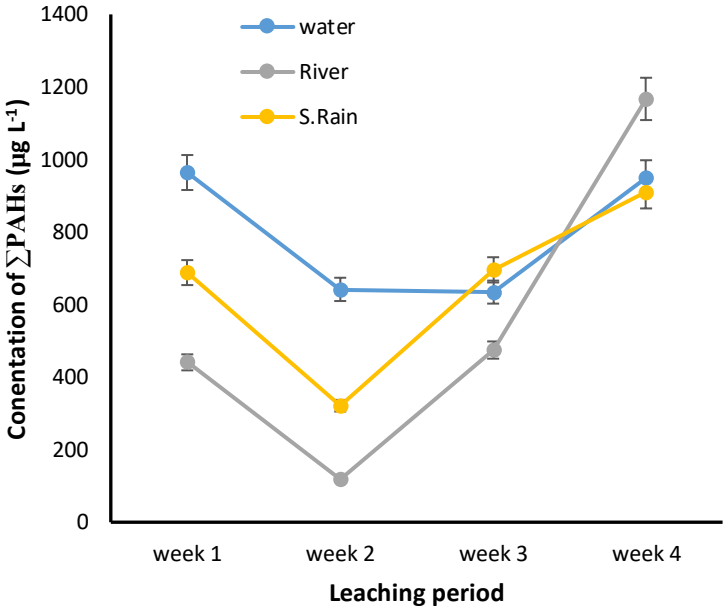

Figure 4-8: Weekly change of PAH concentration in the leachate. Fixed conditions: temperature=room temperature, shaking speed=250 rpm. n=3,RSD

There were more PAHs at week 4 than any other week, implying that, as the exposure time increases, more PAHs were progressively leached into the water, a scenario likely to happen in environmental water if the conditions are conducible. Although a large amount of PAHs was leached from coal tar in week 1, further interaction between water and coal tar over time allowed the weakening of interactions between the more stable PAHs and coal tar, eventually resulting in the breakage of bonds through hydrolysis and their release in solution. Hence, there is a sharp increase of PAH content in the leachate from week 3 to week 4. The same trend is observed with all the other lixiviants (demin water, river water and S. rain). Unlike demin water, the leaching rate does not slow down for the other two lixiviants. River water leached more PAHs than the other two lixiviants used in this study.

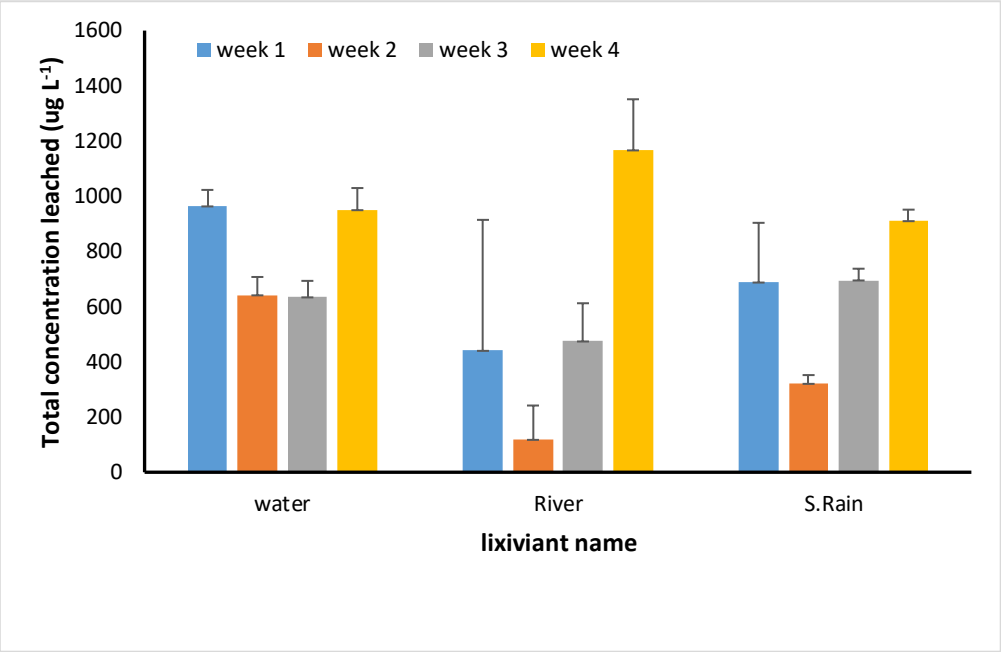

Figure 4-9: Effect of lixiviant type and time on colunm leaching on PAHs. Fixed conditions: temperature= room temperature. N=3, RSD

4.3.3.2 Mobility of PAHs with different ring size

Assessing the fractions of PAHs in the leachate with a different number of rings can give insight into how the mobility of heavier and lighter PAHs differs. As shown in Figure 4-10, the mobility of lighter and heavier PAHs differs considerably. Lighter PAHs (with shorter rings) were more easily leached than heavier PAHs (those with longer rings). For all the lixiviants, the concentration of two and three ring PAHs was higher each week. The proportion of PAHs with more than two rings increases as the leaching time increases. As the leaching period increases, heavier PAHs start to be released. It is evident from Figure 4-10a that, at the beginning of leaching (week 1), only two and three ring PAHs were leached. PAHs with four or more rings started being released into the solution in the second week of the leaching test. Figure 4-10d does indicate that five and six ring PAHs were present in high concentrations in the leachate at the last week of the leaching test. Generally, PAHs with shorter rings are easily mobilised. They are also easily released into the environment (Abdel-Shafy & Mansour, 2016), while a more extended leaching period is required for the release of heavier PAHs. Figure 4-11 clearly shows which PAHs were leached in week 1; as evidenced, only naphthalene, anthracene, fluorene, acenaphthene and acenaphthylene were detected in the leachate. The reason for the release of heavier PAHs only after a longer leaching period may be because they have more binding sites interacting with the coal tar, therefore requiring more energy for the breakage of bonds. Once the lighter PAHs are leached, the heavier PAHs become exposed and start directly interacting with the leaching solution. Consequently, the leaching solution progressively weakens the binding sites with coal tar. Chen *et al.* (2019) found that shorter PAHs were appreciably released from soil into water sources, and the results from Xiaoxing *et al.* (2013) showed that, when the leaching period was longer, heavier persistent PAHs start being leached.

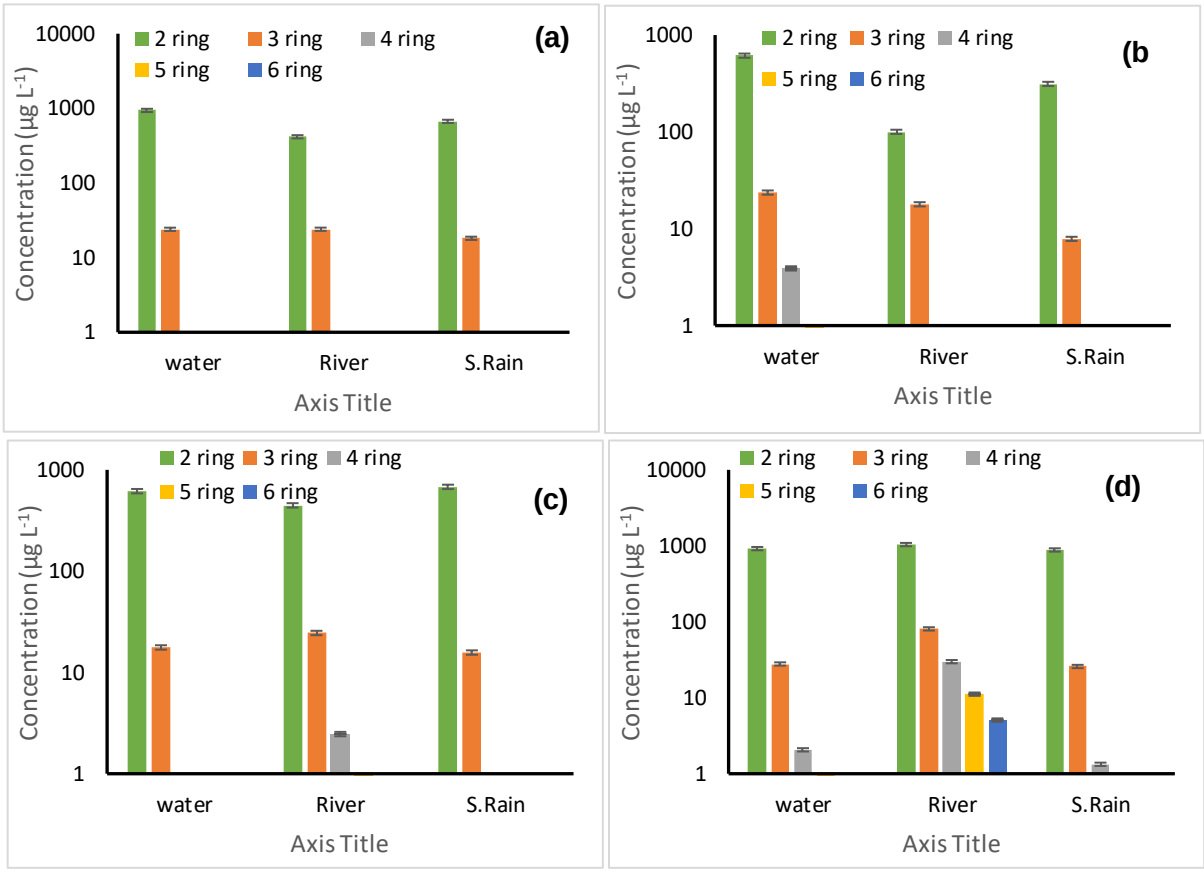

Figure 4-10: Effect of different number of rings of PAHs on the leaching process for week (a) 1 week (b) 2 weeks (c) 3 weeks and (d) 4 weeks. Fixed conditions: temperature= room temperature. n=3, RSD.

Although there was a linear correlation between the leaching period and the occurrence of heavier PAHs in the leachate, there was no positive correlation between the total concentration of PAHs in the leachate and the leaching period. Heavier PAHs may be leached when the leaching period is longer, but their total concentration is still less than that of lighter PAHs in week 1 (shorter leaching period). This observation is well depicted in Figure 4-11, where the total concentration of lighter PAHs (two rings) leached weekly was not increasing with time. For example, the total concentration of two ring PAHs leached in river water after one week was 416.7 µg L^{-1}, and the total concentration of six ring PAHs in week 4 was less than 10 µg L^{-1}.

In week 1, 2, 3 and 4, the concentration of two ring PAHs leached was higher than that of PAHs with more rings for all the lixiviants. This observation implies that the mobility of lighter PAHs was higher than the mobility of heavier PAHs. The type of lixiviant also seems to have an effect on the type of PAH leached over time; river water was found to be the only solution leaching PAHs of five and six rings, while demin water and S. rain water could only leach PAHs of two, three and four rings. Apart from the size of benzene rings, the mobility of PAHs may be enhanced by the constituents of the leaching lixiviants. Therefore, in this case, constituents (such as microorganisms and metals) that

are contained in the river water and pH may stimulate the mobility of PAHs; hence river water was the only lixiviant that could leach PAHs with more than four rings.

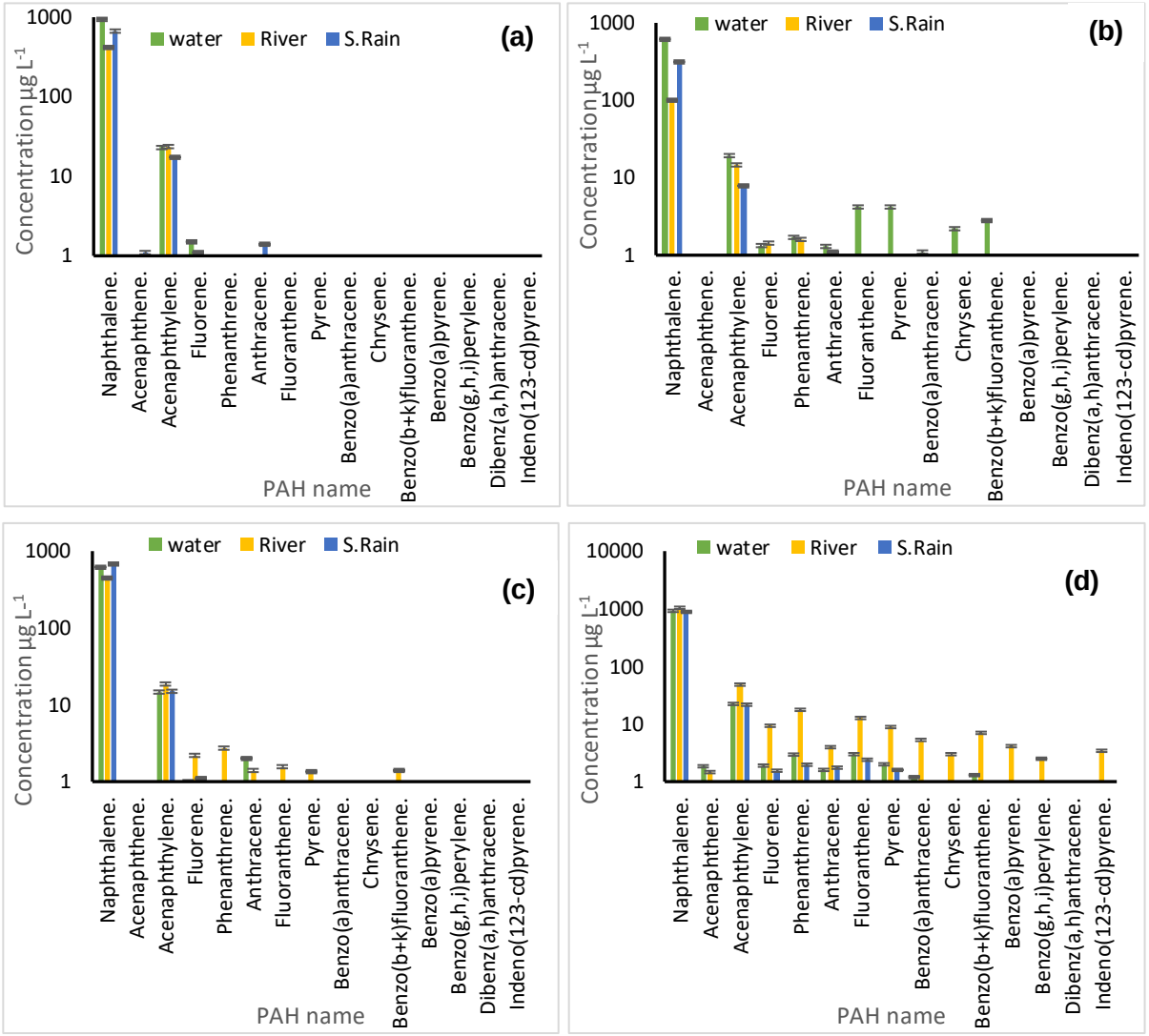

Figure 4-11: Behaviour of individual PAHs with increasing leaching time,(a) 1 week, (b) 2 weeks , (c) 3 weeks,and (d) 4 weeks

4.4 Conclusion

This study aimed to establish the potential of various environmental aqueous solutions to mobilise PAHs from coal tar deriving from the coking process. It was found that the ability to mobilise PAHs varied with a different type of solution; river water was found to be more effective in the quantitative removal of PAHs, and more importantly, was the most effective solution for the mobilisation of benzo(a)pyrene, which is one of the most toxic PAH. Overall, more PAHs were easily mobilised at above room temperature (25˚C), while acidic and moderate alkaline pH values were suitable for the mobilisation of PAHs. More exposure time was required to mobilise heavy PAHs (five to six membered benzene rings) compared to light PAHs (less than four membered benzene rings), which were already mobilised from the first week. This study is a pioneering work in understanding the effect of the properties of environmental water on the mobilisation of PAHs from coal tar derived from the coking process.

References

Abdel-shafty, H.I., & Mansour, M.S. 2016. A review of polyclic aromatic hydrocarbons: source, environmental impact, effect on health and remediation. *Egyptian Journal of Petroleum*, (25) 107-123.

Arcelor Mittal South Africa, Parliament colloqium on beneficiation, 24 August 2014, 2014. https://www.thedti.gov.za/parliament/2014/ArcelorMittal.pdf. Accessed 15 June 2019.

Bhutto, A.W., Bazmi, A.A., Zahedi, G. 2013 Underground coal gasification: From fundamentals to applications, *Progress in Energy and Combustion Science*, 39, 189 – 214.

Bieda, B., Grzesik, K., Sala, D. and Gawel, B. 2015. Life cycle inventory processes of the integrated steel plant (ISP) in Krakow, Poland – coke production, a case study, *International Journal of Life Cycle Assess*, DOI 10.1007/s11367-015-0904-9,20:1089-1101

Blignaut, J.N. and Hassan, R.M. 2002. Assessment of the performance and sustainability of mining sub-soil assets for economic development in South Africa, *Ecological Economics*, 40, 89-101.

Cai, T., Ding, Y., Zhang, Z., Wang, X., & Wang , T. 2019, July 29. Effects of total carbon content and leaching water volume on migration of Polyclic aromatic hydrocarbons in soils by column leaching. *Environmental Pollution* (254) 112981.

Chen, X., Yang, L., Myneni, S.C., & Deng, Y. 2019. Leaching of polycyclic aromatic hydrocarbons (PAHs) from sewage sludge-derived coal biochar. *Chemical Engineering Journal*, 1385-8947.

Covell, J.R., Thomas, M.H. 1996. Combined air sparge and bioremediation of an underground coal gasification site. US DOE. DOE/MC/31346-97/C0830.

Fosso-Kankeu, E., Barlow, B. Lemmer, N. & Waanders, F. 2017. Geochemical speciation of metal ions in the leachate of tailings treated with synthetic rain water. 9th Int'l Conference on Advances in Science, Engineering, Technology & Waste Management (ASETWM-17). 27-28 November 2017, Parys, South Africa. Editors: F. Waanders, E. Fosso-Kankeu, B. Topcuoglu, M. Plaisent, Y. Thaweesak. ISBN: 978-81-934174-6-1. Pp. 19-23.

Hancox, P.J. & Gotz, A.E. 2014 South Africa's coalfields – A 2014 perspective, *International Journal of Coal Geology*, 132, 170-254.

Haritash, A. & Kaushik, C. 2009. Biodegradation aspects of polycyclic aromatic hydrocarbons (PAHs): a review. *Journal of Hazardous Materials*, 169(1) 1-15.

Hartnady, C.J.H. 2010. South Africa's diminishing coal reserves, *South African Journal of Science*, 106(9/10), 369-374.

Heinberg, R. & Fridley, D. 2010. The end of cheap coal, *Nature*, 468, 367-369.

Kapusta, K. & Stanczyk, K. 2011. Pollution of water during underground coal gasification of hard coal and lignite, *Fuel*, 90, 1927-1934.

Kruger, O., Kalbe, U., Simon, F., & Lopez Meza, S. 2012. Leaching experiments on the release of heavy metals and PAH from soil and waste materials. *Journal of Hazadous Materials* (207-208) 51-55.

Lindblom, S.R., Smith, V.E. 1993. Rocky Mountain 1 underground coal gasification test Hanna, Wyoming. Groundwater Evaluation. Final Report. US DOE. DOE/MC/25038-3652.

Quass, J.D. and Skinner, F.D. 1987. Process description of the Sasol I coal gasification plant: Topical report. Gas Research Institute, *Environment and Safety Research*, Chicago, USA.

Shafiee, S., Topal, E. 2008. An econometric view of worldwide fossil fuel consumption and the role of US. *Energy Policy*, 36, 775-786.

Shu-qin, L., Jing-gang, L.I., Mei, M., Dong-lin, D. 2007. Groundwater pollution from underground coal gasification, *Journal of China University of Mining and Technology*, 17(4), 467-472.

Stuermer, D.H., Ng, D.J., Morris, C.J. 1982. Organic contaminants in groundwater near an underground coal gasification site in northeastern Wyoming, *Environmental Scientific Technology*., 16, 582 – 587, 1982.

United States Environmental Protection Agency (USEPA). 2009. PAH priority pollutants.

Walker, L.1999. Underground coal gasification: a clean coal technology ready for development, *Australian Coal Review*, 19-21.

Wolde-Rufael, Y. 2010. Coal consumption and economic growth revisited, *Applied Energy*, 87, 160-167.

World Energy Council, Survey of Energy Resources. 2010. available at http://go.nature. com/hde5r7.

Xiaoxing, L., Yeqing, S., & Jingru, Z. 2013. The influence of pH on extraction of PAHs in environmental water by solids phase microextraction. *Advanced Material Research* (726-731) 479-482.

CHAPTER 5: PAPER 3

Bi_2MoO_6 nanoplates supported on reduced graphene oxide: An effective nanocomposite for removal of naphthalene via adsorption-photodegradation

Shelter Maswanganyi, Rashi Gusain, Neeraj Kumar, Elvis Fosso-Kankeu, Frans Waanders, Suprakas Sinha Ray

ABSTRACT

Polycyclic aromatic hydrocarbons (PAHs) are a class of persistent organic water pollutants causing serious concerns due to their carcinogenic and other negative impact on humans and the ecosystem. In this study, RGO-Bi_2MoO_6 nanocomposites were designed and prepared for the adsorption-assisted photodegradation of naphthalene molecules in an aqueous medium. Synthesised Bi_2MoO_6 and RGO- Bi_2MoO_6 nanocomposites were characterised by XRD, FTIR, SEM, HRTEM, XPS, UV, BET and PL. The photocatalytic characteristics of the synthesised samples were assessed by the photodegradation of naphthalene molecules under visible light. A dosage of 0.3 g L^{-1} of the synthesised material was introduced into the 50 mg L^{-1} naphthalene-contaminated simulated wastewater and exposed to visible light irradiation for the degradation of naphthalene. RGO-Bi_2MoO_6 exhibited significantly improved photocatalytic efficiency in comparison to pure Bi_2MoO_6. Comparing the photocatalytic efficiency of all RGO-Bi_2MoO_6 nanocomposites, RGO-Bi_2MoO_6 (2 wt %) showed the best photocatalytic activity. It was observed that the incorporation of RGO enhanced the visible light absorption and delayed the recombination rate of photogenerated charge carriers. Moreover, RGO-Bi_2MoO_6 nanocomposite showed excellent reusability for the five cycles.

Keywords*:* Graphene, Two-dimensional (2D) materials, Water purification, Photocatalysis, Adsorption, PAHs

5.1 Introduction

Water pollution remains a global challenge that cannot be eliminated because the majority of the water pollutants come from anthropogenic activities that are crucial to human lives. These anthropogenic activities may release water effluents with contaminants, which include heavy metals, pesticides, chemical waste, hydrocarbons and persistent organic pollutants (Kabra *et al*., 2004; Quesada *et al*., 2019; Gusain *et al*., 2020; Ray *et al*., 2020). Persistent organic pollutants, particularly polycyclic aromatic hydrocarbons (PAHs), attract a lot of attention in water pollution studies, owing to their toxic, mutagenic and carcinogenic potential (Abdel-Shafy & Mansour, 2016; Mojiri *et al*., 2019). PAHs are defined as a group of organic compounds that comprises two or more benzene rings attached to each other in a clustered, linear or angular arrangement. Around 16 PAHs in the environment are listed as priority contaminants by the US Environmental Protection Agency (US-EPA) (Mojiri *et al*., 2019). Most of the environmental hazardous PAHs originate from industries (coke production, sewage sludge, organic waste), domestic heating (burning coal, wood, gas, incomplete combustion of fossil fuels, cigarettes), agricultural sources (pesticides), and natural sources (volcanic eruption, decaying organic matter, forest fires) (Mojiri *et al*., 2019; Walaszek *et al*., 2018). PAHs from industrial processes can enter water bodies through leachates from dump sites, coal mines and steel making plants (García-Martínez *et al*., 2018).

Continuous exposure to PAHs in the environment results in detrimental impacts on the flora and fauna. Humans are exposed to PAHs through breathing, drinking, dermal contact and ingestion of food grown in PAH contaminated soil (Rengarajan *et al*., 2015). Additionally, regular exposure to PAHs can lead to different health effects in humans, which include skin irritation, diarrhoea, breathing problems, skin and lung cancer (Mojiri *et al*., 2019). Due to the negative health impacts, there has been widespread attention on investigating effective methods for the removal of PAHs from water. Removal of PAHs from the aquatic environment can be achieved through different techniques, such as physical, chemical and biological methods (Adeola & Forbes; Lamichhane *et al*., 2016; Zeng *et al*., 2000; Zheng *et al*., 2007; Gusain *et al*., 2020). According to previous studies, physical and biological methods have the potential to remove PAHs from water; however, they are inefficient, as they cannot completely remove or degrade PAHs. They remain in the environment as secondary generated waste. Due to challenges such as the toxic nature, complexity and costs associated with using physical and biological methods, chemical wastewater treatment such photocatalysis, Fenton's reagent, peroxonation, ozonation methods have been widely used as an alternative for removing PAHs from the aquatic environment (Oturan & Aaron, 2014; Mukwevho *et al*., 2018; Mukwevho *et al*., 2019). Among all chemical methods, photocatalytic degradation has been widely investigated due to its advantages of being clean, cost-effective, simple and more efficient than other chemical methods.

In recent years, several organic and inorganic materials have been used as photocatalysts for PAH degradation purposes (García-Martínez *et al*., 2006; Nguyen *et al*., 2020). Recently, bismuth-based semiconductor materials have been extensively studied for photocatalysis purposes due to their high light application efficiency, corrosion resistance, low cost, ability to respond to both UV and visible light, chemical inertness, non-toxicity and catalytic properties (Guo *et al*., 2018; Wang *et al*., 2016). Owing to its narrow band gap (~2.7 eV), bismuth molybdate (Bi_2MoO_6) is a preferable semiconductor material, among many bismuth based photocatalysts, for water contaminant degradation under visible light irradiation (Martinez-de La Cruz & Alfaro, 2010; Zhang *et al*., 2015; Ding *et al*., 2017,). However, the fast recombination of photo-generated charge carriers (i.e. electrons and hole pairs), reduces the efficacy of Bi_2MoO_6 photocatalysts. To further improve the photocatalytic performance of Bi_2MoO_6 and address this limitation, Bi_2MoO_6 is usually supported with organic or inorganic materials to supress the recombination of electrons and holes.

In this study, Bi_2MoO_6 nanoplates were grown over different amounts of reduced graphene oxide for the formation of the RGO-Bi_2MoO_6 nanocomposite using the hydrothermal method; its photocatalytic performance on the degradation of naphthalene in simulated wastewater was examined. The impact of different factors such as reaction time, amount of dopant, and pollutant concentration in water was used to assess the efficiency of the prepared catalyst. To test the PAH degradation efficiency of RGO-Bi_2MoO_6, naphthalene was used as a representative model of PAH as a water contaminant. The performances of pure Bi_2MoO_6 and RGO-Bi_2MoO_6 nanocomposites during the photodegradation of naphthalene were then compared.

5.2 Experimental Section

5.2.1 Chemicals

Bismuth(III)nitrate pentahydrate ($Bi(NO_3)_3.5H_2O$-98%), sodium molybdate dehydrate ($Na_2MoO_4{\cdot}2H_2O$ - 99%), and ethylene glycol (99%) were purchased from Sigma-Aldrich,Kempton park,South Africa and were used together with ethanol (99%), which was obtained from Minema, Roodepoort,South Africa for the synthesis of Bi_2MoO_6. The synthesis of graphene oxide involved the use of H_2O_2, HCL, H_2SO_4/H_3PO_4, $KMnO_4$, and graphite powder. Naphthalene flakes used for the preparation of PAH contaminated water was purchased from Associated Chemical Enterprises (ACE), Johannesburg, South Africa. Deionised water was used in all experiments. All chemicals were analytically pure and were utilised with no further purification.

5.2.2 Synthesis of Bi_2MoO_6

Bi_2MoO_6 was prepared by mixing the Bi and Mo precursors at room temperature. $Bi(NO_3)_3{\cdot}5H_2O$ (1.212 g) was taken as Bi precursor and dissolved in ethylene glycol (5 mL), whereas the Mo precursor, i.e. $Na_2MoO_4{\cdot}2H_2O$ (0.0302) was dissolved in ethanol (30 mL). This was followed by mixing both solutions at room temperature for 200 minutes until a brownish solution was acquired.

The obtained brownish solution was transferred into a Teflon lined stainless steel hydrothermal autoclave for hydrothermal treatment at 160°C for 16 hours. Subsequently, the solution in the autoclave was allowed to naturally cool down at room temperature. After hydrothermal treatment, the obtained precipitate was collected from the solution via centrifugation. For the removal of impurities, the precipitate was washed thoroughly using deionised water via centrifugation several times and dried in a vacuum oven for 24 hours at 60°C.

5.2.3 Synthesis of Graphene Oxide (GO)

GO was synthesised by following the improved Hummer's method. In this typical procedure, 3.0 g commercially available graphite powder was added to the concentrated 400 mL H_2SO_4/H_3PO_4 (9:1 by volume) solution. In the above solution, 18.0 g $KMnO_4$ was added slowly and uninterruptedly stirred for 12 hours (Kumar *et al*., 2020). Due to the exothermic nature of the reaction, the reaction mixture produces slight heat, and the reaction temperature was maintained at 50°C. Thereafter, the reaction mixture was allowed to cool at room temperature and charged with ice (500 mL) and 3 mL 30% H_2O_2. The oxidised GO was collected via centrifugation, and the supernatant was decanted away. The solid brown precipitate was washed several times with deionised water, 10% HCl, and finally with ethanol. The obtained brown GO was exfoliated up to a few layers ofGOthrough ultra-probe sonication in the water. The GO solution in aqueous media was further employed to prepare the RGO-Bi_2MoO_6

5.2.4 Synthesis of RGO-Bi_2MoO_6

Several RGO-Bi_2MoO_6 nanocomposites were prepared using different amounts of RGO (2, 5 and 10 wt %) with Bi_2MoO_6. In a typical procedure, to synthesise RGO-Bi_2MoO_6 (10 wt%), it was prepared as follows: 0.7272 g Bi $(NO_3)_3 \cdot 5H_2O$ was dissolved in 5 mL of ethylene glycol and followed by the addition of 40 mg GO in water dispersion. The reaction mixture was stirred for 10 minutes at room temperature. Subsequently, 0.1812 g $Na_2MoO_4 \cdot 2H_2O$ was dissolved in 30 mL ethanol and added to the above solution and further stirred for 30 min. The prepared mixture was poured into the Teflon lined stainless steel hydrothermal autoclave for hydrothermal treatment at 180°C for 16 hours. The resulting sample was naturally cooled at room temperature and followed by washing and drying in the same way as the Bi_2MoO_6 sample. Other samples of RGO-Bi_2MoO_6 were prepared following the same route, using 20 mg and 8 mg GO for RGO-Bi_2MoO_6 (5 wt%) and RGO-Bi_2MoO_6 (2 wt%) nanocomposite, respectively.

5.2.5 Characterisation techniques

An x-ray diffraction (XRD) analysis was utilised to determine the crystallinity, purity and phase of the synthesised samples. XRD patterns were obtained from Philips Analytical X'Pert PRO PW 3050/60, at 40 kV voltage with Cu Kα radiation in a range of 5-90° (2θ) diffraction angle. Fourier transformation infrared spectra (FT-IR) were acquired in the range 400-4000 cm^{-1} with a Perkin Elmer Spectrum

100 FTIR spectrophotometer using KBr pellets. The morphology and the structural features of synthesised materials were investigated utilising scanning electron microscopy (SEM) on a Zeiss Auriga Cobra FIB magnifying instrument. The characteristic elemental distribution of the samples was analysed using an energy-dispersive x-ray spectrometer (EDX, Oxford, UK) coupled with the FESEM. The size and high resolution structural images of the samples were further investigated using high resolution transmission electron microscopy (HRTEM) on JEOL JEM-2100. To investigate the chemical composition, the oxidation states and binding energies of each element in the nanocomposite material, x-ray photoelectron spectroscopy (XPS) measurements were done using Kratos Axis Ultra device (Kratos, UK) using a monochromatic (Al Kα) excitation source for the Bi_2MoO_6 and RGO-Bi_2MoO_6. The background of the XPS spectrum for each material is corrected using Shirley background correction, and all the recorded XPS peaks were constructed using Gaussian functions. The specific surface area and porosity of the samples were recorded on a Micromeritics (ASAP 2020, USA) analyser using nitrogen adsorption desorption isotherms. UV–vis absorbance analysis was executed using LAMBDA 750 UV−vis−NIR spectrophotometer (PerkinElmer, USA). Photoluminescence (PL) spectroscopy was conducted on a Horiba Jobin-Yvon NanoLog spectrometer with a Xe lamp, excited at 325 nm.

5.2.6 Adsorption and photodegradation studies

The prepared nanocomposite was examined for its adsorption and photocatalytic potential in wastewater treatment sample. In the adsorption process, 30 mg of the RGO-Bi_2MoO_6 (2 wt %) was added in 100 mL of naphthalene aqueous solution with a concentration of 50 mg L^{-1} under dark conditions. The mixture was continuously agitated using a magnetic stirrer for 90 minutes. The sampling of the solution was done at consistent time intervals and filtered with single use syringe filters. Then, the filtered solution was used to monitor the amount of naphthalene remaining in the solution after the interactions between the naphthalene molecules and the surface of the adsorbent. The remaining concentration was checked using UV-vis adsorption spectra. The change in the naphthalene concentration in the solution were interpreted using the height of the peak at 275 nm wavelength in the spectra (changes in intensity of the UV-vis absorbance). The data from the UV-vis spectra were used to calculate the remaining concentration in the solution.

The photocatalytic potentials of the prepared Bi_2MoO_6 and RGO-Bi_2MoO_6 nanocomposites were assesed by measuring the degradation of naphthalene in an aqueous solution under visible light. Naphthalene was used as a model PAH water contaminant. Simulated wastewater was prepared by dissolving naphthalene flakes in a 10% methanol aqueous solution at room temperature. In each test, 30 mg photocatalyst was completely suspended in 100 mL of 50 mg L^{-1} simulated naphthalene contaminated wastewater. Prior to exposure to UV-visible light, the solution was magnetically agitated in the dark for 30 minutes to establish an adsorption-desorption equilibrium between naphthalene and the surface of the photocatalyst. A volume of 5 mL reaction solution was extracted

before the light was turned on to initiate the photocatalytic degradation of naphthalene present in water. Then, simulated naphthalene contaminated wastewater was exposed to visible light for 60 min. At different time intervals, approximately 5 mL of the reaction solution aliquot was added. To ensure that the collected reaction solution does not contain the catalyst, the sample aliquot was passed through a syringe filter (0.45 µm). The remaining concentration of naphthalene after the photodegradation process in collected samples were analysed under a Lambda 750S UV/VIS spectrophotometer (PerkinElmer) at 200-500 nm wavelength, using distilled water as the background. The intensity at 275 nm of UV-vis diffuse spectra indicated the amount of the remaining naphthalene in the wastewater. To evaluate the adsorption ability of the prepared photocatalyst, another reaction was set in the dark for 60 minutes and was sampled at the time intervals mentioned above. All collected samples were analysed using a UV-vis spectrometerResults and discussion

5.3 Results and discussion

5.3.1 Characterisation

Figure 5-1 shows the XRD peaks of the prepared pure Bi_2MoO_6 and RGO-Bi_2MoO_6 nanocomposite materials. On comparing the XRD peaks of pure Bi_2MoO_6 and various RGO-Bi_2MoO_6 nanocomposites, no significant changes can be observed. The RGO XRD diffraction peaks were not detected in the XRD of RGO-Bi_2MoO_6, which could be a result of high crystallinity and strong diffraction pattern of Bi2MoO6 and low concentration of RGO. The sharp and intense peaks in XRD indicated that the samples prepared have a high degree of crystallinity. All as-prepared samples showed characteristic peaks of (020), (111), (131), (200), (002), (151), (062), (331), and (262) planes at 2θ = 10.98 °, 23.54°, 28.31°, 32.17°, 35.96°, 46.97°, 55.87° and 88.36°. These diffraction peaks can be perfectly assigned to the pure orthorhombic phase of Bi_2MoO_6, which are consistent with the standard card JCPDS no.76-238 (Zhang et al., 2010). Moreover, no diffraction peaks from other phases were detected, indicative of high purity and structure stability of RGO-Bi_2MoO_6 nanocomposites.

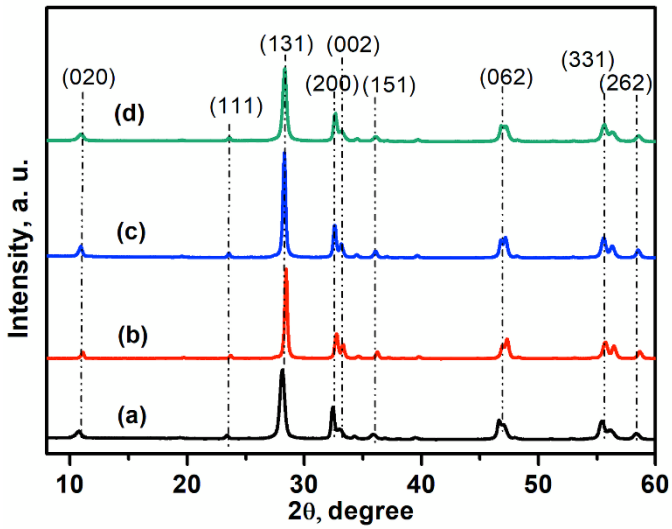

Figure 5-1: XRD diffractions patterns of (a) Bi_2MoO_6, and RGO-Bi_2MoO_6 at (b) 2 wt%, (c) 5 wt%, and (d) 10%

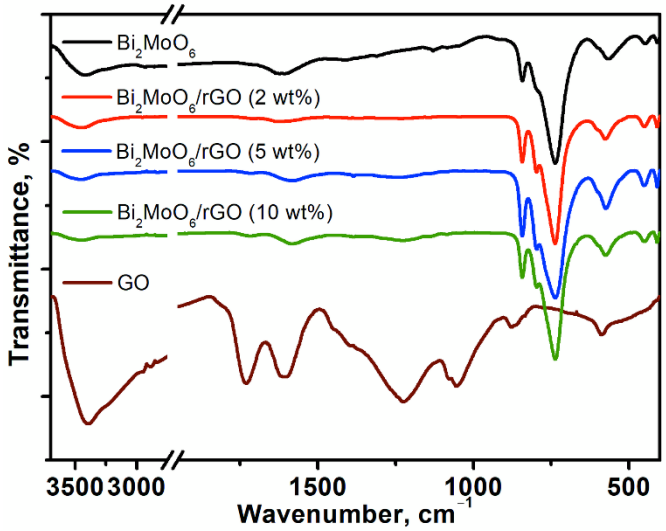

Figure 5-2: FTIR spectra of Bi_2MoO_6 nanoplates,GO and RGO-Bi_2MoO_6 (2,5 and 10 wt%) nanocomposites

The standard GO spectrum exhibited relatively small absorbance bands at wavenumbers between 3500-1000 cm^{-1}, which can be attributed to the representative oxygenic functional groups. The absorbance band identified in the GO spectrum is due to O-H stretching (3394 cm^{-1}), C=O (1724 cm^{-1}), C=C bending (1604 cm^{-1}), C-OH (1215 cm^{-1}) and C-O (1047 cm^{-1}) (Xiao *et al*., 2018, Kumar *et al*., 2016). Another peak is observed at the 590 cm^{-1} wavenumber, which can be ascribed to the O-H out of plane band. However, some of these peaks did not appear in the RGO-Bi_2MoO_6 FTIR spectrum, or the intensity of these peaks were reduced significantly, which further confirmed that the GO was reduced to RGO during the preparation of the nanocomposite.

The surface morphologies of pure Bi_2MoO_6 and RGO-Bi_2MoO_6 (2 wt %) composites were examined by scanning electron microscopy (SEM). The SEM images in Figure 5-3a clearly showed the

formation of irregular nanoplates, like the structure of pure Bi_2MoO_6. Figure 5-3b-c shows the SEM images of RGO-Bi_2MoO_6 (2 wt %) nanocomposites, which illustrated that the formation of hybrid nanostructure material was composed of irregular nanoplate morphologies. Owing to this, it was deduced that the incorporation of RGO in Bi_2MoO_6 particles strongly influences the surface morphology of Bi_2MoO_6. The SEM images of the RGO-Bi_2MoO_6 (2 wt%) nanocomposite also revealed that there exists a strong interaction between RGO nanosheets and Bi_2MoO_6 nanoplates, as it can be clearly seen from the images, that almost all Bi_2MoO_6 particles were perfectly embedded on the RGO thin nanosheets.

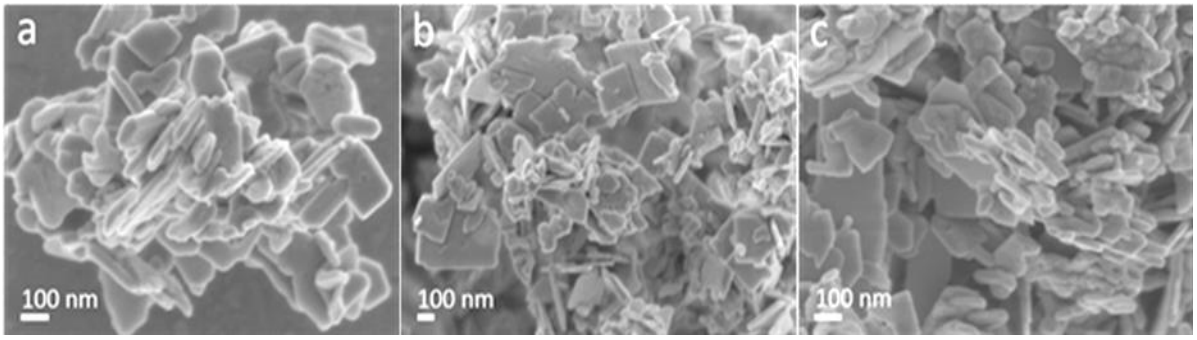

Figure 5-3: SEM images of Bi_2MoO_6 nanoplates (a) and RGO-Bi_2MoO_6 (2 wt%) nanocomposite (b-c)

The high-resolution images of the RGO-Bi_2MoO_6 (2 wt %) nanocomposite was further investigated by TEM, which provided the internal structure of the synthesised monohybrid material. Figure 5-4a showed a high-resolution morphological image of GO thin sheets with a multilayer structure. Figures 5-4b and d showed the high-resolution morphological images of flat-like irregular nanoplates of pure Bi_2MoO_6. The lattice fringe d-spacing in Figures 5-4c-d of 0.319 nm corresponds to the (111) plane of orthorhombic Bi_2MoO_6. In contrast to GO, the RGO in Figure 5-4e-f exhibited transparent wrinkled surface nanosheets, which was an indication that RGO has a good transmittance compared to GO. Figures 5-4e-f clearly revealed the interfacial cross-mixing structure of RGO nanosheets and Bi_2MoO_6 nanostructured material. Figure 5-4g exposed the interlayer spacing of 0.36 nm in RGO nanosheets, which is characteristic of the (002) plane of a few layer reduced GO.

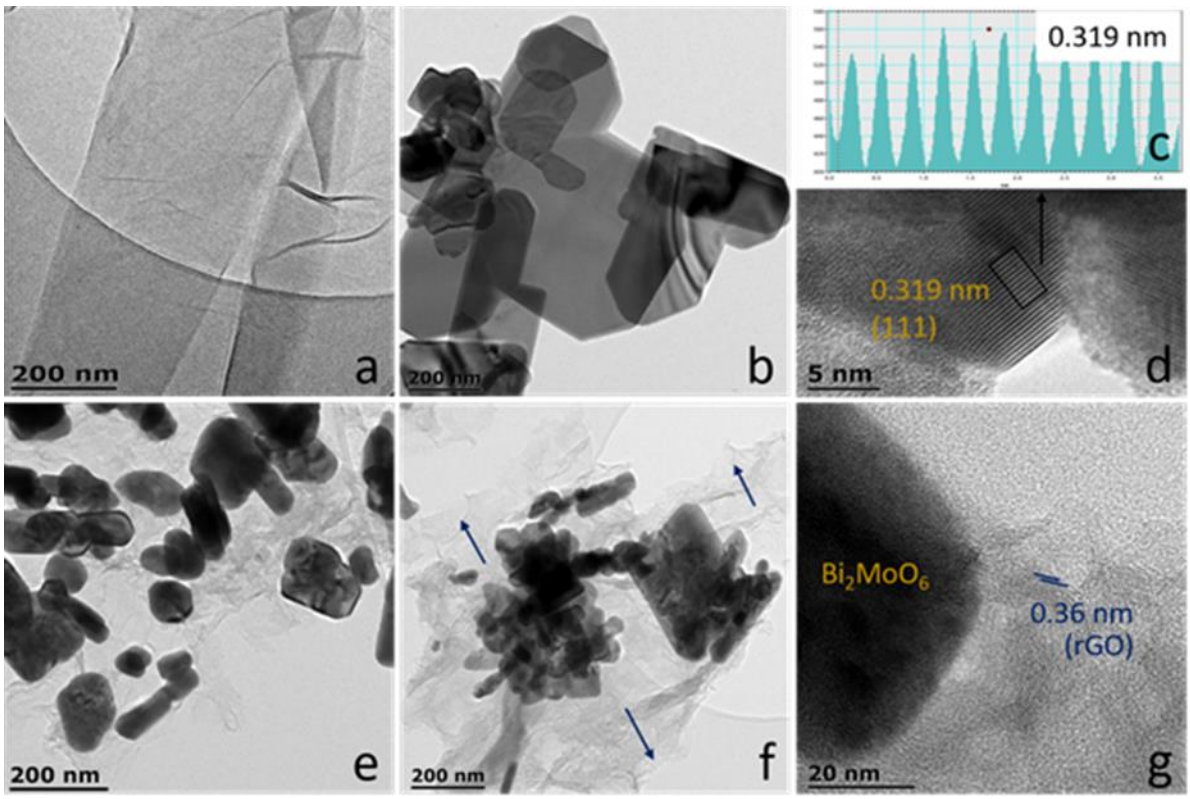

Figure *5-4*:TEM image of GO (a), Bi_2MoO_6 nanoplates (b, d), d-spacing calculation using the average of 10 fringes of a particular area of Figure d (c),and RGO-Bi_2MoO_6 (2 wt %) nanocomposit(e-f)

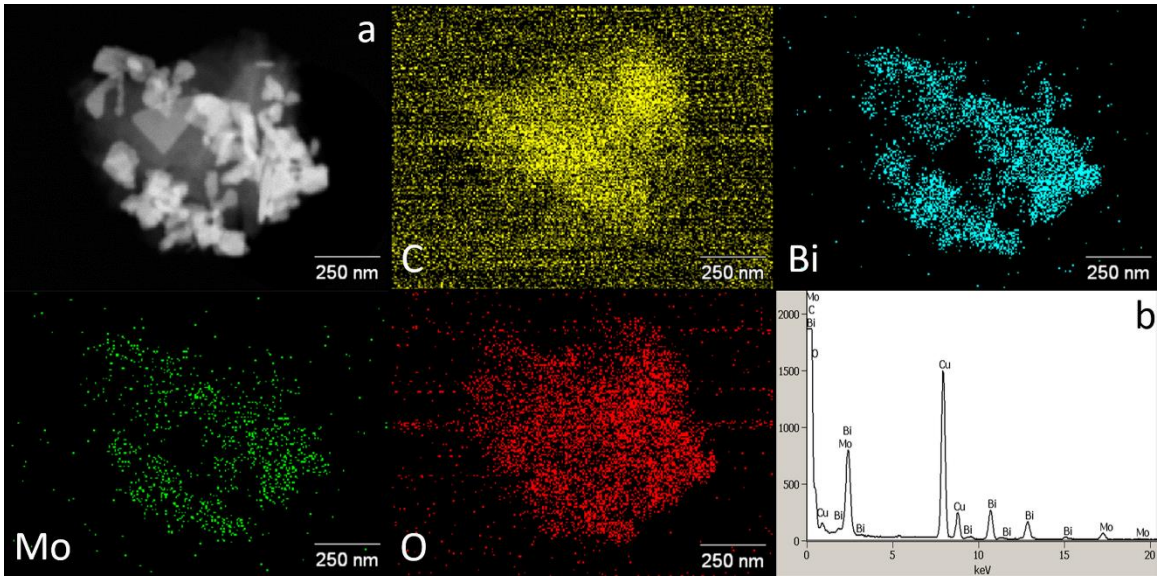

Figure 5-5: Scanning tunnelling electron microscopy (STEM) image, followed by energy-dispersive X-ray (EDX) mapping images that exhibit the homogenous distribution of C,Bi,Mo and O; (b) EDX spectrum of RGO-Bi_2MoO_6 (2 wt%) nanocomposite

The X-ray photoelectron spectroscopy was utilised to analyse the surface composition and the elemental chemical states of the RGO-Bi_2MoO_6 nanocomposite. Figure 5-6a depicts the survey spectrum for the RGO-Bi_2MoO_6 (2 wt%) and pure Bi_2MoO_6, which exhibited characteristic peaks for O 1s, C 1s, Mo 3d and Bi 4f, with no other impurities. In addition, the spectrum for the RGO-Bi_2MoO_6 (2 wt%) showed a much stronger peak of the carbon element (C 1s) compared to that of pure Bi_2MoO_6, which indicated the comparatively high concentration of C due to the presence of RGO. Figure 5-6b depicts the C 1s high resolution spectrum, which can be simplified into four peaks at 284.7, 286.2, 287.5 and 288.7 eV. The peaks at 284.7 and 286.2 eV are associated with the sp^2 carbon (C=C) and sp^3 carbon (C-C/C-O-C/C-OH) in the material, respectively (Kumar *et al*., 2018). Other peaks at 287.5 and 288.7 eV are ascribed to the carbonyl carbons (C=O) and COOH, respectively. The O 1s XPS spectra for pure Bi_2MoO_6 (Figure 5-6c) shows three separated peaks at 529.8, 530. and 531.7 eV, which can be indexed to Mo-O, Bi-O and surface hydroxyl groups, respectively (Zhao *et al*., 2015). However, the O 1s spectrum for RGO-Bi_2MoO_6 showed four separated peaks with a high intensity of 531.7 eV peak and one extra peak at 533 eV, which was due to the C-O and C=O functional groups, respectively.

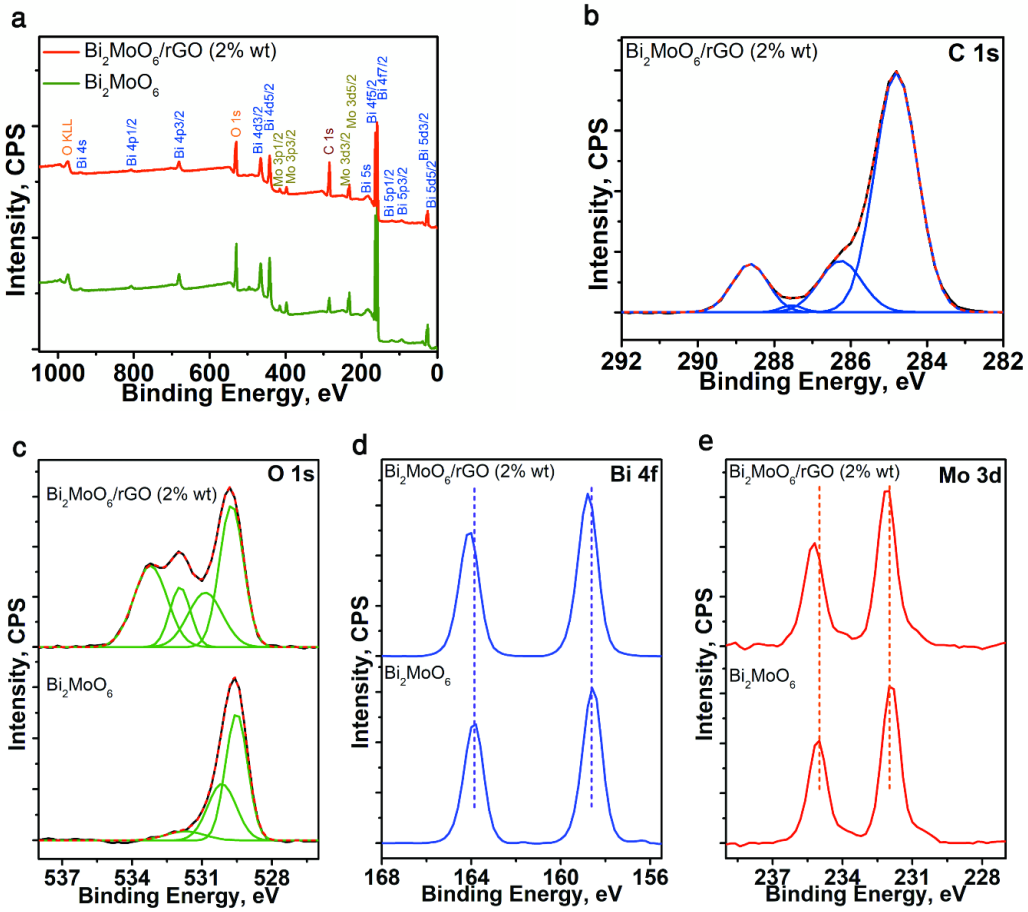

Figure 5-6: (a) XPS survey spectra of Bi_2MoO_6 and RGO-Bi_2MoO_6 (2 wt %). High-resolution XPS binding energy spectra: (b) C 1s, (c) O 1s,(d) Bi 4f and (e) Mo 3d

The high-resolution XPS spectrum of Bi (Figure 5-6d) consisted of only two peaks, which have binding energies at 158.8 and 164.1 eV. These binding energies may be ascribed to Bi $4f^{7/2}$ and Bi $4f^{5/2}$, which demonstrateed that Bi in Bi_2MoO_6 is in Bi^{3+} oxidation state (Liu *et al*., 2018). Furthermore, the Mo 3d spectrum in Figure 5-6e show two peaks at 232.1 and 235.2 eV, which are attributed to Mo $3d^{5/2}$ and Mo $3d^{3/2}$ and indicated that Mo is present in Mo^{6+} oxidation state (Kumar *et al*., 2019). The XPS analysis confirmed that the RGO-Bi_2MoO_6 (2 wt %) photocatalyst was successfully synthesised.

The optical properties of pure Bi_2MoO_6 and RGO-Bi_2MoO_6 samples were studied using the UV-vis absorbance spectra. Figure 5-7a displays a UV-vis absorbance pattern results for all the prepared samples. Pure Bi_2MoO_6 showed a typical UV-vis absorbance spectrum, with a steep edge near 430 nm. Compared to the pure Bi_2MoO_6, the enhanced absorbance of visible light region was noticed in all RGO-Bi_2MoO_6 nanocomposite materials. The observation for the spectrum revealed that the visible light response wavelength range of Bi_2MoO_6 broadens in the presence of RGO, which is crucial to enhance its photocatalytic properties under solar irradiation. The broadening of visible light response was attributed to the presence of black RGO particles, which increase the electric surface charge of RGO-Bi_2MoO_6 nanocomposites and further improves the electron-hole pair formation process during photocatalysis. In addition, the reduced oxygen functional groups and an increase of aromatic rings in RGO are more likely to cause electrons to be easily excited at a lower energy level. These results confirmed that the addition of GO in the Bi_2MoO_6 significantly improves the visible light response. Band gaps of all the samples were also estimated using the Tauc's plot, as depicted in Figure 5-7b. The plot was obtained by drawing a graph of (αhυ) 2 versus (hv) using the following equation:

$$\alpha h\upsilon = A(h\upsilon - E_g)^{n/2} \qquad \textit{Equation 5-1}$$

Where A, E_g (Ev), υ(Hz), h(J-s) and α are constant, band gap, optical frequency, Planck constant, and absorption coefficient, respectively; n was assumed to be 4 (Kasinathan *et al*., 2020). The estimation of band gaps from Tauc's plot were found to be 2.7, 2.1, 2.2, and 2.45 eV for pure Bi_2MoO_6, RGO-Bi_2MoO_6 (2 wt %), RGO-Bi_2MoO_6 (5 wt %), and RGO-Bi_2MoO_6 (10 wt %), respectively. All RGO-Bi_2MoO_6 nanocomposites exhibit a smaller band gap than pure Bi_2MoO_6, which might be due to the interaction between unpaired π electrons of RGO and electrons on the surface of Bi_2MoO_6 (Sharma *et al*., 2018). This is a promising characteristic for enhanced photocatalytic activity. The band gap increases slightly with a higher amount of RGO, which might be due to the aggregation of the RGO nanosheets.

Figure 5-7c shows the nitrogen adsorption-desorption isotherms of pure Bi_2MoO_6 and RGO-Bi_2MoO_6 samples. The isotherm curves of the RGO-Bi_2MoO_6 samples and pure Bi_2MoO_6 are the same, and they are classified in the type IV group. The type IV class exhibits a hysteresis loop and mesoporous structure (Donohue & Aranovich, 1998). The BET surface area of the RGO-Bi_2MoO_6 (2 wt %) (23.74

$m^2.g^{-1}$) was found to be higher than pure Bi_2MoO_6 (16.66 $m^2.g^{-1}$), RGO-Bi_2MoO_6 (5 wt %) (13.62 $m^2.g^{-1}$), and RGO- Bi_2MoO_6 (10 wt %) (10.24 $m^2.g^{-1}$) nanocomposites. The high surface of nanocomposite material provides more surface-active sites, which leads to the enhanced photocatalytic activity of the photocatalyst. The pore size distribution of the synthesised samples (Figure 5-7d) were measured through the Barrett–Joyner–Hanlenda (BJH) interpretation and are summarised in Table 5-1. Incorporation of GO in Bi_2MoO_6 reduced the pore size in the nanocomposite materials.

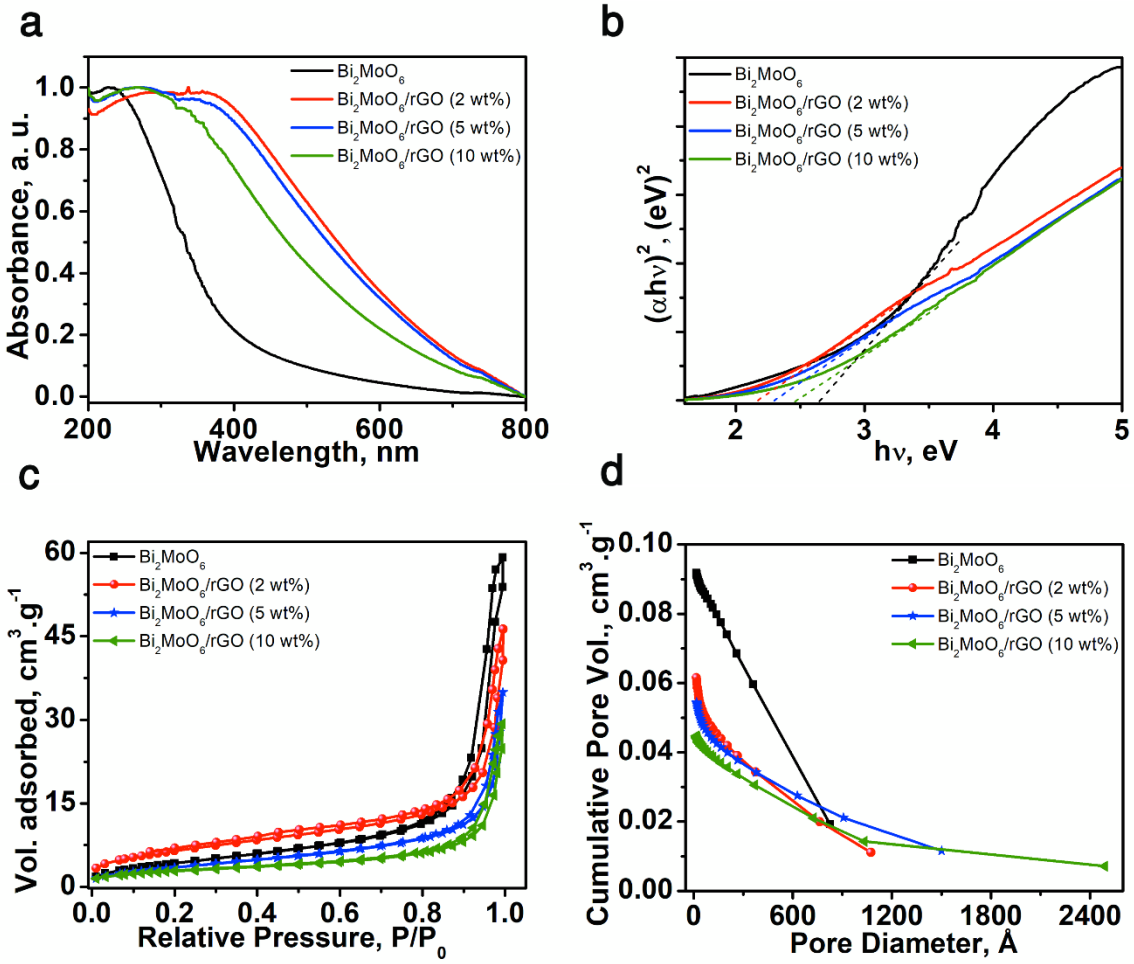

Figure 5-7: UV-vis absorbance spectra (a), the band gaps calculation by Tauc's plots (b), N_2 adsorption-desorption isotherms (c), and pore size distribution of Bi_2MoO_6 and RGO-Bi_2MoO_6 (0 ,2, 5, and 10(wt%) nanocomposites (d).

Table 5-1: Effect of different quantity of RGO on the surface area and porosity of Bi_2MoO_6

Materials	Specific Surface area (m^2 g^{-1})	Average pore volume (cm^3 g^{-1})	Average pore diameters (Å)
Bi_2MoO_6	16.66	0.092	105.16
RGO-Bi_2MoO_6 (2 wt %)	23.74	0.066	54.94
RGO-Bi_2MoO_6 (5 wt %)	13.65	0.054	67.07
RGO-Bi_2MoO_6 (10 wt %)	10.24	0.045	69.54

5.3.2 Removal of naphthalene via adsorption-photodegradation

5.3.2.1 Adsorption studies

Figure 5-8a demonstrate the effect of contact time on the adsorption efficiency of RGO-Bi_2MoO_6 (2 wt %). The results for the graph depict that the adsorption of naphthalene by RGO-Bi_2MoO_6 was very quick; as can be seen, within 5 min of the adsorption process, over 50% of naphthalene was adsorbed and naphthalene molecules were continuously adsorbed on the photocatalyst surface as the reaction progressed, until the adsorption-desorption equilibrium was reached. After 60 min, at least 80% of naphthalene was adsorbed. After 60 mi, an adsorption-desorption equilibrium was built up between the adsorbate and adsorbent. It can therefore be concluded that 60 mi was the most effective time for naphthalene adsorption using RGO-Bi_2MoO_6, and it was chosen for the rest of the study. The effect of the amount of reduced graphene added in Bi_2MoO_6 particles in the adsorption efficiency was also investigated and presented in Figure 5-8b. It is evident from the graph that the efficiency of the RGO-Bi_2MoO_6 (0, 5 and 10 wt %) nanocomposites was behaving in the same way as that of RGO-Bi_2MoO_6 (2 wt %). Nonetheless, the adsorption rates are different for all the synthesised material. Among all, RGO-Bi_2MoO_6 (2 wt %) shows the highest adsorption efficiency for the naphthalene, which might be due to the highest active surface area of the nanocomposite. Therefore, RGO-Bi_2MoO_6 (2 wt %) was chosen as the model adsorbent/photocatalyst for rest of the study. Owing to the RGO skeleton in RGO-Bi_2MoO_6 nanocomposites, all nanocomposites show a higher adsorption efficiency for naphthalene than pure Bi_2MoO_6. The RGO in the nanocomposite material is intensified with π-electrons, which facilitate the naphthalene adsorption via π–π interactions with the aromatic naphthalene (Mukwevho *et al*., 2020). It has also been noticed that the adsorption efficiency of nanocomposites reduced on increasing the RGO content in the nanocomposite. This might be due to the observation that, on increasing the RGO content in the

nanocomposite, the specific surface area also reduces, which reduces the active sites for the adsorption of naphthalene. The continuous increase in the adsorption efficiency for all the nanocomposites as the contact time increases was due to the occupation of the number of active sites of adsorbent by contaminants that increase as time progresses.

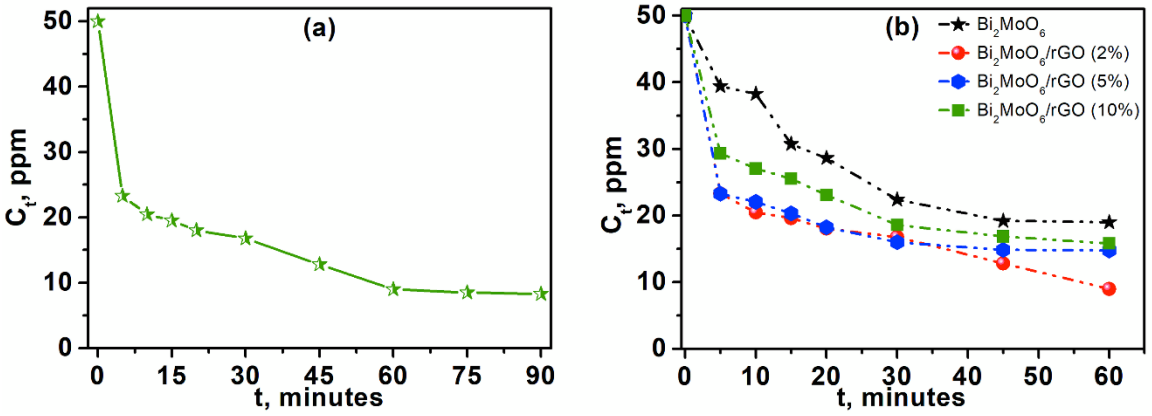

Figure 5-8: Figure 5 8: (a) Effect of contact time on the naphthalene adsorption using RGO-Bi_2MoO_6 (2 wt %). (b) Effect of different RGO-Bi_2MoO_6 nanocomposites on the removal of naphthalene from the wastewater. Conditions: adsorbent (RGO-Bi_2MoO_6) = 30 mg, naphthalene solution = 50 ppm, 100 mL, temperature = room temperature and time total reaction time = 60 minutes.

The effect of the initial concentration on the adsorption of naphthalene by RGO-Bi_2MoO_6 (2 wt %) was analysed by varying the initial concentration of the naphthalene solution (25, 50, 75 and 100 ppm). Figure 5-9a reveals that, as the initial concentration of the contaminant increases, the removal efficiency of the adsorbent decreases. This behaviour can be explained by the fact that, although the amount of contaminant molecules was increasing, the amount of active sites on the adsorbent for adsorption was constant. Therefore, due to limited available active sites for the naphthalene adsorption on adsorbent, the removal efficiency was decreased on increasing the naphthalene amount.

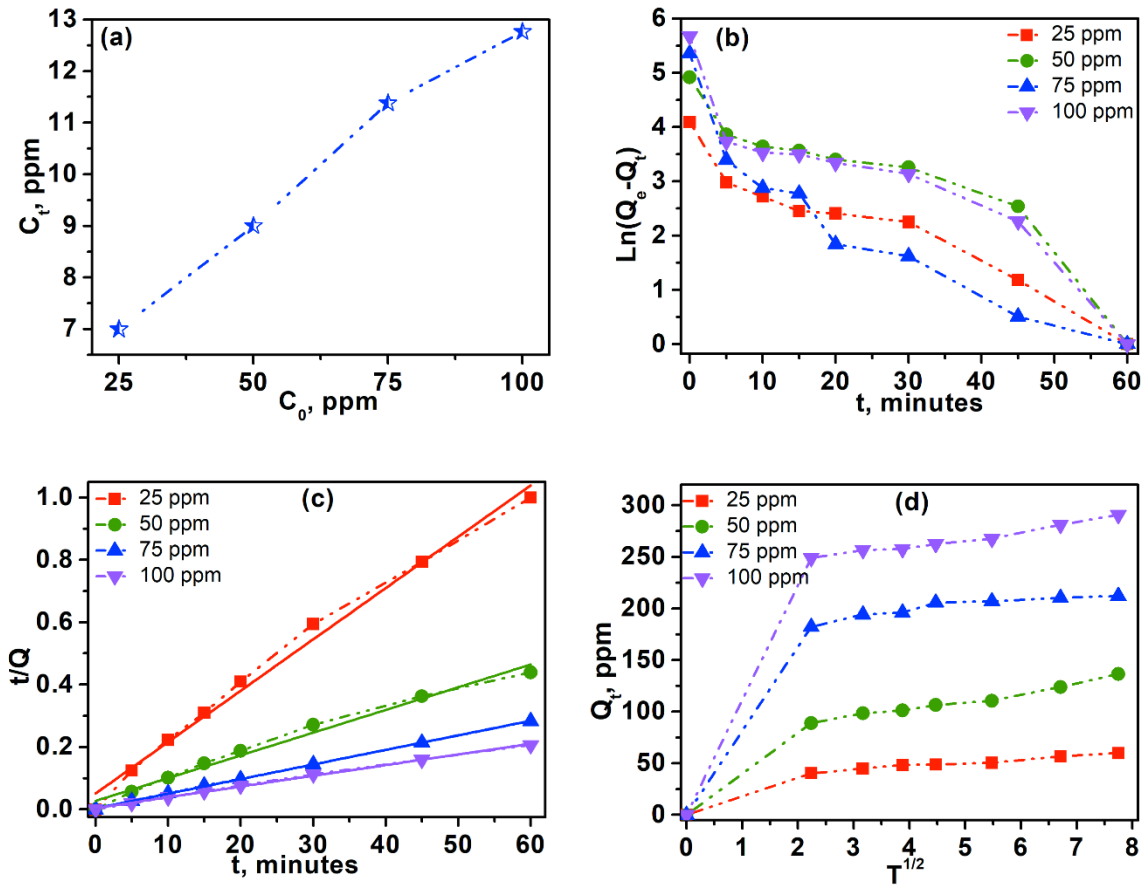

Figure 5-9: (a) Effect of initial naphthalene concentration on the removal efficiency of RGO-Bi_2MoO_6 (2 wt%), (b) Pseudo first order, (c) Pseudo second order adsorption kinetics and (d) Intraparticle diffusion of naphthalene adsorption using RGO-Bi_2MoO_6 (2 wt%). Conditions: adsorbent [RGO-Bi_2MoO_6 (2 wt %)] = 30 mg, naphthalene solution=100 mL (25, 50, 75 and 100 mg.L-1), temperature = room temperature and total reaction time = 60 minutes.

The study of the naphthalene adsorption kinetics was done to help interpret the adsorption mechanism of RGO-Bi_2MoO_6 as an adsorbent for naphthalene removal in water. Three kinetic models, namely pseudo first-order, pseudo second-order and intraparticle diffusion, were used for understanding the adsorption mechanism. In addition, the study of kinetics helps determine and express the rate of determining steps for pollutant removal from the aqueous solution. The linear pseudo first-order kinetics is expressed in Equation 5-2 as:

$$ln(Q_e - Q_t) = lnQ_e - k_1 t \qquad \textit{Equation 5-2}$$

where Q_t and Q_e represent the amount of adsorbed naphthalene molecules (mg) per gram of adsorbent at time t (min) and equilibrium, respectively, and k_1 is the rate constant of pseudo first-order (min^{-1}). The values of k_1 and Q_e can be obtained from the slope and intercept values of the linear plot of ln (Q_e - Q_t) versus t (Figure 9b). The value of Q_t can be calculated using Equation 5-3, as follows:

$$Q_t = (C_o - C_t).\frac{V}{m} \qquad \textit{Equation 5-3}$$

where C_o and C_t are the amount of initial and remaining concentration (mg) of naphthalene after time t (min) in the solution, V is the volume of solution (mL), and m is the weight of adsorbent (mg).

The R^2 value (coefficient of determination) is calculated from the linear graph and used to find the best kinetic model that fits the adsorption process. Higher R^2 values indicate the best fitted model. The graph plotted for pseudo first-order kinetics from the experimental values shows a poor R^2 value and also does not yield a linear relationship (Figure 5-9b). This implied that the pseudo first-order model was not applicable in describing the adsorption mechanism of naphthalene using RGO-Bi_2MoO_6.

The pseudo second-order kinetic model was also studied to check if it is applicable in the adsorption process of naphthalene. The pseudo second-order equation is given as:

$$\frac{t}{Q_t} = \frac{1}{k_2 {Q_e}^2} + \frac{t}{Q_e} \qquad \textit{Equation 5-4}$$

where k_2 is the pseudo second order rate constant ($g.mg^{-1}.min^{-1}$). Figure 5-9c depicts the pseudo second-order kinetics, which is the plot of t/Q_t versus t. The kinetics parameters for the pseudo second-order model were estimated using the slope and intercept values of the graph in Figure 5-9c. The calculated values were found to be very similar to the experimental values, as shown in Table 5-2. Furthermore, Figure 5-9c indicates the linear relationship of the graph with a high R^2 value, which allows the conclusion that the pseudo second-order model can be used to describe the adsorption mechanism of naphthalene. Figure 5-9d reveals the intraparticle diffusion model for the adsorption of naphthalene. The linear intraparticle diffusion kinetic model is expressed as:

$$Q_t = k_{id} t^{\frac{1}{2}} + C \qquad \textit{Equation 5-5}$$

where k_{id} is the intraparticle diffusion constant ($mg.g^{-1}.min^{-1/2}$). The plot of Q_t versus $t^{1/2}$ also does not give a linear relation between the two variables with a poor R^2 value. This confirms that the model was not applicable in the adsorption process of naphthalene, and intraparticle discussion cannot be the rate determining step.

Adsorption isotherm studies were conducted to analyse the interactions between the amounts of naphthalene adsorbed on the photocatalyst surface and the concentration of naphthalene in the solution at equilibrium state. This relationship was analysed using the well-known isotherms, Langmuir and Freundlich. The Langmuir adsorption assumes that the adsorption process is of monolayer form, meaning that it occurs on a surface with a finite number of sites that are distributed homogenously on the adsorbent surface. In contrast, Freundlich adsorption assumes a multilayer adsorption of adsorbate molecules on the surface of the adsorbent that is of a heterogeneous nature and has different energies. The Langmuir isotherm is expressed as follows:

$$Q_e = \frac{Q_m K_L C_e}{1 + K_L C_e} \qquad \textit{Equation 5-6}$$

This expression can be further linearised to transform into Equation 5-7 as:

$$\frac{C_e}{Q_e} = \frac{C_e}{Q_m} + \frac{1}{Q_e K_L} \qquad \textit{Equation 5-7}$$

where Q_m represents the maximum adsorption capacity of the adsorbent ($mg.g^{-1}$), K_L ($L.mg^{-1}$) is the Langmuir sorption constant at a specific temperature, and C_e is the equilibrium concentration of naphthalene in the solution.

The Langmuir adsorption isotherm was plotted between C_e versus C_e/Q_e, and the values of Q_m and K_L can be calculated using the slope and intercept values of the graph (Figure 5-10a).

The Freundlich isotherm equation is shown by Equation 5-8, and its linearised form is given as Equation 5-9.

$$Q_e = k_f C_e^{\frac{1}{n}} \qquad \textit{Equation 5-8}$$

$$lnQ_e = lnk_f + \frac{1}{n} lnC_e \qquad \textit{Equation 5-9}$$

where k_f symbolises the Freundlich adsorption constant referred to as the adsorption capacity, and n is the Freundlich constant that represents the degree of adsorption. The parameters in both the isotherm models are summarised in Table 5-3 as well as the values of the linear correlation coefficient. The values of k_f and 1/n were calculated using the slope and the intercept of the log Q_e versus log C_e plot in Figure 5-10b. It can be clearly seen that both models showed high R^2 values with slight prevalence of the Langmuir adsorption isotherm. The maximum adsorption capacity of naphthalene onto RGO-Bi_2MoO_6 (2 wt %) was determined as 173.611 mg g^{-1}.

Table 5-2: Pseudo second-order kinetic parameters for the adsorption of naphthalene using RGO-Bi_2MoO_6 (2 wt%).

Initial Naphthalene Concentration, $mg.L^{-1}$	Pseudo Second Order Kinetic Parameters			
	$Q_{e,cal}$	$Q_{e,exp}$	k_2 X 10^{-4}, $g.mg.min^{-1}$	R^2
25	60	60.75	2.95	0.99
50	133.33	137.174	2.82	0.98
75	212.066	214.13	2.49	0.99
100	290.78	291.54	2.2	0.99

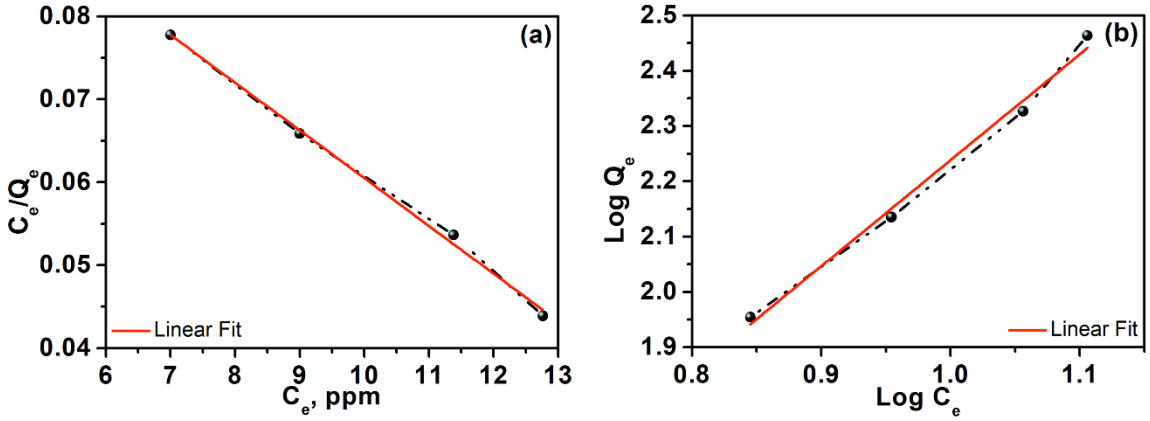

Figure 5-10: (a) Langmuir Adsorption Isotherm and (b) Freundlich Adsorption Isotherm plots for the adsorption of naphthalene from wastewater using RGO-Bi_2MoO_6 (2 wt %). The red line in the graph shows the linear fitting. Conditions: adsorbent [RGO-Bi_2MoO_6 (2 wt %)] = 30 mg, naphthalene solution =100 mL, temperature = room temperature and total reaction time = 60 minutes

Table 5-3: Langmuir and Freundlich adsorption isotherm parameter values for the adsorption of naphthalene from wastewater using RGO-Bi_2MoO_6 (2 wt %).

Adsorption Isotherm Model	Isotherm parameter	Isotherm parameter palues
Langmuir	Q_m, $mg.g^{-1}$	173.611
	K_L, $L.mg^{-1}$	4.8×10^{-2}
	R^2	0.99
Freundlich	K_f, $(mg.\ g^{-1})(L.\ mg^{-1})$	1.38097
	1/n	1.19
	R^2	0.97

5.3.2.2 Photo-degradation studies

To investigate the photocatalytic potential of RGO-Bi_2MoO_6 nanocomposite on the degradation of naphthalene in simulated polluted water, 100 mL of 50 ppm naphthalene aqueous solution with 30 mg of photocatalyst were mixed together and regularly stirred using a magnetic stirrer for 30 minutes in the absence of light in order to reach the adsorption-desorption equilibrium. Thereafter, a sample aliquot was extracted before the solution was exposed to the 250 UV-vis light. After sampling, UV-vis light was beamed on the solution for 60 min for the photodegradation reaction to take place. Figure 5-11a represent the photocatalytic ability of Bi_2MoO_6 and all RGO-Bi_2MoO_6 samples on the photodegradation efficiency of naphthalene in an aqueous solution. Similar to the adsorption process, naphthalene concentration in the solution decreased as the contact and exposure to UV-vis light time increased until equilibrium was reached. The photocatalytic efficiency of all photocatalysts was found to be in the order of: Bi_2MoO_6 < RGO-Bi_2MoO_6 (10 wt %) < RGO-Bi_2MoO_6

(5 wt %) < RGO-Bi_2MoO_6 (2 wt %). It has been noticed that all RGO-Bi_2MoO_6 performed better photocatalytic activity towards naphthalene degradation than Bi_2MoO_6.

The effectiveness of the photocatalyst decreased as the amount of RGO increased, which implies that a large amount of RGO in the Bi_2MoO_6 decreases the number of active sites, which will subsequently lead to a poor photocatalytic degradation process. Among all, RGO-Bi_2MoO_6 (2 wt %) showed the highest potential towards the photocatalytic degradation of naphthalene. Approximately 95% of naphthalene was successfully degraded using RGO-Bi_2MoO_6 (2 wt %) under visible light irradiation. Figure 5-11b shows the decreasing absorbance intensity of naphthalene with the course of photocatalysis degradation, using RGO-Bi_2MoO_6 (2 wt %) as photocatalyst. The intensity decreased as the irradiation time increased. The intensity curves indicate that photodegradation of naphthalene is very fast during the initial 5 min (>80%) under light irradiation. The rapid decrease in intensity at the beginning of the process is due to the abundant availability of active sites on the surface of the photocatalyst, and this will eventually lead to the recombination rate of photogenerated carriers to reduce.

The photocatalytic degradation rate of naphthalene was studied using the Langmuir-Hishelwood (LH) kinetic model, which is commonly used to elucidate the rates of the heterogeneous catalytic process. The model is expressed as:

$$ln\left(\frac{C_o}{C_t}\right) = k_1 t \qquad \textit{Equation 5-10}$$

where k_1 is the pseudo first-order rate constant and is obtained from the product of k_T and K as follows:

$$k_1 = k_T . K \qquad \textit{Equation 5-11}$$

where k_T is the limiting rate constant of the photocatalytic reaction, and K is the adsorption equilibrium constant of the substrate. The plot of lnC_o/C_t versus t represented in Figure 5-11c helps to determine the values of k_1 and confirmed that the LH kinetic model can be applied in the study of the naphthalene photodegradation process. The values of R^2 for all the RGO-Bi_2MoO_6 photocatalysts are very close to 1, which indeed confirms the feasibility of the LH kinetic model in naphthalene photodegradation.

To further examine the performance of RGO-Bi_2MoO_6, the recyclability and recovery of the photocatalyst were explored. Recycling experiments of the RGO-Bi_2MoO_6 (2 wt %) after the photodegradation reaction of naphthalene were perfomed for 5 cycles. After each cycle, RGO-Bi_2MoO_6 was recovered by centrifugation and purified with distilled water several times. The recovered photocatalyst was then used again for photodegradation reactions under the same reaction conditions. As depicted in Figure 5-11d, the performance of the photocatalyst was almost unaffected by the recycling cycle, since it was slightly decreased from about 96% to about 82% efficiency after 5 cycles. Therefore, the photocatalyst can be recycled several times and still show

good photocatalytic activity because, from this experiment, the photocatalyst was used more than four times and still showed good photocatalytic results.

The effective potential of the RGO-Bi_2MoO_6 photocatalyst compared to pure Bi_2MoO_6 in the photocatalytic degradation of naphthalene can further be explained by photoluminescence spectroscopy. Figure 5-12 shows the PL spectra of pure Bi_2MoO_6 and RGO-Bi_2MoO_6 (2 wt %) samples, which were utilised to investigate the transfer activity of photo-excited charge carriers. The emission spectrum of both samples depicts main peaks centred at 450, 482 and 545 nm. These peaks represent the intrinsic luminescence of Bi_2MoO_6. The fluorescence intensity of the RGO-Bi2MoO6 (2 wt %) sample is almost half the intensity of pure Bi_2MoO_6. The lower emission intensity of RGO-Bi_2MoO_6 (2 wt%) implies that the incorporation of RGO in the Bi_2MoO_6 matrix reduces the recombination rate of photo-excited electron-hole pairs in the transfer activity and can behave as an electron acceptor during a photocatalytic process (Yang *et al*., 2015). Therefore, the use of RGO-Bi_2MoO_6 (2 wt %) as a photocatalyst resulted in a lower recombination rate of photo-induced electrons. As a result, during the photocatalytic process, more reactive species would be generated, promoting the separation of electron-hole pairs, and RGO could further facilitate the splitting of electron-hole pairs by its conducting nature. In this way, RGO-Bi_2MoO_6 (2 wt %) exhibits stronger photocatalytic activity, and more pollutant could be degraded.

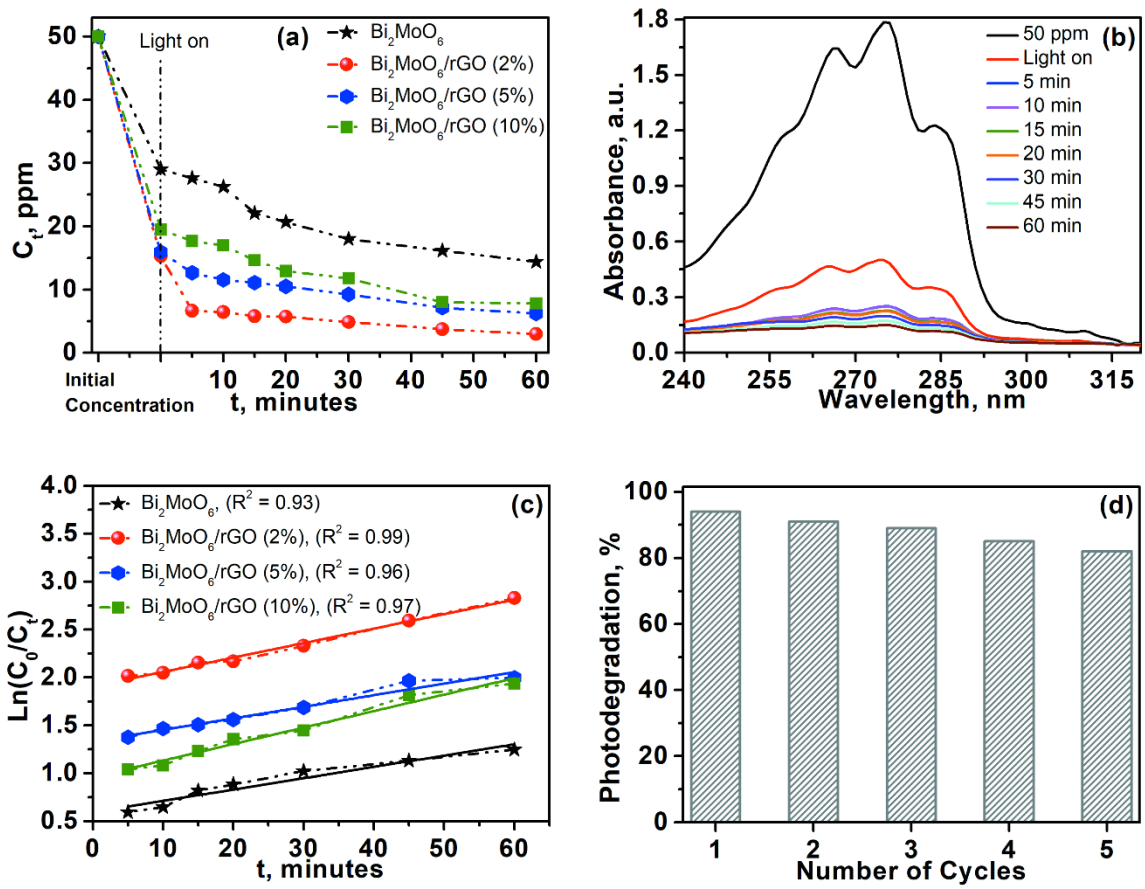

Figure 5-11: (a) Effect of contact time on the photodegradation of 50 ppm naphthalene under 250W UV-visible light irradiation using RGO-Bi_2MoO_6, (b) Decrease in the absorbance intensity of naphthalene with light irradiation time during photocatalytic degradation using RGO-Bi_2MoO_6, (c) Langmuir-Hinshelwood kinetics model for the photocatalytic degradation of naphthalene solution, and (d) Recyclability of the RGO-Bi_2MoO_6 (2 wt%) for naphthalene photocatalytic degradation up to 5 cycles.

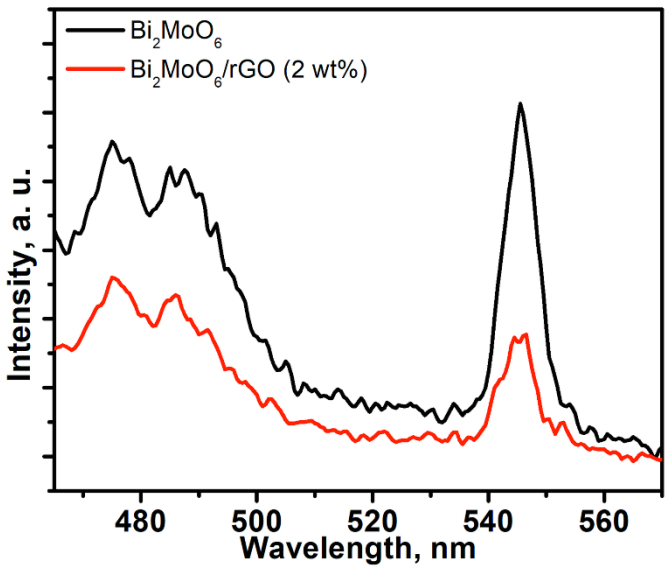

Figure 5-12: PL spectra of Bi_2MoO_6 nanostructure and RGO-Bi_2MoO_6 (2 wt %) nanocomposite (excitation wavelength = 350 nm)

The naphthalene removal mechanism (Figure 5-13) onto the RGO-Bi_2MoO_6 nanocomposite can be described as follows: initially, naphthalene molecules adsorbed onto the RGO-Bi_2MoO_6 nanocomposite through the π-π interactions between naphthalene and the aromatic rings of RGO. Later, these naphthalene molecules started to degrade upon irradiation of visible light. When light irradiated on Bi_2MoO_6 nanoplates, formation of photogenerated electrons and holes take place, which consequently generates active superoxide anion radicals and hydroxyl radicals, respectively for the photodegradation of naphthalene (Kumar *et al*., 2017, Byrne *et al*., 2018). Therefore, naphthalene first adsorbed onto the RGO-Bi_2MoO_6 nanocomposite from an aqueous solution and degraded into less harmful products through photodegradation.

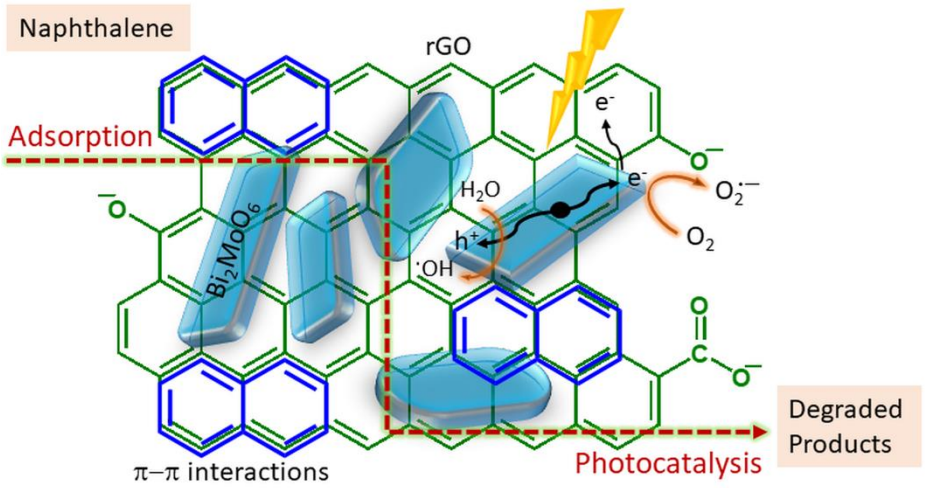

Figure 5-13**:** Plausible mechanism for the removal of naphthalene via adsorption-photodegradation

5.4 Conclusion

The heterogeneous photocatalytic materials (Bi_2MoO_6 and RGO-Bi_2MoO_6 nanocomposite) were successfully synthesised via the hydrothermal method. These materials were further employed for the adsorption-assisted photodegradation of naphthalene (50 ppm) in simulated wastewater. The results revealed that RGO-$Bi_2MoO_6$6 nanocomposite displayed better adsorption and photocatalytic efficiency than pure Bi_2MoO_6 towards the naphthalene degradation in an aqueous solution. Bi_2MoO_6 exhibits a narrow band gap, which is sufficient to generate electrons and hole pairs under visible light, whereas the fast recombination of charge carriers limits its activity for photo-catalysis. The incorporation of RGO in RGO-Bi_2MoO_6 played a significant role in improving the adsorption and photocatalytic efficiency of nanocomposite material. The RGO in RGO-Bi_2MoO_6 improves the adsorption of naphthalene molecules on the surface of the photocatalyst through π-π interaction, which could successfully be degraded. The adsorption of naphthalene was followed by Langmuir adsorption and pseudo second-order kinetics. Furthermore, RGO acts as electron sink and suppresses the recombination activity of photo-generated charge carriers, which promotes the photocatalytic efficiency of material. Among all RGO-Bi_2MoO_6 nanocomposites, RGO-Bi_2MoO_6 (2

wt%) exhibited better photodegradation efficiency, which might be due to a large active surface area, efficient electron transfer, and lower rate of recombination of electrons and holes. Approximately 95% of naphthalene was degraded under the 60 minutes visible light irradiation using RGO-Bi_2MoO_6 (2 wt %). The photocatalyst was successfully recovered through centrifugation and successfully employed for recyclability. Based on the stable and remarkable performance of Bi_2MoO_6, this study suggests a clean and sustainable approach to the remediation of wastewater.

5.5 Graphical abstract

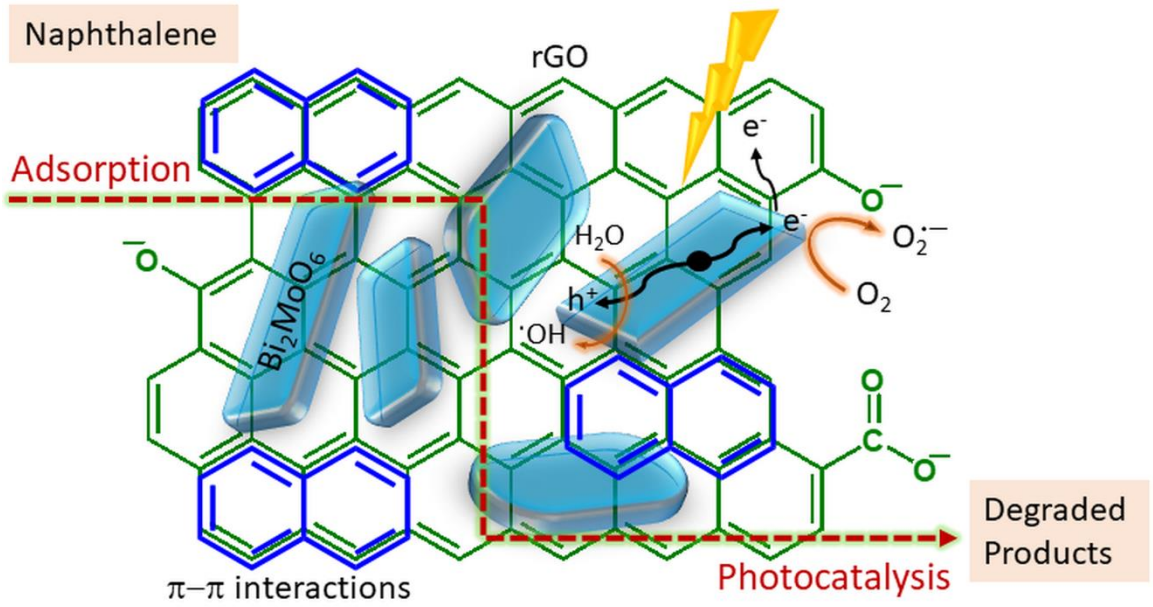

References

Abdel-Shafy, H.I. & Mansour, M.S.M. 2016. A review on polycyclic aromatic hydrocarbons: source, environmental impact, effect on human health and remediation. *Egyptian Journal of Petroleum,* 25:107-123.

Adeola, A.O. & Forbes, P.B.C. Advances in water treatment technologies for removal of polycyclic aromatic hydrocarbons: existing concepts, emerging trends, and future prospects. *Water Environment Research*.

Byrne, C., Subramanian, G. & Pillai, S.C. 2018. Recent advances in photocatalysis for senvironmental applications. *Journal of Environmental Chemical Engineering,* 6:3531-3555.

Ding, J., Yang, Z., He, .C, Tong, X., Li, Y., Niu, X. & Zhang, H. 2017. Uio-66 (zr) coupled with Bi_2MoO_6 as photocatalyst for visible-light promoted dye degradation. *Journal of Colloid and Interface Science,* 497:126-133.

Donohue, M. & Aranovich, G. 1998. Classification of gibbs adsorption isotherms. *Advances in Colloid and Interface Science,* 76:137-152.

García-Martínez, M., Ortega, M., Bolonio, D., Llamas, J. & Canoira, L. 2018. Leaching of polycyclic aromatic hydrocarbons (PAHs) from coal dumps reclaimed with apple trees: a mechanistic insight. *Environmental Geochemistry and Health,* 40:2695-2706.

García-Martínez, M.J., Da Riva, I., Canoira, L., Llamas, J.F., Alcántara, R. & Gallego, J.L.R. 2006. Photodegradation of polycyclic aromatic hydrocarbons in fossil fuels catalysed by supported tio2. *Applied Catalysis B: Environmental,* 67:279-289.

Guo, J., Shi, L., Zhao, J., Wang, Y., Tang, K., Zhang, W., Xie, C. & Yuan, X. 2018. Enhanced visible-light photocatalytic activity of Bi_2MoO_6 nanoplates with heterogeneous Bi_2MoO_6-x@Bi_2MoO_6 core-shell structure. *Applied Catalysis B: Environmental,* 224:692-704.

Gusain, R., Kumar, N. & Ray, S.S. 2020. Recent advances in carbon nanomaterial-based adsorbents for water purification. *Coordination Chemistry Reviews,* 405:213111.

Kabra, K., Chaudhary, R. & Sawhney, R.L. 2004. Treatment of hazardous organic and inorganic compounds through aqueous-phase photocatalysis: a review. *Industrial & Engineering Chemistry Research,* 43**:**7683-7696.

Kasinathan, M., Thiripuranthagan, S., Sivakumar, A., Ranganathan, S., Vembuli, T., Kumaravel, S. & Erusappan, E. 2020. Fabrication of novel Bi_2MoO_6/n-RGO catalyst for the efficient photocatalytic degradation of harmful dyes. *Materials Research Bulletin,* 125**:** 110782.

Kumar, N., Fosso-Kankeu, E. & Ray, S.S. 2019. Achieving controllable mos2 nanostructures with increased interlayer spacing for efficient removal of pb(ii) from aquatic systems. *ACS Applied Materials & Interfaces,* 11**:** 19141-19155.

Kumar, N., Kumar, S., Gusain, R., Manyala, N., Eslava, S. & Ray, S.S. 2020. Polypyrrole-promoted RGO–mos_2 nanocomposites for enhanced photocatalytic conversion of CO_2 and H_2O to CO, CH_4, and H_2 products. *ACS Applied Energy Materials,* 3**:** 9897-9909.

Kumar, N., Mittal, H., Alhassan, S.M. & Ray, S.S. 2018. Bionanocomposite hydrogel for the adsorption of dye and reusability of generated waste for the photodegradation of ciprofloxacin: a demonstration of the circularity concept for water purification. *ACS Sustainable Chemistry & Engineering,* 6**:** 17011-17025.

Kumar, N., Mittal, H., Parashar, V., Ray, S. S. & Ngila, J. C. 2016. Efficient removal of rhodamine 6g dye from aqueous solution using nickel sulphide incorporated polyacrylamide grafted gum karaya bionanocomposite hydrogel. *RSC Advances,* 6: 21929-21939.

Kumar, N., Sinha Ray, S. & Ngila, J.C. 2017. Ionic liquid-assisted synthesis of ag/ag2te nanocrystals via a hydrothermal route for enhanced photocatalytic performance. *New Journal Of Chemistry,* 41**:** 14618-14626.

Lamichhane, S., Kc, B.K. & Sarukkalige, P. 2016. Polycyclic aromatic hydrocarbons (pahs) removal by sorption: a review. *Chemosphere,* 148**:** 336-353.

Liu, Y., Yang, Z.-H., Song, P.-P., Xu, R. & Wang, H. 2018. Facile synthesis of $Bi_2MoO_6/ZnSnO_3$ heterojunction with enhanced visible light photocatalytic degradation of methylene blue. *Applied Surface Science,* 430**:** 561-570.

Martinez-De la Cruz, A. & Alfaro, S.O. 2010. Synthesis and characterization of γ-Bi_2MoO_6 prepared by co-precipitation: photoassisted degradation of organic dyes under vis-irradiation. *Journal of Molecular Catalysis A: Chemical,* 320**:** 85-91.

Mojiri, A., Zhou, J. L., Ohashi, A., Ozaki, N. & Kindaichi, T. 2019. Comprehensive review of polycyclic aromatic hydrocarbons in water sources, their effects and treatments. *Science of the Total Environment,* 696**:** 133971.

Mukwevho, N., Fosso-Kankeu, E., Waanders, F., Kumar, N., Ray, S.S. & Yangkou Mbianda, X. 2018. Photocatalytic activity of gd2o2co3·zno·cuo nanocomposite used for the degradation of phenanthrene. *Sn Applied Sciences,* 1**:** 10.

Mukwevho, N., Gusain, R., Fosso-Kankeu, E., Kumar, N., Waanders, F. & Ray, S.S. 2020. Removal of naphthalene from simulated wastewater through adsorption-photodegradation by zno/ag/go nanocomposite. *Journal of Industrial and Engineering Chemistry,* 81: 393-404.

Mukwevho, N., Kumar, N., Fosso-Kankeu, E., Waanders, F., Bunt, J. R. & Sinha Ray, S. 2019. Visible light-excitable ZnO/2d graphitic-c3n4 heterostructure for the photodegradation of naphthalene. *Desalination and Water Treatment,* 163: 286–296.

Nguyen, V.-H., Thi, L.-A. P., Van Le, Q., Singh, P., Raizada, P. & Kajitvichyanukul, P. 2020. Tailored photocatalysts and revealed reaction pathways for photodegradation of polycyclic aromatic hydrocarbons (PAHS) in water, soil and other sources. *Chemosphere,* 260: 127529.

Oturan, M.A. & Aaron, J.-J. 2014. Advanced oxidation processes in water/wastewater treatment: principles and applications. A review. *Critical Reviews in Environmental Science and Technology,* 44**:** 2577-2641.

Quesada, H.B., Baptista, A.T.A., Cusioli, L.F., Seibert, D., De Oliveira Bezerra, C. & Bergamasco, R. 2019. Surface water pollution by pharmaceuticals and an alternative of removal by low-cost adsorbents: a review. *Chemosphere,* 222**:** 766-780.

Ray, S.S., Gusain, R. & Kumar, N. 2020. Chapter two - classification of water contaminants. *In:* Ray, S.S., Gusain, R. & Kumar, N. (eds.) *Carbon Nanomaterial-Based Adsorbents for Water Purification.* Elsevier.

Rengarajan, T., Rajendran, P., Nandakumar, N., Lokeshkumar, B., Rajendran, P. & Nishigaki, I. 2015. Exposure to polycyclic aromatic hydrocarbons with special focus on cancer. *Asian Pacific Journal of Tropical Biomedicine,* 5**:** 182-189.

Sharma, M., Behl, K., Nigam, S. & Joshi, M. 2018. TiO_2-GO nanocomposite for photocatalysis and environmental applications: a green synthesis approach. *Vacuum,* 156**:** 434-439.

Sindhu, S., Sanghi, S., Agarwal, A., Seth, V. & Kishore, N. 2005. Effect of Bi_2O_3 content on the optical band gap, density and electrical conductivity of $Mo{\cdot}Bi_2O_3{\cdot}B2O_3$ (m= ba, sr) glasses. *Materials Chemistry and Physics,* 90**:** 83-89.

Walaszek, M., Bois, P., Laurent, J., Lenormand, E. & Wanko, A. 2018. Micropollutants removal and storage efficiencies in urban stormwater constructed wetland. *Science of the Total Environment,* 645**:** 854-864.

Wan, S., Ou, M., Zhong, Q., Zhang, S. & Song, F. 2017. Construction of z-scheme photocatalytic systems using ZnIn2S4, COOX-loaded Bi_2MoO_6 and reduced graphene oxide electron mediator and its efficient nonsacrificial water splitting under visible light. *Chemical Engineering Journal,* 325**:** 690-699.

Wang, Y., Niu, C.-G., Zhang, L., Wang, Y., Zhang, H., Huang, D.-W., Zhang, X.-G., Wang, L. & Zeng, G.-M. 2016. High-efficiency visible-light Agi/Ag/Bi_2MoO_6 as a z-scheme photocatalyst for environmental applications. *RSC Advances,* 6**:** 10221-10228.

Xiao, J., Zhang, J., Liu, W., Huang, T., Qu, Y., Chen, H. & Lin, Z. 2018. Construction of RGO/Bi_2MoO_6 2d/2d nanocomposites for enhancement visible light-driven photocatalytic reduction of cr (vi). *Materials Research Express,* 5**:** 115031.

Yang, J., Wang, X., Zhao, X., Dai, J. & Mo, S. 2015. Synthesis of uniform Bi_2WO_6-reduced graphene oxide nanocomposites with significantly enhanced photocatalytic reduction activity. *The Journal of Physical Chemistry C,* 119: 3068-3078.

Zeng, Y., Hong, P. A. & Wavrek, D. A. 2000. Chemical–biological treatment of pyrene. *Water Research,* 34**:** 1157-1172.

Zhang, J., Liu, Z. & Ma, Z. 2019. Facile formation of Bi_2O_2CO3/Bi_2MoO_6 nanosheets for visible light-driven photocatalysis. *ACS Omega,* 4**:** 3871-3880.

Zhang, J., Niu, C., Ke, J., Zhou, L. & Zeng, G. 2015. Ag/AgCl/Bi_2MoO_6 composite nanosheets: a plasmonic z-scheme visible light photocatalyst. *Catalysis Communications,* 59**:** 30-34.

Zhang, L., Xu, T., Zhao, X. & Zhu, Y. 2010. Controllable synthesis of Bi_2MoO_6 and effect of morphology and variation in local structure on photocatalytic activities. *Applied Catalysis B: Environmental,* 98: 138-146.

Zhao, J., Lu, Q., Wei, M. & Wang, C. 2015. Synthesis of one-dimensional α-Fe_2O_3/Bi_2MoO_6 heterostructures by electrospinning process with enhanced photocatalytic activity. *Journal of Alloys and Compounds,* 646**:** 417-424.

Zheng, X.-J., Blais, J.-F., Mercier, G., Bergeron, M. & Drogui, P. 2007. PAH removal from spiked municipal wastewater sewage sludge using biological, chemical and electrochemical treatments. *Chemosphere,* 68**:** 1143-1152.

CHAPTER 6: OVERALL CONCLUSION AND RECOMMENDATIONS

6.1 Overall ronclusion

It can be concluded that coal tar contains a variety of PAHs; all 16 priority PAHs were identified in the coal tar derived from the coking process and were used in this project. The results from the experiments confirmed that PAHs can be leached when the coal tar is exposed to aqueous solutions such as demin water, river water and synthetic rain. It was also observed that the chemical properties of water sources affect the quantity and type of PAHs leached from the coal tar; lighter PAHs were more easily leached from coal tar than heavier PAHs. These findings are very important in understanding the dispersion of PAHs in receiving water sources and carrying out environmental risk assessments related to the inappropriate discharge of coal tar. A number of carcinogenic and toxic PAHs were detected in coal tar, therefore suggesting that dumping coal tar in the environment can lead to adverse health impacts on both humans and animals. Furthermore, it is necessary and very important to ensure that water sources in close proximity to coal tar dump sites and industrial areas producing coal tar are analysed for PAHs.

The second objective of this study involved developing a suitable catalyst for the sustainable degradation of one of the main PAHs identified in the coal tar derived from the coking process, which was naphthalene. Bi_2MoO_6, which is the recently discovered material for the decomposition of organic pollutants, was tested for its performance in the removal of naphthalene. To further enhance the photocatalytic activity of the photocatalyst, Bi_2MoO_6 was modified with RGO to obtain RGO-Bi_2MoO_6 as the final photocatalyst product. This material was successfully synthesised using the hydrothermal method. The prepared RGO-Bi_2MoO_6 was applied in the decomposition of naphthalene from simulated wastewater. It was found that the narrow band gap that Bi_2MoO_6 exhibits is sufficient to operate under visible light conditions as a photocatalyst. However, its photodegradation efficiency is limited by the fast recombination rate that takes place during the photocatalysis process. Therefore, this limitation was addressed by adding RGO to the pristine Bi_2MoO_6. The results obtained proved that the addition of RGO to the material enhanced the photocatalytic performance of pristine Bi_2MoO_6. The 2% RGO-Bi_2MoO_6 was found to be the best performing photocatalyst when compared to the 5 and 10%. The addition of 2% RGO improved the photodegradation efficiency of Bi_2moO_6 by over 20%.The photodegradation activity of RGO-Bi_2MoO_6 was seen to be greatly assisted by the adsorption process. It was found that over 50% of the naphthalene was degraded during the adsorption phase (in the absence of UV-vis light).Therefore, it can be concluded that, based on the results of this study, photodegradation techniques can be employed to remove PAHs present in the water. Furthermore, it can be concluded that doping photocatalysts with non-metals can significantly improve the performance of the material.

6.2 Overall recommendations

As it is possible with many scientific studies,this study may need to be expanded by conducting furthur investigations to add more insights and support the findings from this work. The following are recommendations for furthur research:

- The study investigated only 3 types of leaching llixiviants, namely normal water, river water and synthetic rain. Therefore, other lixiviants such as acid mine drainage water and sea water can be tested to see how they can influence the leaching process of PAHs.
- Another investigation that would be of interest, would be testing how the concentration and the consitituents in the leachate changes after a certain period.
- Since all photodegradation experiments in this study were conducted on a laboratory scale, it is necessary to investigate the feasilibity of using RGO-Bi_2MoO_6 in large scale.
- Since this study investigated PAHs removal process from water using Naphthalene as the representative of PAHs, more degradation and adsoption experiments can be conducted using other heavier and potent PAHs such as benzo (a) pyrene, phenanthrene and pyrene.
- The efficiency of RGO-Bi_2MoO_6 must also be tested with other types of PAHs solutions.